DNA LINKERS SURFING ON COLLOIDS:

How surface-mobile DNA linkers affect colloidal self-assembly

Stef Aris Jurriaan van der Meulen

DNA LINKERS SURFING ON COLLOIDS:

How surface-mobile DNA linkers affect colloidal self-assembly

PROEFSCHRIFT

ter verkrijging van de graad van doctor
aan de Technische Universiteit Delft,
op gezag van de Rector Magnificus prof. ir. K. Ch. A. M. Luyben,
voorzitter van het College voor Promoties,
in het openbaar te verdedigen op
vrijdag 19 februari 2016, om 15:00 uur

door

Stef Aris Jurriaan van der Meulen

Master of Science in Medical Natural Sciences
geboren te Edam, Nederland.

The dissertation has been approved by the

promotor:	Prof. dr. M. Dogterom
copromotor:	Dr. M. E. Leunissen

Composition of the doctoral committee:

Rector Magnificus	
Prof. dr. M. Dogterom	promotor
Dr. M. E. Leunissen	copromotor
Independent members:	
Prof. dr. ir. S. J. Tans	TU Delft
Prof. D. Frenkel	U-Cambridge, UK
Prof. dr. A. van Blaaderen	U-Utrecht
Dr. R. Richter	CIC biomaGUNE, Spain
Dr. D. J. Kraft	U-Leiden
Prof. C. Dekker	TU Delft (reservelid)

ISBN 978-90-8593-247-5
Casimir PhD Series, Delft-Leiden, 2016-03

The work described in this thesis was performed at the FOM Institute AMOLF, Science Park 104, 1098 XG Amsterdam, The Netherlands and at the TU Delft, Faculty of Applied Sciences, Department of Bionanoscience, Marileen Dogterom Lab, Lorentzweg 1, 2628 CJ Delft, The Netherlands. This work is part of the research program of the Stichting voor Fundamentaal Onderzoek der Materie (FOM), which is financially supported by the Nederlandse Organisatie voor Wetenschappelijk Onderwijs (NWO).

For digital copies:
http://repository.tudelft.nl/
http://www.amolf.nl/

For printed copies:
library@amolf.nl

Printed by Ridderprint BV

CONTENTS

SAMENVATTING

De manier waarop onze huizen gebouwd worden of hoe onze dagelijks gebruikte apparatuur wordt geproduceerd, volgt over het algemeen de richtlijnen van assemblage. Assemblage is het proces waarbij individuele, niet-functionele onderdelen aan elkaar worden gehecht om uiteindelijk functionele structuren of patronen van hogere orde te vormen. De basis benodigdheden voor de assemblage van een functioneel object met behulp van losse onderdelen zijn (i) verplaatsing, iets moet de verschillende onderdelen naar elkaar toebrengen en (ii) verbinding, iets moet de onderdelen aan elkaar verbinden opdat de constructie niet direct weer uit elkaar valt. In reguliere assemblage wordt de verplaatsing gerealiseerd door de omgeving: iets of iemand levert mechanische energie welke de betreffende onderdelen in de juiste oriëntatie naar elkaar toe manoeuvreert. Vervolgens worden de onderdelen aan elkaar verbonden door ofwel de directe koppeling tussen de onderdelen zelf (e.g. klittenband) of door toevoeging van een derde component (e.g. lijm) die de objecten aan elkaar plakt. Hoewel deze vorm van assemblage voorziet in een grote mate van controle, is het vaak een tijdrovend en arbeidsintensief proces en wordt het naarmate de beoogde constructies complexer worden ook steeds financieel uitdagender. Deze nadelen worden extra duidelijk in de assemblage van structuren op micro en nano schaal, met name vanwege de complexiteit van de benodigde apparatuur. Mede vanwege bovengenoemde nadelen is de interesse naar een alternatieve vorm, genaamd zelf-assemblage, op het moment sterk aan het groeien.

We spreken van zelf-assemblage of spontane assemblage wanneer het vormen van de uiteindelijke secundaire structuur zonder een externe bron van energie plaatsvindt. In dat geval zijn er twee energie componenten die de balans opmaken: de enthalphie (H) en de entropie (S). De enthalpie is de energie die vrij komt of geabsorbeerd wordt bij het vormen of verbreken van een verbinding. De entropie bepaalt de energie die is gekoppeld aan de hoeveelheid mogelijkheden waarin een bepaalde toestand zich kan ten toon stellen. Des te meer mogelijkheden des te hoger is de entropische energie. Hieraan moet worden toegevoegd dat de entropie van een systeem altijd spontaan naar een zo hoog mogelijke waarde beweegt en dat er energie voor nodig is om het omgekeerde te bewerkstelligen. Of een assemblage proces spontaan zal verlopen hangt uiteindelijk af van de mate van verandering van deze componenten tussen de initiële situatie en het eindproduct. Bij constante temperatuur (T) en druk verhouden deze variabelen zich volgens de vergelijking

$$\Delta G = \Delta H - T\Delta S \tag{1}$$

waarbij ΔG de vrije energie wordt genoemd. Een proces verloopt spontaan wanneer het eind product een kleinere hoeveelheid vrije energie heeft dan de beginsituatie, dus wanneer ΔG negatief is. Ten gevolge van vergelijking (1) zijn er slechts een beperkt aantal energie verdelingen die hiertoe leiden:

i) ΔS is positief en ΔH is negatief.

ii) ΔS is positief en ΔH is positief.
iii) ΔS is negatief en ΔH is negatief.

De assemblage verloopt in de eerste situatie altijd spontaan terwijl het in de laatste twee situaties afhangt van de relatieve waarden van zowel ΔS en ΔH en de temperatuur.

Geïnspireerd door de overduidelijke successen van zelf-assemblage in de biologie, hebben we in dit proefschrift de mogelijkheid onderzocht om componenten uit de natuur te gebruiken om niet-functionele, inerte deeltjes spontaan te laten assembleren tot een geordende structuur. Een cruciaal aspect dat voor een groot deel verantwoordelijk is voor het succes van de zelf-assemblage processen die bijvoorbeeld plaatsvinden in de cel, is de relatief zwakke moleculaire interacties die de koppeling tussen de bouwstenen bepalen. Deze interactie-typen worden geschaard onder de zogenaamde 'zwakke', specifieke interacties, omdat ze door thermische energie geleverd door de omgeving een grote kans hebben om te dissociëren, in tegenstelling tot sterke, covalente verbindingen die praktisch irreversibel zijn. In termen van vergelijking (1) gaat het maken van een verbinding gepaard met een negatieve entropie verandering. De ongebonden situatie kan simpel gezegd in meer configuraties voorkomen dan de gebonden situatie. Als gevolg zal de verbinding enkel spontaan verlopen in situatie (iii), wanneer de enthalpie ook een negatieve verandering doorstaat. Daarbij moet de waarde van deze negatieve verandering voldoende groot zijn om te compenseren voor de negatieve entropie verandering. Bij een zwakke verbinding is de enthalpie verandering van zodanige grootte dat de uiteindelijke vrije energie erg dicht tegen 0 komt te liggen met als gevolg dat de kans op ontbinding significant wordt. De kans om los te gaan geeft de bouwstenen de mogelijkheid om binnen een assemblage traject te herschikken naar een meer optimale organisatie in plaats van vast komen te zitten in een minder gewenste oriëntatie.

Een tweede essentiëel aspect is de hoge specificiteit van de verbindingen tussen de onderdelen. De assemblage van bijvoorbeeld eiwitten is niet afhankelijk van één type interactie maar wordt gereguleerd door een specifieke combinatie van interactie-typen alsmede de positie van de betreffende interacties op het molecuul. Dit maakt dat enkel de best passende (ook wel complementaire) bindingspartner het meest efficiënt bindt, zoals er maar één type sleutel in een slot past.

Om te onderzoeken hoe deze componenten geïmplementeerd kunnen worden voor de zelf-assemblage van inerte deeltjes hebben we een bestaand modelsysteem gekozen welke gebaseerd is op ontwikkelingen op het gebied van DNA-bedekte silica deeltjes. Hierin zijn de silica microdeeltjes de bouwstenen die we laten organiseren tot een secundaire ordelijke structuur. Op het oppervlak van elk deeltje zijn korte strengen DNA zodanig gekoppeld dat ze loodrecht op het oppervlak van de deeltjes zijn georiënteerd. De laatste reeks van 11 nucleotiden van elke DNA streng fungeert als koppelingsstuk: de specifieke sequentie is complementair met de uiteinden van de DNA strengen op het oppervlak van een tweede set aan silica deeltjes. Als gevolg zullen de deeltjes met complementair DNA met elkaar binden terwijl de deeltjes met hetzelfde DNA ongebonden blijven. Op deze manier wordt specificiteit in de binding gecontroleerd door de specifieke DNA sequenties en zijn de bindingen – in dit geval de waterstofbruggen die de nucleotiden met elkaar verbinden – zwak en omkeerbaar.

Hoewel er aan de juiste voorwaarden lijkt te worden voldaan, is het vormen van geordende structuren met behulp van de DNA-strategie nog niet heel succesvol geble-

ken. Het blijkt namelijk dat, hoewel de individuele bindingen zwak en reversibel zijn, een grote reeks aan parallelle verbindingen een effectief sterke, irreversibele connectie verzorgt met als consequentie dat twee complementaire deeltjes direct sterk aan elkaar plakken zonder de mogelijkheid om zich te herschikken naar een betere geometrische positie in het aggregaat van deeltjes. In theorie is in twee dimensies een hexagonale organisatie van de deeltjes meest optimaal aangezien in dat geval het hoogst mogelijk aantal verbindingen tussen de deeltjes behaald kan worden. Echter het hoge 'hit' and 'stick' gehalte van de deeltjes zorgt ervoor dat de route hiernaartoe geblokkeerd wordt. Deeltjes komen op verkeerde plekken vast te zitten waar ze vervolgens niet of nauwelijks meer uit komen om vervolgens een ongeordend aggregaat te formeren.

Een in deze context nuttige eigenschap van de DNA verbindingen is dat ze temperatuurreversibel zijn. Dat wil zeggen, door het verhogen van de omgevingstemperatuur dehybridizeren de DNA strengen zich, met als gevolg dat de micro-deeltjes dissociëren ofwel smelten. In vergelijking (1) wordt dit duidelijk aangezien de entropie verandering wordt vermenigvuldigd met de temperatuur. Omdat in deze situatie van zwakke verbindingen de vrije energie al dichtbij nul ligt zal bij een stijgend aandeel van de entropie de vrije energie op een zeker moment positief worden, met dissociatie als gevolg. Het vervolgens weer verlagen van de temperatuur heeft het omgekeerde effect.

De relatie tussen het aantal gedissocieerde deeltjes en de temperatuur wordt sterk bepaald door de hoeveelheid mogelijke DNA verbindingen tussen elk deeltjes-paar. Nu blijkt uit verschillende studies dat al bij meer dan één DNA verbinding per deeltjespaar, de verhouding tussen de temperatuur en de kans dat een deeltje gebonden is een behoorlijk scherpe transitie laat zien. In andere woorden de deeltjes zitten of vast of zijn volledig los van elkaar terwijl het temperatuur bereik voor elke situatie er tussen in slechts 1 tot 2 °C beslaat. Omdat juist in deze tussenfase de mogelijkheid voor herschikking ligt, is het praktisch erg moeilijk om dergelijke deeltjes te laten zelf-assembleren tot hun ordelijke grondtoestand zonder vast komen te zitten in een wanordelijke tussentoestand. Enkel met een proces waarbij de temperatuur voortdurend langzaam oscilleert om de smelt-transitie heen, is aangetoond dat er na een periode in de orde van dagen geordende structuren verschijnen.

Om met dit modelsysteem op een effectievere manier geordende structuren te realiseren is een aanpassing dus nodig. In dit proefschrift laten we zien hoe het toevoegen van een extra vrijheidsgraad in dit modelsysteem het zelf-assemblage proces kan verbeteren. De extra vrijheidsgraad die we hebben toegepast is de mogelijkheid voor het DNA om over het oppervlak van de deeltjes te manoeuvreren. In hoofdstuk 2 geven we als motivatie voor deze modificatie een overzicht van de huidige kennis over de rol van oppervlakte-mobiliteit in moleculaire interacties zowel in biologische als in gesynthetiseerde systemen. We geven een overzicht van de verschillende in de literatuur bekende model-systemen waarin de invloed van oppervlakte-mobiele verbindende moleculen zijn onderzocht. Duidelijk wordt hoe clustering van moleculen de interactie-sterkte beïnvloedt en hoe mobiele verbindingen zelfs gebruikt kunnen worden om kristallen met gecontroleerde orde-parameters te verkrijgen.

In hoofdstuk 3 en 4 beschrijven we hoe we het model systeem van DNA-bedekte micro-deeltjes hebben aangepast opdat de DNA over het oppervlak kan diffunderen. Hiervoor hebben we gebruik gemaakt van de vloeibare eigenschappen van de lipide bi-

laag. De karakterisering van de verankering van het DNA in een lipide bilaag met verschillende hydrofobe modificaties is te vinden in hoofdstuk 3. Het blijkt dat een DNA streng wanneer verankerd met de lipide bilaag via slechts één hydrofobe groep niet stabiel in de bilaag blijft, maar dat de thermische fluctuaties in het systeem voldoende zijn om de verankering ongedaan te maken. Verscheidene methoden om de stabiliteit van de verankering te verhogen worden hier gepresenteerd. In hoofdstuk 4 laten we vervolgens zien hoe we de DNA-lipide-bilaag constructie toepassen op de micro-deeltjes, tonen we aan dat het DNA daadwerkelijk mobiel is en demonstreren we het effect van de oppervlakte mobiliteit op de zelf-organisatie van de micro-deeltjes.

Om nog beter de zelf-assemblage van de micro-deeltjes te kunnen voorspellen en dus controleren is meer kennis nodig van de interactie-energie tussen de complementaire DNA strengen op twee met elkaar verbonden deeltjes. Een methode om de interactie sterkte tussen twee objecten te bepalen is het meten van de kracht die nodig is om de twee objecten los van elkaar te bewegen. In hoofdstuk 5 beschrijven we twee microscopische technieken die geschikt zijn om bovenstaand experiment uit te voeren met onze micro-deeltjes. Een van de twee technieken hebben we zelf ontwikkeld en dit proces staat in dit hoofdstuk beschreven. Resultaten van daadwerkelijke krachtmetingen ontbreken echter nog, omdat de ontwikkeling van deze opstelling ten tijde van het schrijven van dit proefschrift nog niet was afgerond. Omdat de tweede techniek wel reeds beschikbaar was hebben we hiermee de eerste beoogde krachtmetingen tussen twee gebonden deeltjes bij verschillende DNA dichtheden wel kunnen uitvoeren, waarvan de resultaten ook in dit hoofdstuk worden gepresenteerd. Hieruit kan geconcludeerd worden dat de interactie kracht, zoals verwacht sterk afhangt van de hoeveelheid DNA per deeltje. Over hoe de interactie kracht daadwerkelijk samenhangt met de DNA dichtheid kan door de beperkte hoeveelheid metingen nog geen uitspraak worden gedaan.

Ten slotte beschouwen we in hoofdstuk 6 hoe dit onderzoek kan worden voortgezet en geven we onze visie op waarom verder onderzoek interessant is. Dit wordt geïllustreerd aan de hand van voorbeelden van potentiële toepassingen die uit dit onderzoek zouden kunnen voortvloeien. Waarvan één, namelijk het bestuderen van de flexibiliteit van een lineaire keten van deeltjes gekoppeld met mobiel DNA, ook al voorzichtig door ons is verkend.

SUMMARY

The way the buildings we live in are built and the devices that we use to fulfill our daily needs are produced, nearly always follow the guidelines of assembly. Assembly is the act of combining individual, non-functional building blocks into functional structures or patterns with higher organizational order and basically relies on two actions: i) displacement, the building blocks need to get into close contact and (ii) connection, once close enough together the parts need to be held stably together. In ordinary assembly, a person either directly or indirectly delivers the mechanical energy required to position the building blocks in the right place and orientation. After which the surface properties of the building blocks (e.g. Velcro) or a secondary component (e.g. glue) provides the means to fix them together. Although this type of assembly provides excellent control during the process, it can be very time-consuming, labor intensive and expensive. These drawbacks become especially substantial in the assembly of structures on the micro and nano length scales due to the complexity of the required specialized equipment. Consequently, the interest in the development of another type of assembly called self-assembly is currently rapidly increasing.

Self-assembly or spontaneous assembly, is the formation of secondary structures out of individual building blocks without the need for an external person guiding the process. Instead, the assembly process is completely driven by the properties of the building blocks and the properties of the medium by which they are surrounded. Formally, this can be described by two energy components: the enthalpy (H) and the entropy (S). The enthalpy is the energy released or absorbed when bonds break or form and the entropy is defined as the energy that is coupled to the number of states in which a certain configuration can exist. The larger the number of possibilities, the larger is the entropic energy. It should be added that the entropy of a system always spontaneously evolves to the highest possible value while it requires energy to accomplish the opposite. Whether the assembly will take place spontaneously depends on the magnitude of the change of both of the energy components between the final and initial situations. At a constant temperature (T) and pressure these quantities relate to each other according the equation

$$\Delta G = \Delta H - T\Delta S \tag{2}$$

Where ΔG is referred to as the free energy. A process proceeds spontaneously only when the end product has less free energy as compared to the initial situation, so when ΔG is negative. As a result, Eq. (2) prescribes only three energy distributions that can lead to spontaneity:

i) ΔS is positive and ΔH is negative.
ii) ΔS is positive and ΔH is positive.
iii) ΔS is negative and ΔH is negative.

A process described by the first situation always occurs spontaneously, while the latter two depend on the relative magnitudes of ΔS, ΔH and T. Inspired by the great successes of self-assembly in biology, this thesis describes our endeavor in exploring the possibilities of using nature inspired components to steer the self-assembly of inert micro-particles into ordered secondary structures.

A crucial aspect which is largely responsible for the success-rate of the self-assembly processes occurring in nature, is the relative weak magnitude of the molecular interactions that mediate the coupling between the basic building blocks. These interactions are called weak because the thermal energy delivered by the environment is already enough to dissociate the bonds, as opposed to the strong, covalent bonds which are practically irreversible. In terms of Eq. (2), the formation of a bond is associated with a decrease in entropy. Simply said, the number of arrangements that two disconnected molecules can possibly occupy is higher than for the bound structure. Therefore, such a bond will only occur spontaneously if the binding process can be described by situation (iii), when the enthalpy change is negative as well. If that is the case, the magnitude of the enthalpy change also needs to be large enough for it to compensate for the negative entropy change. For weak bonds the enthalpy change is just enough to meet this requirement, setting the free energy change to be only slightly below zero, thereby increasing the unbinding probability. The enhanced likelihood of unbinding facilitates the possibility for the building blocks to rearrange towards a more optimal position within the assembly instead of getting stuck in an undesired configuration.

A second essential aspect for self-assembly is the high specificity of the interaction. The binding of a ligand to a receptor for example does not depend on solely one type of interaction but relies on a combination of different interaction types as well as their exact position along the molecules. Consequently, only the molecules exposing the right interaction types in the correct orientation will form an efficient bond.

To investigate how these aspects can be applied for the self-assembly of inert micro-particles into ordered structures, we have adapted an already existing model system of DNA-coated silica micro-particles. The DNA coating consists of short DNA strands that are through one end coupled to the surface of the silica micro-particles, such that they orientate perpendicular to the surface. The terminating eleven nucleotides of each DNA strand are designed as the linking bridges; the specific sequence is complementary to the DNA ends displayed by a second set of silica micro-particles. By forming DNA bridges the silica micro-particles that expose complementary ends will bond whereas the particles showing the same sequence remain unbound. This way the preconditions for self-assembly are supposed to be met: the specificity is controlled by the DNA sequence and the interactions – in this case the hydrogen bonds between the complementary nucleotides – are weak and reversible.

Even though the requirements seem to be fulfilled, steering the silica micro-particles into ordered structures has so far not been very successful. A theoretically and experimentally demonstrated explanation for the experienced difficulties finds its roots in multi-bond effects. Despite of the interactions between individual DNA strands being weak, the combination of multiple DNA bonds in parallel effectively establishes a strong, irreversible coupling. When two particles meet they immediately stick together, impeding the possibility to rearrange. It is predicted for this specific binary system of two com-

plementary particle types that their equilibrium two dimensional structure is a hexagonally organized packing as this provides the highest number of DNA bonds. However, the 'hit' and 'stick' type of aggregation obstructs the particles in their efforts to get there and the result is a randomly organized aggregate.

And in this context a useful property is the thermo-reversibility of the DNA linkages. By increasing the temperature, the intertwined DNA strands dehybridize and the micro-particle aggregates dissociate also referred to as melting. Speaking in terms of Eq. (2), due to the increasing magnitude of the temperature, the entropy contribution enlarges which at sufficient temperatures favors the unbinding of the DNA strands. Because this procedure does not affect the structure of the individual DNA strands, subsequently lowering the temperature has the reverse effect.

The relation between the number of dissociated particles and the temperature depends strongly on the number of DNA bonds that make up the connection. It has been shown theoretically that already in the case of a single DNA bond per pair of particles, the relation between the number of unbound particles follows a steep transition upon crossing a certain temperature. So either all particles are strongly bound or completely unbound while any intermediate situation can only exist in a temperature window of only 1 or 2 °C. Because the possibility for the particles to rearrange within an aggregate only exists within this narrow temperature window, turning random aggregates into crystals becomes experimentally challenging. Only by oscillating the temperature continuously and slowly about the melting temperature over a period of days, have researchers successfully created crystal structures.

In order to improve the self-assembly of the DNA-coated micro-particles, the current approach has to be adjusted. In this thesis we describe our efforts to introduce an extra degree of freedom into the system and we show how this addition improves the micro-particle self-assembly. The adaptation involves the ability for the linking DNA molecules to diffuse over the surface of the micro-particles. In Chapter 2, we explain our choice for this particular adaptation on the basis of scientific publications that focus on the beneficial role of surface-mobile molecular interactions in both biological and synthetically developed systems. It becomes clear how clustering molecules influence the strengths of interactions and how mobile interactions can be applied to the self-assembly of micro-particles into crystal structures with different order parameters.

In Chapters 3 and 4 we describe how the surface-mobility of the DNA linkers on the micro-particles is achieved. For this we have made use of the fluidic properties provided by the biological structure of the lipid bilayer. We characterized the anchoring stability of hydrophobically modified DNA in a lipid bilayer in Chapter 3. It turns out that anchoring DNA strands to a lipid bilayer by only a single hydrophobic compound, is insufficient to maintain a thermodynamically stable coupling. Several alternatives are presented that enhance the bilayer-anchoring stability. How the lipid-DNA construction subsequently is applied on micro-particles, whether the DNA strands are actually mobile and to what extend the surface mobility affect the micro-particle self-assembly is outlined in Chapter 4.

In order to enhance the predictability and hence the controllability of the micro-particle self-assembly, better understanding of the interaction properties is required. A method to measure the interactions strength between two particles is by monitoring the

force required to pull two connected particles apart. In Chapter 5 we describe two experimental setups that provide the means to perform exactly such measurements. One of these setups we have developed ourselves and this process is described in this chapter. Actual results are lacking, as the setup was not yet suitably functional at the time of writing this thesis. However, we do present in this chapter the results of the force measurements performed on pairs of interacting particles using a slightly different but readily available setup. From this data it can be concluded that the interaction strength depends strongly on the density of DNA strands per particle. The acquired statistics are however too limited to make statements on the exact relation between the DNA density and the interaction strength.

Finally, we elaborate on the possible future directions this research could be going in Chapter 6 and why continuing this research would be of great interest. We illustrate this by giving examples of potential applications that could emerge from our obtained achievements and by presenting the our efforts concerning one such application, namely to use mobile DNA linkers to make very flexible linear particle chains.

1

INTRODUCTION

This thesis revolves around exploiting the specificity of DNA interactions to guide the assembly of micro-colloids into higher order structures. The concept of DNA mediated interactions between micro-colloids is a field of study that has ramified from the field on DNA guided self-assembly of nano-colloids. Despite the great potential that the use of DNA could offer for self-assembling micro-colloids, so far the predicted astounding results are still to be accomplished. As compared to the wide variety of self-assembled higher order structures that have been realized with DNA coated nano-colloids, for micron-sized colloids new strategies appear to be needed. Motivated by the high potential of the field and the challenges that are confronted herein, we initiated an experimental project aimed to design and implement a novel strategy aimed to uplift the self-assembly process. This is achieved by both modifying the way the DNA strands are coupled to the particles' surface and in parallel exploiting sensitive force spectroscopy techniques to elucidate the interaction strengths of the DNA bridges at different conditions. For this purpose, we modified an existing system of micro-colloids coated with DNA in such a way that while the DNA is confined to the surface of the particles, its lateral diffusivity is maintained. The surface mobility is accomplished by surrounding silica micro-particles with a lipid bilayer into which the DNA strands are embedded. This way the lipid bilayer functions as a two dimensional platform in which the DNA strands can 'float' like sea beacons that are drifting in water. The size and composition of the silicon oxide micro-particles permit easy visualization by various optical microscopy techniques and facile manipulation with optical tweezers, making them excellent platforms for probing the strength of the DNA-mediated interactions.

1.1. DNA-MEDIATED COLLOIDAL SELF-ASSEMBLY

The incentive of the research presented in this thesis is to provide a contribution to the understanding of the self-organization of micron-sized particles mediated by DNA linkers. The current goal in this field is to control the self-assembly of micro-particles into complex, functional structures. DNA linkers are very promising candidates to achieve this. Namely, by coupling short single stranded oligonucleotides at one end onto the

surface of micron-sized particles, the extended single strands can reach out to hybridize with the extending complementary strands attached to surrounding particles. With the right number of long enough DNA linkers per particle, and appropriate buffer conditions, such particles will at room temperature self-assemble into aggregates. However, while exploring this parameter space, researchers have run upon obstacles that hinder the controlled self-assembly into ordered crystal structures. Although the predicted equilibrium structure might be an ordered crystal, the micro-particles often become kinetically trapped and form random aggregates.

By registering the number of unbound, individually dispersed particles as a function of increasing temperature, a profile appears that shows that the transition from fully aggregated particles to fully dispersed particles occurs within a very narrow temperature window. Consensus exists that this narrow temperature window arises because the probability of particle-dissociation being doubly exponentially proportional to the temperature, when mediated by multiple DNA linkers. Only within this temperature window the particles are just weakly enough bound to allow them to rearrange, but because this window is so narrow, experimentally establishing such conditions turns out to be not trivial. Typically, equilibrium structures can be obtained if the particles are repeatedly cycled from a fully associated to a fully dissociated state by repeatedly crossing the melting temperature of the DNA bonds for several days. Furthermore, the crystallization is hampered by the difficulty to get an homogeneous DNA surface density on each particle. It is therefore desired to improve the current model system of DNA coated micro-particles in order to optimize their self-assembly into functional, ordered structures.

The research field in which DNA is used for the assembly of nano/micro-particles into higher ordered structures dates back to 1996. Back then, two research papers were published in Nature demonstrating experimental methods to couple short DNA strands to nano-particles, revealing ways to enhance the control over the particles' organization [1, 2]. This has to do with the molecular composition of DNA. A more detailed description is provided later in this section, yet in short DNA consists of two intertwined strands, each composed of a sequence of molecules called nucleotides. There are 4 different types of nucleotides, which are labeled A, T, C and G, of which an A can only bind to a T and a C can only bind to a G. Due to these binding constraints, a certain arrangement of nucleotides can form a DNA molecule only with a strand that displays the matching/complementary nucleotides. Then, by designing a set of different pairs of complementary strands and attaching them to different subsets of particles, only those particles displaying complementary strands will link together. Thus, the specific nucleotide sequence of the strands on each of the particles, orchestrates which of the particles bind together and hence control the way the particles organize, see Fig. 1.1.

Given the nearly limitless amount of possible nucleotide arrangements, a huge number of complementary particles could theoretically be made. Moreover, one could decorate particles with different strands, allowing for the particles to bind with more than one other type, generating particle-assemblies of even higher complexity. However, before such high degree of control becomes possible, a new number of challenges had to be or are still to be overcome. For example, methods had to be developed to efficiently couple the DNA to the surface of particles. The ends of DNA have fortunately proven to lend themselves very suitable for a large range of chemical modifications. Different mod-

ifications like thiol, carboxyl or biotin groups can relatively easily be added to the DNA synthesis process so as to link them to the ends or somewhere in the middle of the DNA strand. This also accounts for the insertion of fluorescent or radioactive labels which makes subsequent characterization of the DNA coating feasible.

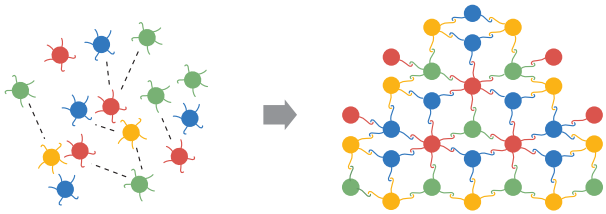

Figure 1.1: Steering the self-assembly of particles using DNA linkages.

Furthermore, new models are needed to relate the chemical and physical properties of the DNA interactions with the resulting assembled structure. Using these extending DNA strands namely introduces new parameters that make existing models inadequate. The DNA linkers introduce new concepts like the length that the DNA strands extend outward thereby increasing the interaction range or their discrete distribution over the surface making continuum models less suitable. These concepts have already led to new models for nano-particles that have helped in the development of a large variety of crystal structures [1–8].

For micro-particles guiding the self-assembly turns out to be more complicated. The apparent difference between nano- and micro-particles has primarily to do with the ratio, σ, between the range of the DNA interaction, i.e. the length of the DNA strands L, and the radius of the particles r, see for a schematic representation Fig. 1.2. In the case of nano-particles, σ~1, hence the maximum number of linking strands between particles is on the order of tens or less. For micro-particles however, $\sigma \ll 1$, assuming the same strand length. As a consequence, a lot more linkers will contribute to the interaction when two particles come into close proximity. This can not be circumvented by simply extending the length of the DNA to compensate for the larger particle size. DNA strands of such lengths behave more like coiled polymers, whereas the short DNA strands can be considered as semi-flexible rods. These different mechanical properties would merely introduce new physics leading to totally new behavior [9]. Also decreasing the DNA density per particle will not improve much, as the necessary density decrease will reduce the encounter rate between two strands to a minimum, which substantially slows down or even inhibits the particle self-assembly completely.

These nano- versus micro-particle differences have been studied in detail and have been verified by a number of research groups [10–13]. Using that obtained understanding, people have come up with possible strategies to optimize the crystallization, of which the first experimental evidences have been published [14–19]. Now that the understanding of the mechanisms of the self-assembly of simple systems of DNA coated colloids is rapidly increasing, the next step is at hand. In this study, we aimed to contribute to this next step in the self-assembly of DNA coated micro-particles by introducing an extra de-

gree of freedom. We developed a system where the DNA strands coupled to the surface of particles are still able to exert lateral motion. This is achieved by surrounding silica micro-particles with a lipid bilayer in which the DNA linkers are embedded. By allowing for the lateral diffusion of the linkers we hypothesize that aggregated particles posses more freedom to maneuver to their energetically most favorable position in the aggregate instead of becoming arrested into a kinetically trapped state. We have observed that this enhanced flexibility facilitates the crystallization and believe that it could even allow for the much desired principle of directional bonding [17], paving the road towards more complex micro-structures.

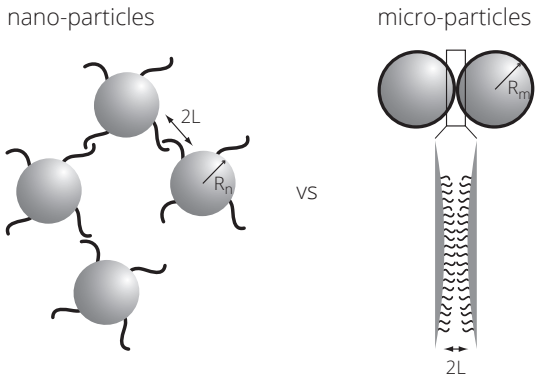

Figure 1.2: DNA mediated self-assembly of nano- versus micron-sized particles. The radius of nano-sized particles, R_n, is in the same order of magnitude as the length L of the DNA linkers, which is typically in the order of tens of nanometers. In contrast, the radius of the micron-sized particles, R_m, is typically $50-500L$. Consequently, the ratio, $\sigma = L/R$, differs by a factor ≥ 50 between nano- and micro-particles and thus for micro-particles, many more DNA linkers will take part in the interaction.

As one may have recognized in this introductory section, there are three main concepts that form the backbone of this thesis. These are colloids, DNA and the lipid bilayer. In the following sections of this chapter we provide some more detailed information on how these concepts are defined and how they are related to our research. Finally, this chapter will end with an outline of this thesis.

1.2. COLLOIDS

The desire to enhance the controllability of assembling particles is triggered by the developments in the established research field of colloids. A colloid is defined as a two phase system, in which one phase is dispersed in a second continuous phase. Nearly any combination of the main three phases, i.e. gas, liquid and solid, are able to form a colloid. As long as the particles forming the dispersed phase are within a size-range of approximately 1-1000 nm. Examples are given in Table 1.1.

Our model system falls under the "Sol" category; solid particles dispersed in a liquid medium. The motivation for studying this particular type of colloid is inspired by examples observed in nature. In the 1930s, researchers noticed the interesting swelling properties of bentonite and the optical properties of Schiller layers in iron oxide sols [20].

The properties of these two examples are a result of the ordering of the monodisperse inorganic particles. Also in biology, one finds monodisperse features forming long-range ordered arrays. Stanley in 1935 examined the organization of tobacco and tomato viruses upon concentrating them in water by centrifuging and discovered their crystalline packing [21]. Later, other virus particles were also seen to organize in crystalline organizations using X-ray diffraction.

Table 1.1: **Examples of colloids**

Continuous phase	Dispersed phase	Colloid type	Example
Solid	Solid	Solid sol	Ruby glass
Solid	Liquid	Solid emulsion/gel	Cheese, agar
Solid	Gas	Solid foam	Aerogel
Liquid	Solid	Sol	Paints, blood
Liquid	Liquid	Emulsion	Milk
Liquid	Gas	Foam	Whipped cream
Gas	Solid	Aerosol	Smoke
Gas	Liquid	Aerosol	Fog
Gas	Gas	N/A	N/A

Some time later, the beautiful optical properties of opal were discovered to be related to the organization of monodisperse silica particles. The long range order exposed by the voids between the silica particles have such dimensions that they provide the specular light reflections. The observation of the natural existence of monodisperse silica particles led to the discovery and optimization of methods to synthesize monodisperse particles of silica, polystyrene and a whole range of other polymers. As a consequence the interest for studying these types of colloids rapidly increased [22].

An important motivator for investigating colloidal crystallization is their structural overlap with the organization of atoms in atomic crystals. It appeared that the basic principles defining the final structure were very similar to the rules dictating atomic crystals. And as their size allows for much easier visualization, colloids provided a powerful model to facilitate the understanding of atomic crystals. Effects of properties like charge, size-ratio and solvents on the ordering of particle mixtures suddenly became much better understood. As well as the mechanisms and kinetics of crystallization, and the emergence of defects.

Besides the added value to the research in the organization of atoms, the colloidal crystallization offers applications in optics and photonic crystals. As first recognized in the Schiller layers and opals, the right arrangement of particles can lead to structures that can capture light and control the way it is transmitted. Other interesting aspects involve the study of self-assembly and cooperative motion as a model system for the molecular self-assembly existing in nature, which has eventually led to the development of mechanically superior biomaterials.

The way colloids crystallize depends on a number of aspects . First, it is defined by the type of interaction between the respective particles. The interaction is mediated by the surface properties of the particles as well as the medium in which they are dispersed. Charged groups on the particles' surfaces can cause like-charge particles to repel and opposite-charge particles to attract [23]. Depending on the exact charge density and the ionic strength of the medium this interaction can extend over a range of up to a micrometer. Other interactions have more to do with the solubility of the surface groups in the medium. Hydrophilic groups for example, dissolve much better in water-based solutions as opposed to organic suspensions. As a consequence, particles that bear hydrophilic surface groups when dispersed in an organic suspension, tend to minimize their surface-exposure to the medium by clumping together. Aside to the chemical properties of the colloids, physical interactions can also play a major role. Neutral particles for example, undergo only steric interactions, which self-assemble into interesting crystals purely driven by entropy. The earliest appreciation of this entropic ordering was Lars Onsager's model for a fluid of thin, hard rods that are capable of self-assembling into liquid crystals [24]. His model has been verified experimentally, and since then a large number of adaptations have been realized using combinations of colloids of all sorts of shapes and sizes [25–30].

Whether chemical or physical interactions actually drive the creation of unique architectures depends strongly on the strength of the interaction. Weak bonds allow for more dynamics within the bonds. The continuous binding and unbinding of particles allow them to explore more configurations. Whereas with too strong bonds, the structure is more likely to become arrested in a less favorable organization. The second contributing factor to the crystallization, is the kinetics at which the suspended particles are moving about. This 'moving about', which is more generally called Brownian motion refers to the random movement of the particles caused by the random collisions with the molecules comprising the continuous phase. Set by the viscosity of the fluid, the temperature and the size, shape and density of the suspended particles, the particles' motion drives the dynamics of the crystallization.

All the parameters defining the aforementioned aspects, can be accurately measured and controlled. One can measure for example the surface charge of the particles and the conductivity of the suspension and image the final crystal structure using optical microscopy or X-Ray diffraction. The measured physical properties of the colloids and their final organization structure can then be compared with simulations and theoretical models providing a complete understanding of the process. This way, a large amount of understanding has been gained in how the self-assembly of colloids can be controlled to create desired architectures.

The majority of this research involves the self-assembly of single-type particles or mixtures of two or three different types of particles [31]. The resulting wide variety of structures possible has given researchers the arguments to search for methods to create more complex structures. Ideally, one finds ways to direct the assembly of many different types of colloids into structures in which the position of each contributing particle is pre-determined. Each particle would then have its own purpose in the structure, like the amino acids in a protein. Such diversity is thought to be realizable with DNA coated colloids. As mentioned in the previous section, the DNA strands can be easily synthesized

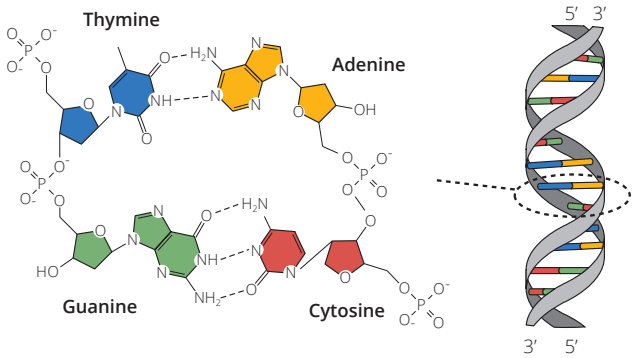

Figure 1.3: The structure of DNA.

and its specificity allows for the design of a huge range of different strands. A current popular strategy is to use short DNA strands of which only the final few nucleotides are complementary to the ends of opposing strands. These functional ends are referred to as sticky ends. In principle, a large number of particles can then be mixed in which each particle carries its own type of sticky ends. Adding the possibility to decorate specific sites of each particle with different sticky ends opens the path to directional bonding providing even more possibilities for self-assembly.

1.3. DNA

The elucidation of the structure of DNA and its relevance to the existence of life is one of the biggest game changing events of the 20th century. Since its recognition of bearing the fundamental information for life on earth in 1940s, a lot of progress has been made in the understanding of its function and its role in evolution. The knowledge is so well established that the central dogma of molecular biology and the role of DNA in it, is nowadays basic curriculum of the biology courses taken by high school students all over the world. Hence, when conversing with someone about DNA, chances are high that the topic of discussion will be its major role in passing on the basic code of life. In contrast, the association of DNA with micro-particle self-assembly is less well known and as a consequence often not directly understood. Therefore, since this is exactly the topic of this thesis, we briefly summarize how DNA got integrated into the field of micro-particle self-assembly and its relation to this study.

DNA is an abbreviation for deoxyribo-nucleic acid and it is well known for its famous double helical structure that was discovered in the 1950's by Watson and Crick. The structure of DNA is illustrated in Fig. 1.3. The basic molecular components are called nucleotides which are covalently coupled into long strings, typically referred to as strands. Each nucleotide type is built of a five-carbon sugar (deoxyribose) and a nitrogenous base. There are four different nucleotide types present in DNA which differ in the exact structure of the associated base. They are referred to as Adenine (A), Thymine (T), Guanine (G) and Cytosine (C). The cytosine and thymine bases are so-called pyrimidines; bases that consist of a heterocyclic aromatic ring structure. Its atomic structure is similar to the

6 carbon ring forming benzene, yet with two carbon atoms replaced by nitrogen atoms. Adenine and Guanine are also built of a pyrimidine compound but with an additional imidazole group fused to it, forming a purine. Lastly, each nucleotide carries a phosphate through which adjacent nucleotides are joined together to form a strand. The strand is asymmetric where either ends are referred to as 3' or 5', with the 3' having a terminal hydroxyl group and the 5' a terminal phosphate group.

Because of the specific linear arrangement of nucleotides, their associated bases are left exposed. The bases all carry one or two hydrogen accepting (oxygen and nitrogen) and donating (hydroxyl and amine) groups. Cytosine and Guanine both have three hydrogen accepting/donating groups, while Adenine and Thymine only bear two. Due to the equal number of hydrogen accepting/donating groups, Cytosine preferably binds with Guanine while Adenine forms a bond with a Thymine. That these combinations of nucleotides structurally fit so well makes them very stable and is why they are called complementary. Other coupling, less thermodynamically preferable combinations between the nucleotides may exist as well, they can appear when melted DNA strands at high temperature are quickly quenched to a low temperature, but these events are beyond the scope of this thesis. For a strand of nucleotides, the base-alignment requirement is most optimally met when two complementary strands align anti-parallel and intertwine to form the well known double helix.

The high stability of the double helical structure allows for the secure storage of the information encoded by the arrangement of the nucleotides in each strand. Having duplicates of the information is at the core for the process of transferring the encoded information to following generations. During cell division, the double helices are split so that the separated strands can be scanned by DNA polymerases, special enzymes that attract and join complementary nucleotides together. This allows for the copying of the entire DNA code so that it can be transferred to each of the daughter cells.

The fact that DNA is found in all organisms currently living on earth as well as in those having lived during the past millions of years, proves its profound effective functionality. Although its exact sequence, the way it is folded and its secondary chemical modifications per organism and between organisms continuously undergo changes, the basic principle of 4 types of nucleotides organized in a double helix is always kept unchanged. In addition, due to the vital role of DNA in living organism, a large number of synthesis and analysis tools have been developed to enhance the understanding of its structure and function. Nowadays, a multitude of techniques exist to visualize the organization of DNA in cells, DNA can be extracted from cells to explore its sequence and it can be physically grabbed and pulled apart to unravel its mechanical properties. Regarding the vast developments in DNA research, it is not surprising that at some point people found methods to synthesize short pieces of DNA. This ability of making DNA strands has led to the emergence of new research fields focused on other topics than understanding life or curing diseases. Food industries are for example interested in modifying the genome of crops to enhance their proliferation, taste or shape. Or, what is more in line with the topic of this thesis, it attracted nano-engineers who are interested in controlling the self-assembly of nano-particles into higher ordered structures. Their search for ways to steer mixtures of many different particles into complex, functional structures led to the demand for functionalizing particles with different recognition sites that only specifically

bind to one type of other particle in the mixture. In this way it becomes possible to create hierarchal organizations of particles in which each particle has a different task in the structure. DNA suddenly appeared as a potential candidate for achieving this goal. As mentioned earlier, the bond strength is determined by the arrangement of nucleotides and the level of complementariness with the opposing strand. Each different arrangement of nucleotides can therefore function as a unique linking molecule, providing the tools for the nano-engineers' whishes. A beautiful example which show the large potential of DNA in the area of self-assembly is the world of DNA-origami. At first recognized by Seeman and co-workers, DNA origami involves the coupling and folding of keenly designed short strands into two or three dimensional secondary structures. [32–34] Others used a combination of one long single strand which is folded by a range of staple strands [35–37]. The research has so far predominantly led to the construction of 'useless' smiley faces or other non-functional structures. However, the first potential 'real' applications are being explored and more and more publications are showing up [38–42]. Particular promising results are obtained in the use of DNA to guide the hierarchical assembly of nanoparticles into plasmonic structures with controllable optical responses [43, 44], to create nanometer-scale transmembrane channels in lipid bilayers [45], and its application in the study of motor proteins [38].

We are specifically interested in a side branch of this self-assembly research field, namely the area of research dedicated to studying the self-assembly of micro-particles composed of an inert material coated with short DNA strands. The advantage of this is that the micrometer size of the particles could potentially allow for the emergence of millimeter or even centimeter sized secondary structures, with material properties (e.g. optical or elecronic) that are tailored by the material of the micro-particles. This area of research is more elaborately discussed in the next section.

1.4. LIPID BILAYERS

The lipid bilayer, as the name already suggests, is a film comprising two layers, known as leaflets, each composed of individual molecules called lipids. It is most well-known for forming the soft, flexible shells that separate cells from their surrounding environment. Thus providing the micron-sized environments that are essential for cellular processes to take place. Without lipid bilayers, no life as we know it would be able to exist [46]. The word lipid comes from the Greek word *lipos* which means fat. Yet, fatty acids are just one of many molecules that fall under the category lipids. Other examples are waxes, sterols, fat-soluble vitamins, monoglycerides and phospholipids.

Only the amphiphilic lipids form bilayers, which are the lipids that are built of two parts, one hydrophilic ("water-loving") head and one or more hydrophobic ("water-hating") carbon tails, see Fig. 1.4. When dispersed in water, the hydrophobic parts of these type of lipids minimize their exposure with the surrounding water molecules by forming a film in which all the carbon tails are aligned. Finally, two leaflets stick together and form a bilayer which reduces the carbon-water contact to a minimum.

Due to the high tendency of the lipid carbon tails to reduce their water contact, the lipids' out of plane motion is very restricted, while they can diffuse freely in the lipid bilayer plane. In two dimensions the lipids continuously diffuse about giving the bilayer a very dynamic character. This gives the bilayer, aside from being a barrier, numerous

other functionalities. Examples are, the incorporation of channel-forming proteins that control the in- and out-let of specific substances, or the integration of proteins that act as sensors that allow the cell to communicate with its surroundings. The high degree of flexibility also gives the bilayer its characteristic mechanical properties. By adding or removing lipids or slightly rearranging the lipids, the membrane easily adepts to a growing or shape-changing cell. And if the membrane gets pierced, the bilayer will not collapse nor stay torn, but instead quickly reseals.

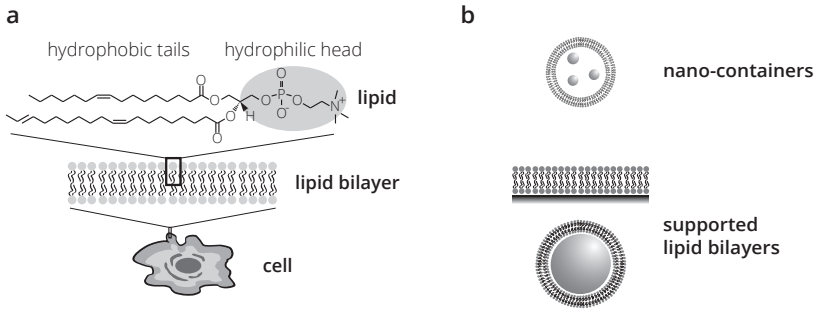

Figure 1.4: a) The chemical structure of lipids and their organization into lipid bilayers. The top image represents the molecular structure of the lipid 1,2-dioleoyl-sn-glycero-3-phosphocholine (DOPC), one of the most abundant lipid in animal cell membranes and also one of the lipids that we have been using for our research. b) Examples of potential applications of lipid bilayers. Lipid bilayers arranged into spherical vesicles can be used as containers transporting biomolecules or diagnostic markers to specific locations in the body. In addition, the bilayers can be deposited onto solid planar or spherical objects to create platforms which could for example be used for the controlled analysis of lipid organization or the behavior of membrane-bound proteins.

It is due to these exceptional properties why lipids are recently receiving increasing interest from the field of nano-technology [40]. Since the ability has emerged to purify or synthesize lipids, the lipids have been used to create self-assembled structures like micelles, reverse micelles and liposomes [47]. These secondary structures hardly undergo any non-specific binding of other biomolecules, which allows them to surpass barriers that are impassable for the biomolecules themselves. As such, they can function for example as carriers transporting medicine to specific diseased locations [48]. In addition, they can be coupled to other soft or hard nano-structures via specific chemical linkages. The resulting combination of the lipids to prevent degradation and the optical properties of nano-particles, allows for the selective diagnoses of for example tumors [49].

Besides their high potential in medicine, lipid-based structures have also many applications for nano-devices . For this, an excessively used platform is the supported lipid bilayer, a planar lipid film confined to a flat substrate. These lipid films are transparent for visible light, allow for heat conductivity, behave as insulators perpendicular to the plane of the membrane and are electrically conductive within the plane, making them excellent platforms for high-throughput sensing or electronic devices [50, 51]. As well as for the study of membrane proteins [52], or the lipids themselves [53].

Next to the planar supports, lipid bilayers can also be formed onto spherical surfaces like on silica micro-particles. This particular combination has been used to study the

interaction potential of bilayer of various lipid composition [54, 55].

During these developments, the lipid bilayer also got associated with the field of DNA nano-technology. By chemically coupling hydrophobic molecules to the ends of short DNA strands, the strands anchor in between the leaflets of the lipid bilayer [56, 57]. Initially developed for getting specific DNA sequences inside cells, the hydrophobically modified DNA strands got used for other applications like the patterning of surfaces with specific moieties [58] or the control of the morphology and properties of liposomal superstructures [59].

in this thesis, we exploit the combination of silica micro-particles, lipid bilayers and hydrophobically modified DNA to built a system of particles that display extended surfacediffusing DNA strands.

1.5. THESIS OUTLINE

In this thesis we studied a modified model system based on DNA interactions to drive the self-assembly of silica micro-colloids. To obtain an overview of what model systems already exist and how they relate to the questions we wish to answer, we review the already existing literature that encompasses the notion of mobile interactions and its relation to self-assembly in **chapter 2**. We review the different model systems that have been developed. Including systems of vesicles of different sizes, emulsion droplets and bilayer coated particles. In addition, we outline the theoretical models that could be applied to these model systems and any potential new strategy to which these models can be extended.

As a potential platform for the realization of surface-mobile oligonucleotides, we used the lipid bilayer. **Chapter 3** revolves around the characterization of the possible ways to couple short oligonucleotides to a lipid bilayer that is supported by a planar silica substrate. How does the type of hydrophobic anchor affect the kinetics and the final stability of the binding? Furthermore, we explored the physical organization of the final oligonucleotide layer, to elucidate the density of oligonucleotide and how far they extend outward. For this, we compared strands of different length and of different rigidity by comparing single and double stranded oligonucleotides.

The realization and characterization of the intended model system of silica microparticles coated with mobile oligonucleotides is explained in **chapter 4**. Here, we outline the procedure with which we achieve this and we reveal the first results regarding the effect of the mobility on the self-assembly. An interesting contrast is revealed between particles with immobile linkers.

In **chapter 5** we explored the possibilities to probe the binding strength of two particles coated with surface mobile oligonucleotides. For this purpose, we developed a microscopic technique based on reflection interference contrast microscopy (RICM). Unfortunately, we have not been able to complete the development to the extent that it is suitable for actual force measurements. To still be able to measure the binding strength we used an already functional setup consisting of an 'ordinary' optical microscopic into which two maneuverable lasers are coupled. These lasers are focused by the objective into the sample to function as optical tweezers. With these tweezers we compiled a protocol that repeatedly moved two particles into close proximity, held them together for 30 seconds after which the beads were pulled apart again. Here, we demonstrate that

the protocol allows for accurately determining the force required to rupture two coupled particles. Furthermore, we show preliminary results on the force distributions acquired for particles held together with surface-mobile DNA bonds.

Lastly, in **chapter 6** we summarize our findings and place them in a broader perspective. With this we aim to give an outlook of the next steps that are to be taken and the interesting directions further research could move forward to.

2

COLLOIDS WITH SURFACE-MOBILE LINKERS: AN OVERVIEW

In this chapter we review the possibilities of using colloids with surface mobile linkers for the study of colloidal self-assembly processes. A promising route to create systems with mobile linkers is the use of lipid (bi-)layers. These lipid layers can be either used in forms of vesicles or as coatings for hard colloids and emulsion droplets. Inside the lipid bilayers molecules can be inserted via membrane anchors. Due to the fluidity of the lipid bilayer, the anchored molecules remain mobile. The use of different lipid mixtures even allows to create Janus-like particles that exhibit directional bonding if linkers are used which have a preference for a certain lipid phase. In nature mobile linkers can be found e.g. as receptors in cells. Therefore, towards the end of the review, we also briefly address the possibility of using colloids with surface mobile linkers as model systems to mimic cell-cell interactions and cell adhesion processes.

The content of this chapter has been published as: S. A. J. van der Meulen, G. Helms, M. Dogterom, *J. Phys.: Condens. Matter* **27**, 233101-14 (2015).

2.1. INTRODUCTION

Since a number of years, DNA-coated colloids have been employed as versatile bio-inspired model systems to study processes of self-assembly and crystal formation. [1, 2, 5, 7, 60–62] The unique feature of these colloids lies in the fact that the nucleotide sequence of the DNA can be chosen specifically to promote interaction with colloids that are coated with complementary nucleotide sequences. In the majority of cases these model systems consist of gold, glass or plastic beads to which DNA molecules are either attached using physical adsorption [9, 63, 64], or covalent chemical bonds [1, 2, 65]. By careful design of the single-strand (sticky) ends of the surface-grafted DNA molecules, interactions between colloids can be made not only specific, but also tunable [14, 66–68]. In addition, methods have recently been developed to create solid colloids with DNA linker molecules that are mobile on the colloid surface (Fig. 2.1a, and Ref. [69])

In this review we discuss the potential of solid colloids with surface-mobile linkers as new model systems for self-assembly processes. We first review previous experimental model systems with surface mobile linkers, and then focus on the recent development of model systems based on DNA-coated spheres. Next, we briefly discuss the potential of these systems for the experimental study of multi-bond interactions with biological relevance. Especially on this last topic, there is a vast theoretical literature on the effect of linker mobility on for example cell-cell interaction forces. We only superficially refer to this literature, and refer the interested reader to excellent previous work for more in-depth information [70–72].

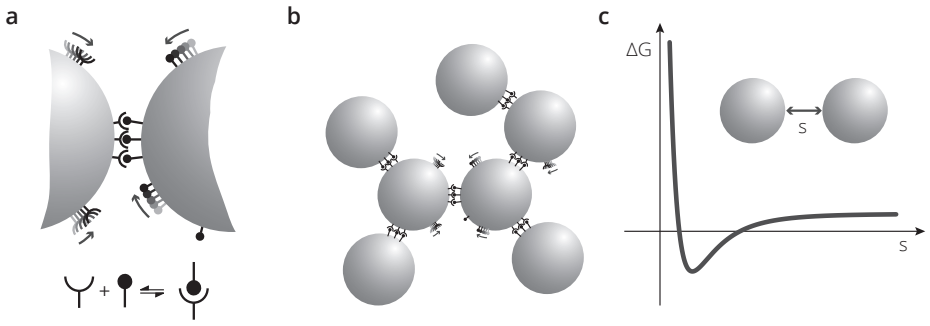

Figure 2.1: (a) Schematic drawing of solid colloids carrying linking molecules that can diffuse over the particles' surface. This system can be used (b) for studying colloidal self-assembly or (c) for measuring multibond interaction energies ΔG. [69].

2.2. SELF-ASSEMBLY PROCESSES

Self-assembly is the process whereby individually non-functional building blocks, in the absence of external guidance, form higher-ordered, organized structures or patterns as a consequence of specific, local interactions among the components themselves. Studying self-assembly processes is of great importance for several reasons. For instance, due to

the huge developments in nano-science and the unprecedented potential applications it has, there is a high demand for practical methods to built nano-structures, which self-assembly could provide. Further, self-assembly is common to many dynamic, multicomponent systems, from smart materials and self-healing structures to netted sensors and computer networks [73]. Finally, many supra-molecular structures in living cells are the result of self-assembly processes. Hence, understanding the principles of self-assembly will also help us understanding cells.

There are a number of features that a structure should have in order for it to be considered a self-assembled structure. One of the features is that the final structure should possess a higher order than the isolated parts. Secondly, the interactions linking the components together should be 'weak' with respect to covalent bonds. The building blocks do not necessarily have to be atoms or molecules but can also be larger mesoscopic objects like lipid vesicles or micro particles. Finally, a self-assembly process is non-dissipative and occurs spontaneously because the free energy of unassembled components is higher than of the self-assembled structure, which is in a (local) static equilibrium, persisting without the need for energy input [74]. There are many ways to direct self-assembly towards a preferred outcome [75]. For example, because the components must be able to move with respect to one another during the self-assembly process, the type of phase in which the components are dispersed dictates the motility of the components and therefore the dynamics of the self-assembly process. In addition, one can use physical boundaries and other templates to restrict the assembly to specific dimensions. Another tunable parameter is the type of interaction between components. By adjusting for example the shape, surface properties, charge, polarizability, magnetic dipole or mass of the building blocks, the direction and/or the affinity with which the components bind to each other can be changed, thereby affecting the kinetics and equilibrium final structure of the self-assembly process.

In this review we primarily consider specific interactions mediated by molecules. Such interactions can be achieved by chemically coupling specific linking molecules to the surface of self-assembling building blocks. Popular examples of such molecules are the biotin/streptavidin couple and the Watson and Crick (DNA) type of bonding between short oligonucleotides. Molecules are coupled to the surface of nano- or micro-particles in such a way that the molecular sites of interaction are left exposed, remaining free to bind to a partner. Especially the use of DNA provides a vast amount of controllability, via e.g. the number of molecules per surface area, the interaction depth (i.e. the length and flexibility of the oligonucleotide strand), the temperature and the interaction strength per molecule (i.e. the number of complementary base pairs). Explorations of this parameter space have led to the development of reliable crystallization strategies for nano-colloids (Fig. 2.2), in which great control is achieved over the crystal structure, the lattice spacing, and other properties [76].

However, comparable control over the self-assembly of larger micron-sized building blocks appears more challenging as reviewed by DiMichele and Eiser. Due to kinetic issues encountered during the self-assembly process, e.g. particles irreversibly sticking together, the structures more frequently develop into amorphous phases (often referred to as gel structures, [77]) than towards the expected thermodynamically more stable crystal phase, inhibiting thus far the development of technological applications such as self-

assembling photonic metamaterials [12]. Fortunately, recent experimental and theoretical progress has led to the development of new rational designs that could potentially facilitate a wider range of self-assembly experiments. The roles of many of the key parameters, e.g. the length of inert spacers, the combinatorial entropy and the presence of competing linkages are now far better understood which already has led to the creation of crystal structures with a wide variety of order parameters [8, 78–80].

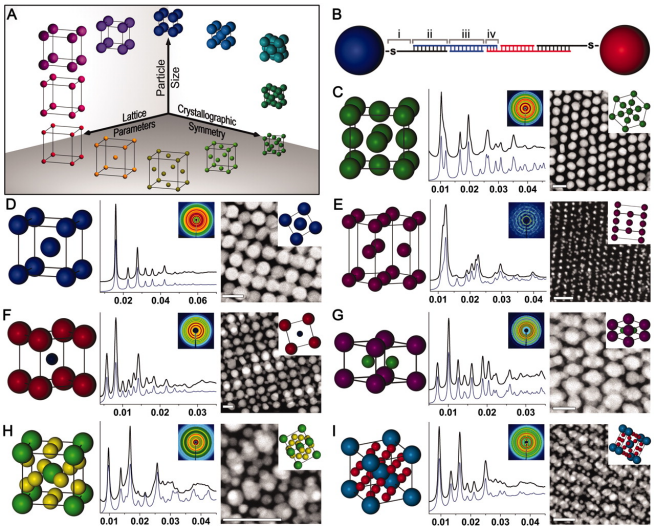

Figure 2.2: Examples of crystal structures that are accessible by self-assembly of nanoparticles mediated by nucleic acid linkers [5]. (A) By varying the parameters that control the assembly of the nanoparticle building blocks (e.g. particle size and the length of the nucleic acid linkers), it has been shown that over 100 different crystal structures, covering 17 distinct crystal symmetries, can be made. (B) The DNA strands mediate these nanoparticle assemblies, are composed of (i) an alkyl-thiol moiety and 10-base nonbinding region, (ii) a recognition sequence that binds to a DNA linkers, (iii) a spacer sequence of programmable length to control interparticle distances, and (iv) a "sticky end" sequence that drives nanoparticle assembly via DNA hybridization interactions. The superlattices displayed here are isostructural with (C) fcc, (D) bcc, (E) hcp, (F) CsCl, (G) AlB_2,(H) Cr_3Si, and (I) Cs_6C_{60} lattices. From [5]. Reprinted with permission from AAAS.

2.2.1. THE NEED TO EQUILIBRATE

As illustrated in the last paragraph of the previous section, an essential requirement for the self-assembly process to successfully take place is the ability of the system to equilibrate. A common equilibration method is to allow for the building blocks to be able to transiently switch between aggregated and non-aggregated states. In the case of DNA functionalized colloids, this can be achieved by successively crossing the temperature at which the DNA strands melt [79]. During the melting of the DNA strands, the colloids inside the disordered aggregates get more loosely connected and hence have more freedom to relocate to finally get to their expected ordered ground state. However, calculations, simulations and measurements on colloidal pair potentials have revealed an extreme sensitivity on environmental variables like temperature, which makes the for-

mation of ordered structures a very difficult process [1, 64, 65, 81, 82].

The temperature acts like an on-off switch for the very short range attraction between the otherwise self-avoiding colloids above the melt temperature [61, 65].. This is because the rate at which the free energy minimum of the interaction is strongly related to temperature changes. According to Ref. [64] a change of only ~3 °C can lead to a change of 10 $k_B T$ in the free energy minimum. The same authors have shown, both experimentally and computationally, that when the number of bonds between two particles is not too small, the temperature-dependence of the probability of unbinding follows a double exponential relation [11, 64]. This is represented by a very sharp melt region (only a few degrees). It is thought that this strong temperature dependence prevents the existence of a stable gas-liquid transition, which has been observed to facilitate the crystallization process [11]. These observations together with kinetic effects as for example delayed nucleation or arrested phase separation [83], outline the possible reasons for the difficulties experienced with the crystallization of DNA-coated micro-particles.

A strategy that could assist in overcoming the challenge of equilibrating the aggregates, but that has not been much looked into yet, is to allow for particles that are already attached to move with respect to each other. Adjusting their position relative to their neighbors within an aggregate gives the colloids the freedom to maneuver to their ordered ground state location within the aggregate without the need for the interactions to transiently open and close. One could for example achieve this by coupling the linking molecules to the surface of the building blocks in such a way that they can still undergo lateral motion along the surface. When in this situation two complementary particles bind, they can move with respect to each other by dragging the binding molecules along the surface while remaining at close proximity. Currently, there is no direct experimental evidence that proves that surface-mobility of linking molecules facilitates the organization of crystal structures. However, there are studies that have reported surface mobility of ligands coupled to gold nanoparticles [84–87]. Consequently, the crystallization presented in the studies on DNA-coated gold nanoparticles might in part be explained by the DNA linkers being able to move position on the particles' surface.

An alternative way to functionalize colloids with surface mobile linkers is to coat them with a lipid bilayer into which binding moieties can be embedded. Lipid bilayers or liposomes spontaneously self-assemble from lipids, which are molecules consisting of hydrophilic, water-loving, heads and hydrophobic, water-hating, tails [88, 89]. Due to the fluidic nature of typical lipid bilayers at room temperature, the embedded linkers can freely diffuse along the bilayer surface. Prior to the combination with colloids, lipid-based model systems have indeed been successfully used in a number of self-assembly studies. These model systems, as well as the insight they provided, are reviewed in some detail in the next section.

2.3. LIPID-BASED MODEL SYSTEMS WITH SURFACE-MOBILE LINKERS

2.3.1. SELF-ASSEMBLING LIPOSOMES

Liposomes, or vesicles, which are themselves the result of a self-assembly process, can undergo a secondary self-assembly process mediated by their lipid composition, solu-

tion properties, or the presence of lipid bound proteins or other active molecules. Similar to colloidal particles, the bilayers of liposomes can be functionalized with molecules like streptavidin/biotin or oligonucleotides. Then, under the appropriate solvent conditions, vesicles displaying complementary molecules or single-type vesicles mixed with linking molecules, will self-assemble into multi-vesicle aggregates. The multi-vesicle aggregates can serve as idealized model systems for biological tissues or can function as multicomponent or multifunctional drug delivery systems [59, 90, 91]. In addition, their spontaneous formation could lead to new methods for developing artificial tissues and soft composite materials [92].

2.3.2. WITH BIOTIN/STREPTAVIDIN BONDS

The high affinity and specificity of the biotin-streptavidin interaction makes this pair attractive for steering liposomal self-assembly. Biotin can be conjugated to lipids without affecting the vesicles' properties [93], and subsequent inter-vesicle bridging can be induced by the addition of streptavidin. This self-assembly process can easily be controlled by e.g. changing the density or affinity of the interactions, and is fully reversible by adding competing binding molecules with a higher affinity for streptavidin in solution. For small vesicles ($\varnothing$ ~ 50-100 nm) controlling the inter-vesicle binding by biotin/streptavidin interactions additionally minimizes the contribution of the whole lipid bilayer surface as compared to vesicles interacting through for example charged lipids, thereby reducing the consequential stresses and deformations and stabilizing the vesicle aggregates (see Ref. [94] and Fig. 2.3).

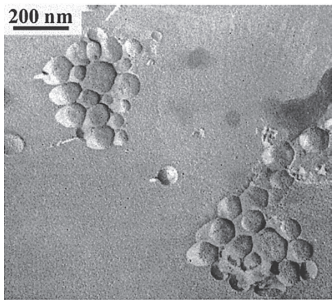

Figure 2.3: Self-assembled clusters of unilamellar vesicles mediated by biotin - streptavidin interactions. Freeze-fracture electron micrograph of aggregates obtained for a streptavidin to biotin ratio of 1.5, after aging for 3 weeks. As the aggregates age, intra-aggregate binding continues and the aggregates grow increasingly compact. Reprinted with permission from [95]. © (2000) American Chemical Society.

Investigation of the self-assembly of streptavidin-biotin presenting liposomes revealed that the aggregation could be very well predicted by a kinetic model based on Smoluchowski kinetics, fractal concepts and Rayleigh and Mie scattering theory [96]. Together with agreeing experimental results, Lynch *et al.* theoretically showed that the aggregation probability of liposomes carrying low amounts of biotin depends on the relative amounts of bound streptavidin and free biotin molecules on the liposome surface [96]. Whereas, for liposomes carrying high densities of biotin, the probability depends upon the relative liposome surface area covered with streptavidin molecules. By tuning the fraction

of streptavidin to biotin-lipids and monitoring the clustering very carefully, Kisak *et al.* were able to create compact, size-limited aggregates of vesicles [95]. A process that is due to a competition between biotin-binding to streptavidin free in solution and streptavidin already bound to another biotin.

Although they did not include it in their model, it was additionally observed that the rearranging intra-aggregate bonds are responsible for the compact shapes of the vesicle-aggregates, making this system different from other aggregation models. Interestingly, at relatively few biotin-ligands per vesicle, intra-aggregate binding can become faster than inter-aggregate bonding meaning that the mobility of the linkers enhances the self-limited aggregation, i.e. the vesicles aggregate into clusters which size depends on the number of vesicles in the cluster.

2.3.3. WITH OLIGONUCLEOTIDES

Inspired by the successes of employing DNA-mediated adhesion for assembly of binary hard-sphere colloids, strategies have been developed to also direct the self-assembly of liposomes with complementary oligonucleotides. Beales and Vanderlick incorporated short oligonucleotides into the bilayers of vesicles (hydrodynamic radius ~50 nm) by means of a cholesterol group on one end of the DNA strand [97]. To induce self-assembly, the other end of the DNA strands comprised a short sequence of nucleotides which was complementary to the end of DNA strands incorporated to a second set of vesicles. In close enough proximity, two vesicles that carry the complementary sequences are bound together by the oligonucleotides forming double stranded DNA duplexes. The self-assembly is reversible since the DNA duplexes dehybridize at temperatures above their melting transition or at low ionic strength of the suspension.

One observation they made was that a minimum number of DNA strands per vesicle was required at which the vesicles started aggregating. This suggests that the strength of only one DNA duplex is insufficient for maintaining vesicle adhesion. More strands must diffuse into the binding site and form a duplex in order to realize a stable coupling. Furthermore, at an intermediate number of strands per vesicle they observed that the aggregate size after some time ceased to increase. Plausibly, too much of the DNA eventually resides in the contact area between two adhered vesicles leaving too few free strands available for a third vesicle to adhere. They support their explanation by measuring the kinetics of aggregation and comparing the effective time for two vesicles to bind with time for a strand to diffuse into the binding site. The former clearly exceeds the latter by several orders of magnitude meaning that there is ample time for the majority of the strands to collect in the binding site. At high DNA densities they observed unrestricted aggregation.

The same group obtained similar results for larger vesicles, so called giant unilamellar vesicles (GUVs) having a diameter the size of several micrometers [97]. Again at low DNA densities no aggregation was seen, limited aggregation was observed at intermediate densities and unceasing aggregation occurred at high densities. Yet, compared to the smaller vesicles, GUVs carry many more DNA strands per vesicle. Therefore, these different aggregation regimes cannot be explained by the same reasoning as for the regimes seen for smaller vesicles. Other aspects like the deformability of the membrane start to play a role. As soon as two GUVs adhere, a large osculating area forms. The growth of the

adhesion plaque is driven by the fluid nature of the membrane which allows for the DNA to diffuse into, and enhance the binding site. With a sufficient number of DNA linkers this growth is only limited by the surface tension it creates on both GUVs. Unlimited aggregation can therefore take place when the maximum plaque size is reached and there is enough DNA on the membrane to saturate the contact zone, while leaving sufficient DNA on the unbound area available to form a stable coupling with another GUV. Also multi-vesicle assemblies of higher complexity have been realized this way [98].

Recently, Parolini et al., utilized the DNA functionalized GUVs to develop a material that displays structural responsiveness to external stimuli [99]. Due to a competition between the attraction of the DNA bonds and the surface tension of the lipid membranes, the adhesion zones between two neighboring vesicles decreases upon cooling. They predict a wide range of applications in which such materials can be used, e.g. tunable filters with temperature-dependent pore sizes and cargo carrying vehicles that not only release their product upon temperature changes but also upon changes in osmotic pressure.

2.3.4. "JANUS" OR DOMAIN CARRYING VESICLES

Recently, there has been an increasing interest in the development of patchy particles and the structures into which they self-assemble. A major consequence of the anisotropy of these particles is that their interactions do not only depend on the inter-particle separation but also on the particles' relative orientation. This provides an additional degree of complexity that allows for greater control and sophistication, which allow for new structures to form.

Janus particles are a subclass of such anisotropic particles, which comprise two opposing faces with different surface chemistry [100, 101]. Self-assembled architectures composed of amphiphilic molecules like lipids turn out to be very useful for the realization of particles that present two distinct phases. In particular, with vesicles comprising lipid mixtures that demix into coexisting liquid-like phases, the initial membrane domains eventually fuse together until the vesicles exhibit two opposing surfaces each having different chemical compositions. The two chemically different phases themselves can have properties that favor the binding of two particles together, for example if the two surfaces have opposing charge. Moreover, one can load the Janus vesicles with specific molecules which preferentially reside in one of the two phases [102]. Including highly unsaturated lipids such as cardiolipin (CL) in the phase separating lipid compositions enhances the partitioning of chol-DNAs into the liquid ordered (L_o) phase. A possible explanation of this effect is that the structure of CL creates large lateral packing stresses in the hydrophobic regions of the membrane. It is likely that these stresses increase the free energy cost of inserting a cholesterol modified DNA strand into the liquid disordered (L_α) phase and hence drive the partitioning of such molecules into the L_o domains [103, 104]. Either way, the splitting of the surface chemical properties into two phases provides a means to realize asymmetric surface distributions of adhesive functionalities.

Higher order valencies may be realizable if the lipid mixture does not separate into two opposing, equally sized surfaces, but separate into multiple spots or rafts. By preparing vesicles or polymersomes using a mixture of neutral and anionic amphiphiles, Christian and colleagues were able to make liposomes that have stable spots or rafts upon adding divalent cations like calcium or copper [105]. The domain sizes were shown to be

controllable by changing the pH, divalent cation concentration, and fraction of anionic amphiphiles.

2.3.5. SELF-ASSEMBLING EMULSION DROPLETS

When more mechanical stability of the self-assembling structures is desired, it is possible to use emulsion droplets instead of liposomes. Emulsion droplets form when two immiscible fluids are mixed in the presence of surface active agents, so that one of the fluid phases gets dispersed into the other. Emulsion droplets exhibit all the classical aspects of colloids: Brownian motion, reversible phase transitions as a result of droplet interactions and irreversible transitions that generally involve their destruction [106]. In addition, just like with liposomes they can be functionalized with ligand-receptor like pairs such as biotin-streptavidin or DNA oligonucleotides [107, 108].

Detailed studies of the self-assembly of DNA-functionalized emulsion droplets have given hints to what the most important control parameters are, and how one can predict the self-assembling structure. One crucial aspect of these systems, just as with vesicle systems, is that the linking molecules can move freely over the surface to which they are attached. As a consequence, during binding of two complementary droplets more linkers are likely to move into the connecting area.

When complementary droplets carry respectively red and green fluorescently labeled linker molecules, the accumulation of binding molecules is clearly seen in confocal micrographs by the yellow color in the area where bound droplets overlap, see Ref. [109] and Fig. 2.4. In these experiments, the degree of accumulation could be tuned by adjusting the number of binders per droplet, which was quantified by measuring the size of the patches as a function of linker density. The results fitted nicely to a mean field thermodynamic model that is based on the assumption that the recruitment of binders continues until the translational entropic cost of the immobilized binders in the patch plus the energy paid to deform the emulsion droplet matches with the energy gained by binding.

Although the number of binders inside a patch with a diameter of for example 1.6 μm was estimated to be large ($2{\cdot}10^3$ connections), the patches remained able to freely diffuse. The motion of the patches was quantified by coupling multiple nano-particles to emulsion droplets with DNA linkers and following their respective motion. Despite the hydrodynamic drag which is expected to be much larger for an adhesive patch than for a single lipid, the nano-particles (i.e. the patches) exhibited an average diffusion constant of $D \sim 0.012\ \mu\mathrm{m}^2 s^{-1}$, which is expected to be two orders of magnitude lower than the diffusion of a single lipid. According to the thermodynamic model, a maximum patch size exists due to the dramatic sensitivity of the deformation energy cost on the patch angle θ: $E_{\mathrm{deform}} \sim \theta^4$, where $\theta = r_{\mathrm{p}}/R$, $\mathrm{r_p}$ is the radius of the patch, and R is the radius of the droplet. Controlling the DNA density therefore controls the number of patches that a droplet can maintain. Both theoretically and experimentally it was shown that with DNA surface densities of 7.5, 15 and 30% (with respect to the maximum DNA coverage possible), respectively monovalent, divalent and multivalent structures are formed (see Fig. 2.4a). In addition, self-arresting structures could be formed using a droplet/nanoparticle hybrid system. The nano-particles are large enough to make it energetically favorable to form a ring around the contact points of two emulsion droplets without actu-

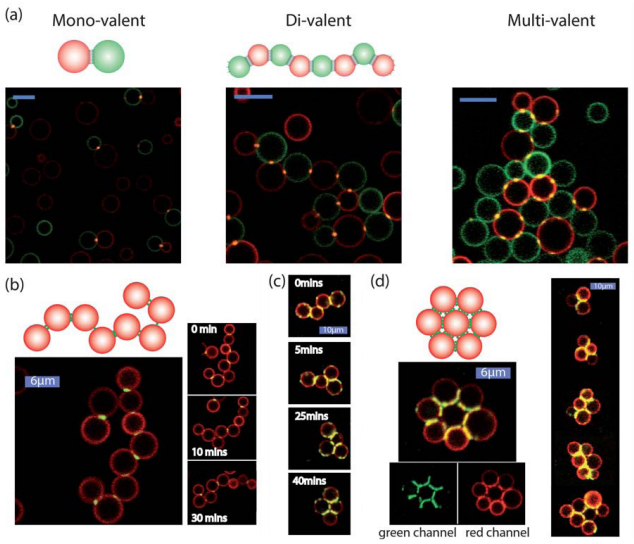

Figure 2.4: Controlling the valency of clusters of emulsion droplets. (a) By varying the number of linkers per emulsion droplet one can create (left) monovalent doublets, (center) di-valent droplet chains and (right) multi-valent aggregates. The scale bars are 10 μm. The same mono- (b), di- (c) and multi-valent (d) clusters can be realized by using DNA-coated nanoparticles as linkers and changing the droplet to nanoparticle ratio. Reproduced from [109] with permission of The Royal Society of Chemistry.

ally reaching the contact points. Because this maximizes the number of nano-particles in the contact zone, the geometry of the final compact structure can be controlled (by tuning the number of droplets and the nano-particle surface density) to favor the formation of linear chains, triangular lattices or flowers (see Fig. 2.4b-d).

2.4. SOLID COLLOIDS WITH SURFACE MOBILE LINKERS

As demonstrated in the previous sections, introducing mobility to the molecules that mediate the self-assembly of larger entities uncovers new interesting strategies to control the organization of the final equilibrium assembly. It was shown with systems of vesicles and emulsion droplets that by carefully tuning the binding interactions, it becomes possible to induce for example self-limited clustering and even to control the valency. The latter is attractive because it potentially allows for the development of open structures that do not form in systems with isotropic interactions. Examples of similar structures in nature are carbon atoms that form diamonds as a consequence of the well-defined electronic valency. Getting colloids to self-assemble into a diamond lattice could potentially lead to the production of photonic band gap materials [110]. A photonic band gap is a location within a material where electromagnetic wave propagation at a specific band of wavelengths is forbidden in all directions [111, 112]. Controlling the properties of such photonic band gaps allows one to control the flow of light inside the structure and hence have a wide range of potential applications in optics. As demonstrated by Ho et al., readily achievable FCC structures are insufficient for the existence of a full photonic

bandgap[110]. They calculated exact solutions of the Maxwell equation for the photonic band structure of periodic arrangements of dielectric spheres in the fcc and the diamond structures. These solutions provided evidence for the existence of a pseudogap rather than a full gap for the fcc structure whereas the diamond lattice possesses a full photonic band gap.

However, so far it has not been straightforward to control the coordination number in solid colloidal systems. Wang et al., made considerable progress by developing a method to deposit patches on colloids at precise locations onto which DNA could be grafted [113]. By limiting the position of DNA strands to specific locations on the colloids they were able to generate small aggregates with controllable coordination number (valency). Although very promising, in order to produce bulk colloidal phases of practical interest the yield of their method needs to be scaled up substantially, which as of today remains a challenge.

2.4.1. CONTROLLING VALENCY WITH MOBILE LINKERS

Recent theoretical and computational studies indicate a potential alternative and less--involved strategy to control the valency. Angioletti-Uberti et al., reported calculations on colloidal particles functionalized with surface-mobile DNA strands [17]. Their results predict that the many-body effects that naturally arise in DNA-coated colloids with surface mobile linkers can be used to enforce the valency. In addition, they demonstrate that the valency can be tuned by changing the density of inert strands or the interaction between individual strands.

Their predictions are based on calculations on a binary model system of colloids, A and B, functionalized with surface-mobile double stranded oligonucleotides. The sequence of the DNA on the colloids of type A is complementary to the DNA sequence on the particles of type B. At the same time, same-type particles repel each other due to the steric hindrance caused by the non-binding DNA strands. When two colloids (A and B) bind, their attraction increases as the number of bonds increases due to their mobility. If a second colloid B_2 binds, any of the mobile DNA strands on A can now bind with B or B_2. As a consequence of the symmetry in the system, both particle connections will eventually contain the same number of DNA bonds. Assuming that the number of DNA strands per particle remains constant, the more particles bind to A the fewer strands remain per particle connection and hence the effective attraction between two particles decreases.

This many-body effect by itself is however not enough to impose valency. Although the addition of another particle makes the inter-particle interactions weaker, it does add one more interacting pair. This can be quantified by adapting a previously developed expression for the binding of DNA-coated particles to account for the mobility of the DNA strands [68, 114]. The authors could show that indeed the binding free energy per pair becomes less negative upon increasing number of neighbors, confirming the weakening of the attraction between particles upon cluster growth. However, the final coordination number of the cluster is controlled by the free energy of the cluster, which was shown to be a continuously decreasing function upon increasing number of neighbors. Only through the addition of non-specific double stranded DNA, they identified a region in parameter space where the free energy of the clusters exhibits a minimum at coordination numbers below the physically attainable maximum. After running Monte Carlo

simulations the authors showed that this free energy minimum was enough to give the colloids valency. Furthermore, this valency could be tuned by changing the binding energy of each individual strand, e.g. by adjusting the temperature or salt concentration, see Fig. 2.5. The introduced valency led to the self-assembly of the colloids into more open structures with limited long-range order, which are potentially good enough to inhabit photonic band gaps [115].

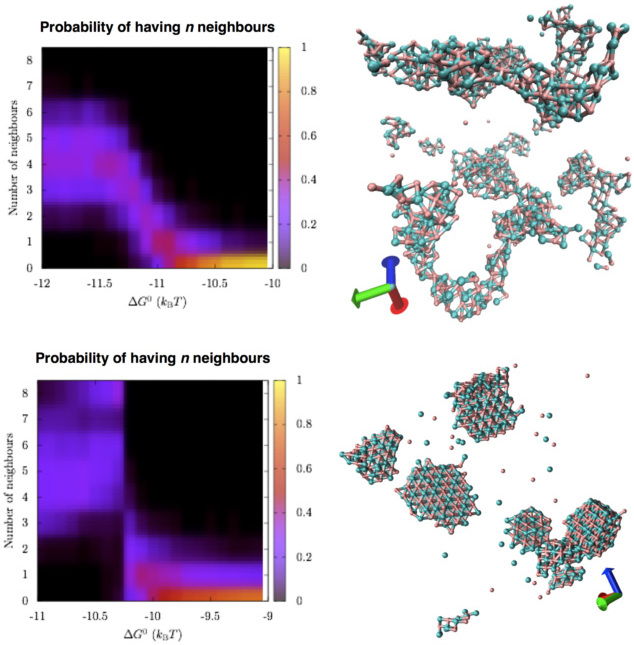

Figure 2.5: Valency distribution as a function of ΔG^0, for colloids with (top) and without (bottom) inert strands. ΔG^0 corresponds to the hybridization free-energy for two DNA strands in solution and depends only on the DNA sequence and is a function of temperature and ionic strength of the solution. The repulsive free-energy at the equilibrium distance between colloids is basically zero except when inert strands are present. The snapshots show typical configurations at low ΔG^0 in the two cases, where the system either assembles open structures of tetrahedral coordination (top, with inert strands) or a more compact NaCl structure (bottom, no inert strands). Reprinted with permission from[17]. © (2014) by the American Physical Society.

2.4.2. EXPERIMENTAL MODEL SYSTEMS FOR CONTROLLING VALENCY

The theoretically obtained guidelines for realizing clusters with controlled valency encourages the search for model systems that provide experimental verification. A potential candidate could be the droplet system developed by Feng and co-workers [109]. In the low-valency structures that they reported, the required repulsion is likely to originate from the deformation of the droplet interfaces. However, whether the deformations alone are responsible for the valency effect has still to be confirmed.

In addition, Lee et al., who studied the self-assembly of gold *nano*-particles functionalized with a monolayer containing a mixture of hydrophobic and hydrophilic lig-

ands, were able to guide the self-assembly from micellar clusters, to extended chain-like assemblies in aqueous solution [87]. They could explain their findings by formulating an assembly mechanism in which the hydrophobic ligands reorganize on the surface to form patches between neighboring particles.

Silicia microparticles coated with DNA-functionalized lipid bilayers such as the ones developed by van der Meulen et al., provide another promising experimental system that may allow for the control of valency [69]. Here, double stranded DNA with short single stranded overhangs are first coupled to small unilamellar vesicles (SUVs) by two cholesterol anchors. Next, the vesicles are mixed with a suspension of monodisperse silicon oxide microparticles. The contact of the SUVs with the surface of the microparticles in combination with the high surface tension of the SUVs triggers the rupture and spread of the vesicles around the particles until they are completely enveloped by a lipid bilayer. The DNA strands incorporated in the bilayer maintain their mobility on the surface and have shown to remain inside the bilayer when a strong enough hydrophobic anchor is used [116, 117]. See Fig. 2.6 for a schematic overview of the model system.

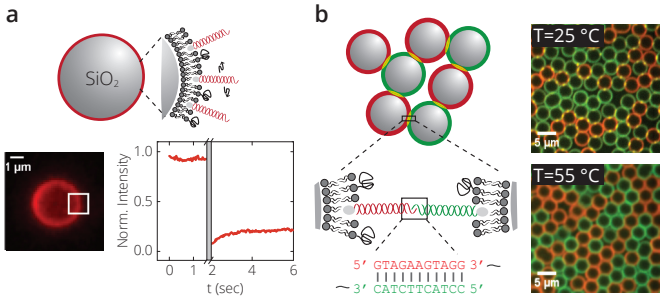

Figure 2.6: Schematic representation of solid microparticles coated with surface-mobile DNA binding groups. (a) Silica microparticles are coated with a lipid bilayer comprising predominantly DOPC and a small percentage of PEGylated DPPE. The DNA interpenetrates the bilayer through a hydrophobic anchor, e.g. cholesterol. The partial recovery of the fluorescence intensity after bleaching one side of a DNA functionalized particle (white square in the fluorescent image) indicated the surface-mobility of the DNA [69]. (b) Controllable self-assembly was achieved by mixing two particle populations carrying DNA with complementary ends. Below the melting temperature of the DNA bonds, the complementary particles bound together indicated by the appearance of bright yellow spots at the contact zone. The particles dissociated upon increasing the temperature indicated by the disappearance of the bright yellow spots. Reprinted with permission from [69]. © (2013) by the American Chemical Society.

Van der Meulen et al., studied the self-assembly properties of their mobile-DNA particles by designing a similar binary mixture of particles decorated with either A or the complementary B strands. These colloids self-assembled into clusters at 25 °C, which dissociated at temperatures of 55 °C. Both DNA strands were fluorescently labeled and the appearing yellow color at the contact zone between two particles (due to overlapping red and green labels) indicated that at low temperatures the DNA molecules accumulated in the contact zone whereas they diffused to a homogeneous surface distribution at high temperatures (see Fig. 2.6b). The packing of the mobile-DNA-coated particles directly upon mixing appeared already more dense than for immobile-DNA-coated particles. Nevertheless, the packing could be enhanced by melting the clusters and subse-

quently slowly cooling (~9 °C/hr) the suspension, which led to slightly more hexagonally packed clusters, see Fig. 2.7. Furthermore, during melting of the clusters of mobile-DNA-coated particles, the transition from a bound to an unbound state is far less sudden as compared with the transition for immobile-DNA-coated particles. From these observations it is speculated that the particles have more freedom to move with respect to each other and rearrange due to a collective mobility of the bonds in the contact zone. The mobility of the linkers and the occurrence of a hexagonal-like crystal phase indicate that the system reproduces the predictions for particles with no additional repulsion reported by Angioletti-Uberti et al. The effect of repulsion is still to be tested, but could easily be realized by adding inert DNA strands of two or three times the length of the complementary DNA strands. As the simulations suggest, tuning the amount of repulsion should than produce particles that obtain valency upon binding. These particles should subsequently self-assemble into 2D structures with a lower coordination number than the 2D hexagonal close-packed structure that has already been experimentally observed. It should be noted, that the described model system only leads to 2D assemblies due to gravity effects. To establish three dimensional structures one could try to density match the particles with the solvent.

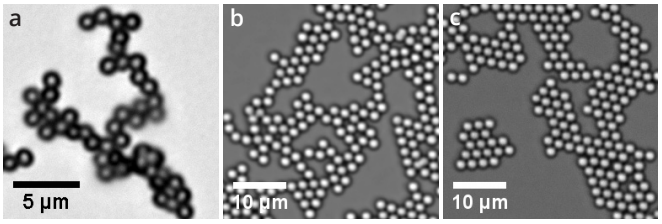

Figure 2.7: Self-organization of complementary micro-particle mixtures functionalized with either immobile or mobile DNA linkers. 1:1 mixtures of S- and S'-functionalized particles were cooled quickly from a fully dissociated state at 52°C to a fully associated state at 25°C in 15 min. The bright-field snapshots show the resulting structures for (a) 1.0 μm diameter particles with immobile DNA linkers and (b) 2.0 μm diameter particles with mobile DNA linkers. (c) The same sample as in panel B after re-dissociating and slowly cooling from 52 to 25°C in 3 h. Reprinted with permission from [69]. © (2013) by the American Chemical Society.

2.5. DIFFUSIVE INTERACTIONS IN BIOMIMETIC MODEL SYSTEMS

As explained above, solid colloids with surface-mobile bonds provide a promising route to creating self-assembled structures with controlled valency. At the same time, these model systems hold the potential of providing a new model system for the study of multi-bond interactions with biological relevance. In fact, one of the earliest appreciations of mobile interactions originates from the study on interactions between cells: immediately when Singer et al. pointed out the fluid nature of lipid membranes and their embedded proteins , it was realized that the mobility of surface receptors should influence the way cells interact with their surroundings [88, 118]. See Fig. 2.8 for a 3D representation of interacting cells.

Since then numerous studies have revealed great variability in the modes of lateral

mobility of proteins inside the membrane, elaborately reviewed by [71]. The different modes of motion have been proposed to play crucial roles in multiple processes, e.g. cell adhesion, signal transduction, cell activation and cell differentiation, yet dissecting the precise reason for the existence of all the different motility modes in cells remains a challenging task [72, 119, 120]. Any of the processes outlined above are a result of an enormously complex network of many components accurately orchestrated to perform the designated task.

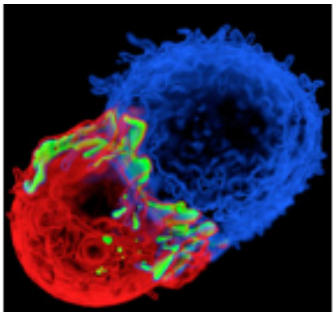

Figure 2.8: 3D rendering of an HEK-293 cell (biochemically engineered to express T cell genes) (red) interacting with an antigen-presenting cell (blue). Signaling between the two cells is initiated by the recruitment of kinase ZAP70 (green) to the area where the two cells interact. Figure adopted from Ref. [121]. Reprinted by permission from Macmillan Publishers Ltd: Nature [121], © (2012).

Despite the great complexity, there are several strategies available to narrow down the roles of each individual player in a particular action of the cell. One could remove or mutate a specific protein of interest and monitor the response. If a change is observed, the manipulated protein is most likely involved in that particular process. By repeating the same process for related proteins or for different mutations the mechanism of interest may become clear. An alternative method is to transfer all the components responsible for a biological phenomenon occurring in a specific cell into a cell that normally does not express the proteins of interest, see for example Refs. [121, 122]. In this way, one can specifically study a particular process in the absence of interfering processes that occur in the original cell, whilst still taking place within the realistic conditions of a cell. This, at the same time poses a major complication for both described strategies. Proteins often have multiple functions and introducing unfamiliar proteins or manipulated ones can have detrimental consequences for the behavior of the cell. Furthermore, living cells are dynamic systems where energy is consumed to up or down regulate protein expression levels and hence molecular concentrations are never constant, thereby complicating quantitative modeling. Therefore, over the years an increasing number of simple model systems have been designed that do not suffer from these variabilities but still provide valuable information about the mechanism of a specific cellular process.

2.5.1. MODEL SYSTEMS BASED ON SUPPORTED LIPID BILAYERS

A proven-to-be essential workhorse for such model systems is the supported lipid bilayer, from here on referred to as SLB. An SLB is a lipid bilayer which is formed on a solid substrate, such as glass, silicon oxide or mica. Because a thin layer of water exists be-

tween the substrate and the bilayer, the bilayer itself remains fluidic and allows for the embedding of other molecules like membrane proteins or other kinds of lipids. SLBs can be prepared either by the Langmuir Blodgett technique [123] or by deposition and spreading of lipid vesicles on the surface [124, 125].

Once a SLB is formed, one can functionalize it with specific proteins or receptors. By subsequently adding cells one can not only monitor the cell's response to the SLB presenting molecules, but the responses can also relatively easily be quantified, given the quasi two dimensional geometry of the SLB. For example Zhu et al. examined the interactions between the cell-receptors CD2 and CD58, both mobile in the bilayer, by monitoring the adhesion of CD2-expressing T-cells with a CD58 containing SLB [126]. It appeared that adhesion is associated with the accumulation of both receptors in the contact area (schematically represented in Fig. 2.9). Furthermore, FRAP analysis of the contact area revealed that the bleached molecules were quickly replaced by molecules from outside the bleaching spot, indicating that the CD2-CD58 dissociation rather leads to partner-exchange than rebinding of the same pairs. Further examples for the interactions of supported lipid bilayers with cells can be found in the papers of Groves and Dustin [127, 128].

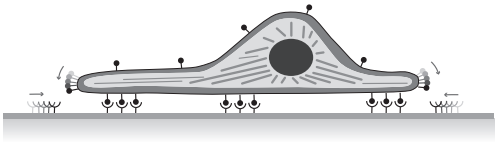

Figure 2.9: Schematic representation of a cell carrying cell-adhering-molecules (CAMs) that bind the cell to a receptor-decorated supported lipid bilayer (SLB). Because the linking molecules in both the cell-membrane and the SLB are mobile, binding groups can cluster to strengthen the adhesion [126].

To reduce the complexity further one can replace the cells by vesicles. This way one has precise control over all the components that could take part in adhesion, e.g. membrane composition and the density of cell-adhering-molecules (CAMs), which allows to study only those interactions that one is interested in [129–131]. Because all the ingredients of the system are known, quantifying the free energy of adhesion becomes easier. A major result of studying these particular biomimetic model systems is the observation that the formation of adhesion domains is an inevitable result of a delicate interplay between short range attraction forces between pairs of cell adhesion molecules (CAMs), long range repulsion forces mediated by the glycocalyx, and the elastic stresses of the lipid protein bilayer [72]. In addition, these mimetic systems have revealed fundamental differences between systems where both the binding partners are mobile versus a situation where one of the two is immobile [129]. A fine balance between mixing entropy and binding enthalpy in the case where both binding partners are mobile, allows for much larger areas of tight adhesion and increases the spreading pressure of each domain.

Furthermore, both the number of bonds and their organization are significantly different when the binding partners are mobile. Many more bonds form and the ability to adjust their location on the membrane allow CAMs to optimize their inter-bond distance, which lowers the free energy of the bound state as a result of the lower entropic penalty the linkers have to pay for the coupling. A property which, in contrast to immo-

bile linkers, allows for the stable formation of domains at physiological linker densities. Another important difference between vesicles that are bound to a SLB with immobile or mobile bonds becomes clear when a force is applied to the vesicle to break the coupling [132]. As opposed to immobile bonds, mobile linkers close to the contact line transverse laterally without unbinding the moment you switch on the force. Sparse domains reorganize into densely packed structures accompanied by the increased probability of forming new bonds due to cooperative effects. As a result, the adhesion strength rises and together with the force-induced linker condensation, repeatedly applying these external forces causes the contact zone to enlarge continuously. The rapid strengthening of cell adhesion upon an applied external force mediated by the mobile linkers can play an important role in situations of changing elastic stresses that require a cell to quickly adapt. An example of such a situation is the attachment of white blood cells to endothelial cells during which the linkages have to withstand high shear stresses governed by the blood flow.

2.5.2. MODEL SYSTEMS BASED ON VESICLES AND EMULSION DROPLETS

Although the systems in which cells or vesicles adhere to supported lipid bilayers appear very suitable for studying the effects of mobile binding groups on the adhesion strength, they have limitations for adhesion-induced membrane deformations. As the solid support causes the SLB to be nearly fully restricted from any form of deformation, only the adhering cells or vesicles undergo deformations. This is interesting for mimicking events where cells adhere to rigid surfaces like the extracellular matrix, but for cell-cell interactions it does not suffice. Biomimetic model systems that are more resembling cell-cell interactions are those made of two liposomes or giant unilamellar vesicles (GUVs) that have receptor/ligand type of molecules incorporated in their membranes. Studying the binding of two GUVs that carry complementary molecules allows one to examine, in a very controlled manner, the binding process and all its potentially important aspects in great detail. For example, with two micro-pipettes one can hold two vesicles and bring them together, while keeping the surface pressure of both vesicles constant. This way Noppl-Simson et al. have shown that for biotin-coated vesicles cross-linked by fluorescently labeled avidin at low surface densities of biotin and avidin on the membrane (<5 mol %), the accumulation of linkers in the contact-zone is driven by the spreading pressure resulting from the clustering avidin molecules [133]. By measuring the contact angle between the two adhered vesicles one can estimate the density of linkages in the contact zone. In contrast, at high surface densities, the spreading-pressure argument breaks down, because the chemical driving force for adhesion far exceeds the mechanical counterforce against spreading [134].

Cell-cell contacts in real tissues are continuously subject to mechanical forces due to homeostatic pressure and active cytoskeleton dynamics. To study the role of pressure Pontani et al. used a dense packing of functionalized emulsion droplets in which surface interactions were tuned to mimic those of real cells [108]. The authors used an emulsion system because compression of the individual droplets with an interfacial tension of $\sim 10 \cdot 10^{-3}$ N/m leads to pressures in a similar range to those found in tissues. Furthermore, the emulsion droplets can easily be modified to reproduce the attractive and repulsive interactions that govern cell adhesion. Their system of emulsion droplets

coated with biotin-streptavidin complexes, negatively charged SDS and PEG-lipids resulted in a mixture of droplets that show homogeneous coverages of streptavidin. No interaction between droplets takes place. Only when applying a pressure by centrifuging, the droplets are pressed sufficiently close together for the biotin-streptavidin bonds to form. Further examples of this approach can be found in Fataccioli et al., who used biomimetic emulsion droplets to study specific wetting processes, and in Bourounina et al., who studied the formation of specific receptor-ligand bonds between liquid interfaces [135, 136].

A general limitation of both the vesicle and emulsion systems is that it is hard to control the size distributions. The developments of microfluidic devices nowadays offer great potential [137, 138], yet are still limited in their yield. Ill-defined knowledge of the sizes of the interacting vesicles complicates quantitative analysis of the processes taking place. Ideally, the density of binding molecules is accurately controlled in order to calculate the interaction forces and subsequently enable the systematic comparison between different conditions, e.g. different linker densities. Furthermore, since vesicles and emulsion droplets are out-of-equilibrium structures, they are unstable and will eventually coalesce with each other. This in turn also limits quantitative analysis, as the structures do not remain constant in size, which constraints the experimenter to a limited time window in which measurements can be done. Using the system of solid colloids with surface mobile linkers introduced above can be a potential candidate to fill in this niche. Silica particles can be synthesized with very narrow size-distributions [139] and the lipid coating has been verified to remain stable for several days [54, 140, 141]. In addition, the micro particles can easily be manipulated with optical tweezers, enabling highly sensitive force measurements. However, the solid support restricts the deformations of the membrane, which is a disadvantage compared to vesicle/emulsion systems. It should therefore be emphasized that the micro particles can be used as an additional model system for interaction measurements, complementary to other model systems.

2.6. PROSPECTS

In this chapter we presented an overview of model systems with surface mobile linkers. We focused on the influence of linker mobility on the self-assembly process of colloids. In these systems, the use of mobile linkers prevents so called “hit and stick” situations and adds another degree of freedom or control parameter. A very promising method for preparing model systems with mobile linkers is to embed these linkers into lipid bilayers. The use of lipids allows a wide range of system variations. They can be used in form of vesicles, solid supported lipid bilayers, or as coatings for emulsion droplets. And besides acting as model systems for studying the self-assembly of colloids into larger structures, they are also an ideal tool to mimic cell-cell interactions and cell adhesions.

In the future one can imagine that the use of lipid-coated colloids with surface mobile linkers offers a wide range of research applications, as they provide a system which can be easily modified. Not only the linker molecules and their anchors can be varied but also the lipid matrix itself, which allows for the preparation of patchy particles or particles with different linker mobility. Furthermore, the solid support itself can have an influence on the mobility of the linkers. The use of a solid colloid allows an easy handling of the particles. They can be handled for example with optical tweezers or attached to atomic

force microscopy cantilevers which then allow to probe the influence of the linker mobility on binding forces. With these possibilities we think it will be possible to create increasingly powerful model systems that enable new strategies for the self-assembly of ordered structures and mimic cell-cell interactions.

Besides all the aforementioned possibilities that mobile interactions offer for self--assembly, e.g. enabling valency control on interacting colloids, the mobile-linker-coated particles have additional potential applications. For example Conway *et al.* reported the successful functionalization of lipid bilayer coated microparticles with DNA nanocages [142]. Also these DNA structures showed to be fully mobile on the particles' surface. By introducing competing DNA strands they could selectively remove parts of the DNA cages, reorient them thereby changing their accessibility, and dimerize the cages with neighboring cages. These developments provide a leap towards the design of methods for programmable dynamic control of protein binding, cell signaling, and drug delivery, as well as methods to control nanoelectronic and optical properties of lipid bilayers, using easy to construct DNA scaffolds.

We thank Mirjam E. Leunissen for initiating and facilitating our research on colloids with surface-mobile linkers, and for a critical reading of the manuscript.

3

THE PHOSPHOLIPID BILAYER ANCHORING STABILITY AND KINETICS OF HYDROPHOBICALLY MODIFIED DNA OLIGONUCLEOTIDES

In this chapter we report the results obtained from measuring the stability and organization of short DNA strands anchored to lipid membranes through various hydrophobic anchors. The binding of DNA oligonucleotides by the absorption of three different frequently used hydrophobic anchors to supported lipid bilayers (SLBs) made of dioleoylphosphatidylcholine (DOPC) was compared by quartz crystal microbalance with dissipation monitoring (QCM-D) and spectroscopic ellipsometry (SE). All three anchors were found to incorporate well into DOPC lipid membranes, yet only the di-stearyl-based anchor remained stable in the bilayer upon rinsing. The reversible anchoring of the cholesterol and stearyl-based oligonucleotides can however be stabilized by hybridization of the oligonucleotides to complementary DNA modified with a second hydrophobic anchor of the same type. In all cases, the incorporation into the lipid bilayer was found to be mass-transport limited, although micelle formation likely reduced the effective concentration of available oligonucleotides in some samples, leading to substantial differences in binding rates. We further found that the surface density and/or thickness of the final DNA layer can be controlled by changing the physical properties of the individual oligonucleotides, e.g. stiffness or length. The presented results are useful for material and biomedical applications that require efficient linking of oligonucleotides to lipid membranes.

The content of this chapter has been published as: S. A. J. van der Meulen, G. V. Dubacheva, M. Dogterom, R. P. Richter, M. E. Leunissen, *Langmuir* **30**, 6525-33 (2014).

3.1. INTRODUCTION

Targeting DNA oligonucleotides to lipid bilayers is an attractive approach to produce new materials, to create highly tunable model systems for studying fundamental questions, and for therapeutic applications [59, 143]. For example, in the design of anti-sense medicine, single-stranded oligonucleotides are targeted to cellular membranes through a hydrophobic moiety, after which they are internalized by the cell allowing the oligonucleotides to hybridize to targeted mRNA strands by sequence recognition and thereby preventing translation of the associated protein [144–146]. Lipophilic oligonucleotides are also used in the site-selective immobilization of lipid vesicles to surfaces by linking complementary strands, incorporated in the lipid bilayer of vesicles on the one hand, and in the planar lipid bilayer on a substrate on the other [58, 147, 148]. The surface-bound vesicles can then function as miniaturized experimental containers to reduce reagent consumption, monitor fast chemical kinetics, or even to study single molecules. DNA-functionalized vesicles have also been shown to be of great value to study vesicle fusion, or to model processes like cell-adhesion and cell-cell interactions [149–152]. Recently, we used lipophilic oligonucleotides to decorate lipid bilayer-coated silica microparticles with specific, surface-mobile binding groups, see chapter 4 and ref. [69]. It was found that the lateral diffusion of binding groups afforded by the lipid bilayer greatly improved the microparticle self-assembly properties as compared to oligonucleotides that were directly immobilized on the particles.

Most applications require stable anchoring of the oligonucleotides in the lipid bilayer. Experimental information on the anchoring characteristics of commercially available oligonucleotides remains however limited. Whereas better understanding of the anchoring kinetics and the organization of oligonucleotides on the surface would provide a better control on functionalization, in particular on the DNA grafting density. We therefore measured the lipid bilayer anchoring characteristics of oligonucleotides with three frequently used hydrophobic moieties by the surface-sensitive techniques quartz crystal microbalance with dissipation monitoring (QCM-D) and spectroscopic ellipsometry (SE). The combination of these techniques allows us to monitor binding events *in situ* at high temporal resolution without the need for labels and at the same time provides information about the molecular organization within the DNA film.

The anchors that we have investigated are cholesterol (Ch), stearyl (C_{18}) and di-stearyl $(C_{18})_2$ of which the chemical structures are shown in Fig. 3.1a. In addition, we have studied the differences between single versus double stranded DNA, one versus two anchors and we made the comparison with shorter oligonucleotides. An overview of all the oligonucleotide types and their hydrophobic terminal modifications included in this study is given in Table 3.1 and Fig. 3.1b.

3.2. EXPERIMENTAL METHODS

3.2.1. MATERIALS AND SAMPLE PREPARATION

We studied the anchoring of hydrophobically modified DNA oligonucleotides to a DOPC supported lipid bilayer (SLB), by first forming a lipid bilayer on a planar silica-coated QCM-D sensor and subsequently flowing in the oligonucleotide suspension. To this end, DOPC (Avanti Polar Lipids, Alabaster, AL, USA) was dissolved in chloroform and then

Table 3.1: **Base sequences of the oligonucleotides used in this study.**

name[a]	sequence (5' → 3')[b]
ss-T_{only}-Long	X-TTTTTTTTTTTTTTTTTTTTTTTTTTTTTTTTTTTTTTTTTTTTTTTTTTTTTTT-TTTTTTTT
ss-Long	X-TTTATCGCTACCCTTCGCACAGTCAATCTAGAGAGCCCTGCCTTACGAC-CTACTTCTAC
ss-Long' (no anchor)	CGTAAGGCAGGGCTCTCTAGATTGACTGTGCGAAGGGTAGCGAT
ss-Long'	CGTAAGGCAGGGCTCTCTAGATTGACTGTGCGAAGGGTAGCGATTTT-X
ss-T_{only}-Short	X-TTTTTTTTTTTT

[a] The sequences ss-Long and ss-Long' with and without anchor are complementary to each other and are used to create the double stranded samples.
[b] A, C, G and T are the nucleotides adenine, cytosine, guanine and thymine, respectively. X denotes the position of the hydrophobic modification.

dried with a gentle stream of N_2(g) and two hours of vacuum desiccation. The dried lipids were subsequently re-suspended to 2 mg/ml (2.5 mM) in a filtered (pore-size: 0.2 μm) and degassed (30 min) buffer solution of 150 mM NaCl, 10 mM HEPES, pH 7.4, in ultra-pure water and homogenized by repeating five freeze/thaw cycles with liquid nitrogen. Small unilamellar vesicles (SUVs) were formed by sonication (30 min) with a tip sonicator (Branson, USA), operated in pulsed mode at 30% duty cycle with refrigeration, followed by centrifugation in an Eppendorf centrifuge (30 min at 60,000 *g*) to remove any titanium particles that may possibly be present. SUV suspensions were stored at 4°C under nitrogen. Before assembling a SLB, the vesicle suspensions were diluted to 50 μg/ml (0.06 mM) in the aforementioned buffer containing an additional 2 mM $CaCl_2$.

After the successful formation of a SLB on the QCM-D sensor, we added the oligonucleotides, see Table 3.1 and Fig. 3.1 for an overview of the different types used. The Ch and C_{18} conjugated constructs were synthesized by Eurogentec (Liège, Belgium), and the sequences modified with $(C_{18})_2$ were produced by ATDBio (Southampton, UK). Upon delivery, the oligo-nucleotides were dissolved to desired concentrations in the same buffer as mentioned above without $CaCl_2$ and stored at -20°C. To study the effect of two anchors, or compare single and double stranded DNA bearing only one anchor, some of the sequences in Table 3.1 were pre-hybridized by mixing equal amounts of two complementary strands and slowly cooling from 90 to 22°C at a rate of 1.5°C/min.

3.2.2. CMC DETERMINATION USING SPECTROPHOTOMETRY

We determined the critical micelle concentration (CMC) of our constructs by measuring the absorbance of 1-(2-pyridylazo)-2-naphthol (PAN), a water insoluble organic dye at 470 nm [153]. Below the CMC, the dye does not dissolve in the aqueous solution, and the absorbance of the solution remains low. At the CMC, a sudden rise in the solution's absorbance is observed, as the dye is encapsulated in micelles and dissolves in solution. For each compound, a titration series was prepared with final sample volumes of 450 μl. Subsequently, 20 μl PAN (Sigma) suspension (0.2 mg/ml dissolved in hexane) was added to each sample. The samples were vortexed and the hexane was allowed to evaporate for 30 minutes. The absorbance of each solution at 470 nm was measured using a Cary300

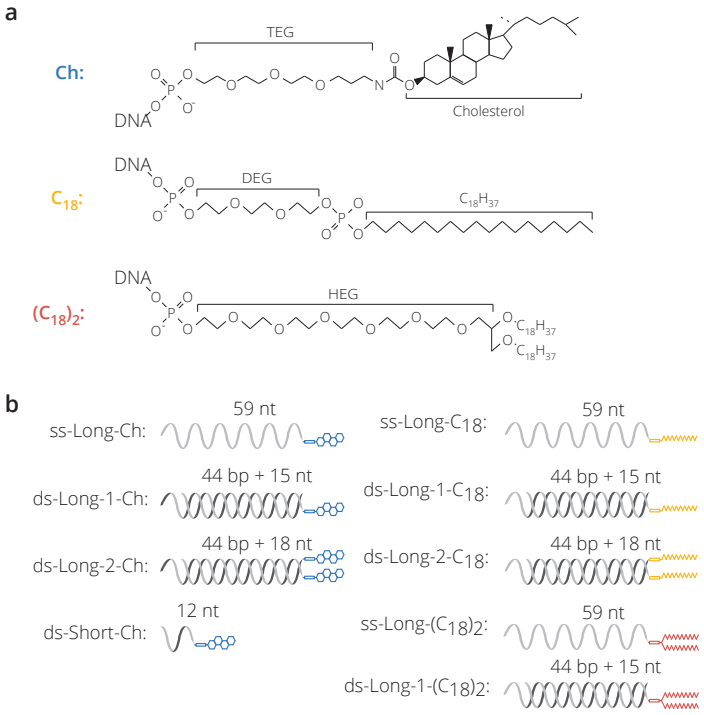

Figure 3.1: Oligonucleotides modified with different lipophilic moieties to anchor them to a DOPC SLB. (a) The three anchors: cholesterol (Ch), stearyl (C_{18}) and di-stearyl ($(C_{18})_2$) are each covalently coupled to one end of the oligonucleotides through the linkers TEG = triethylene glycol, DEG = diethylene glycol and HEG = hexaethylene glycol, respectively. The positions where the oligonucleotides are coupled to the anchor are indicated by 'DNA'. (b) Schematic representations of all the complexes analyzed in this study. Each name is built out of three parts; first, the configuration of the oligonucleotide sequence, i.e. single or double stranded (ss or ds), the length and finally the anchor type. The number of nucleotides (nt) and basepairs (bp) are indicated above each structure.

UV/Vis Spectrometer (Agilent, Santa Clara, CA, USA).

3.2.3. QCM-D

Quartz Crystal Microbalance with Dissipation monitoring (QCM-D) measures the changes in the resonance frequency, Δf, and dissipation, ΔD, of a sensor crystal upon interaction of soft matter with its surface. The QCM-D response is sensitive to the mass (including any hydrodynamically coupled water) and the mechanical properties of the surface-bound layer. To enable SLB formation, we used silica-coated QCM-D sensors (QSX303; Biolin Scientific, Västra Frölunda, Sweden), which were cleaned in a 2% sodium dodecyl sulfate solution for 30 minutes, rinsed with ultra-pure water, blow-dried with N_2(g) and exposed to UV/ozone (BioForce Nanosciences, Ames, IA, USA) for 30 minutes prior to usage. The measurements were performed using the Q-Sense E4 system equipped with four Q-Sense Flow Modules (Biolin Scientific). The system was operated in flow mode at a rate of 20 μl/min at 23 °C unless stated otherwise. The Δf and ΔD responses at 6 over-

tones (i = 3, 5, …, 13, corresponding to resonance frequencies of 15, 25, …, 65 MHz) were simultaneously monitored during SLB formation and subsequent DNA binding and unbinding. Throughout this manuscript only changes in dissipation, ΔD_i and normalized frequencies, $\Delta f_i/i$, for i = 7 are presented. The oligonucleotides were diluted to 1 μM concentrations unless stated otherwise and were added after a proper SLB had formed. We continued the administration of oligonucleotides until saturated binding was reached or for a maximum of 60-75 minutes, after which we rinsed the functionalized SLB with buffer to measure any potential unbinding of the oligonucleotides. The adsorption and desorption of all oligonucleotides were measured two to four times. Representative measurements are presented in the displayed figures.

The thickness and viscoelastic properties of the final DNA film on the SLB were determined by fitting the QCM-D data to a continuum viscoelastic model [154–156]. The model relates the measured QCM-D responses, Δf and ΔD as a function of i, to the viscoelastic properties of the adsorbed layer and the surrounding solution. The oligonucleotide films were modeled as homogeneous viscoelastic layers with acoustic thickness d, density ρ, storage modulus $G'(f)$, and loss modulus $G''(f)$. The frequency dependence of the storage and loss moduli was assumed to follow power laws, with exponents α' and α", respectively. The semi-infinite bulk solution was assumed to be Newtonian with a viscosity of η = 0.89 mPa·s, and a density of ρ = 1.0 g/cm^3. Data at selected time points were fitted with the software QTM (D. Johannsmann, Technical University of Clausthal, Germany[155, 156]). Details of the fitting procedure, including the method used to validate the uniqueness of the fit, have been described by Eisele et al.[157]. The normalized χ^2 value for the best fit was typically around 1.0, indicating a good fit.

3.2.4. SPECTROSCOPIC ELLIPSOMETRY

Spectroscopic ellipsometry (SE) measures the changes in the ellipsometric angles, Δ and Ψ, of polarized light upon reflection at a planar surface. *In situ* combined QCM-D/SE measurements were performed on QCM-D sensors with a special silica coating (QSX335; Biolin Scientific), using the Q-Sense Ellipsometry Module (Biolin Scientific). The special coating consists of Ti, TiO_2 and SiO_2 layers, where the Ti interlayer is thick enough to be treated as a fully opaque film. The flow module was mounted with the Q-Sense E1 system on a spectroscopic rotating compensator ellipsometer (M2000V, Woollam, NE, USA). Ellipsometric data, Δ and Ψ, were acquired over a wavelength range λ = 380 to 1000 nm, at 65° angle of incidence. Prior to measurements, we verified that the polarization of the light beam was not affected by the glass windows of the flow chamber as previously described[158]. Measurements were performed in flow mode (20 μl/min) at 23°C. The oligonucleotides were dissolved to 2 μM concentration and added in injection mode as described elsewhere[158].

The refractive index ($n(\lambda)$) and optical thickness (d) of the oligonucleotide film were determined by fitting the ellipsometric data to a multilayer model, using the software CompleteEASE (Woollam). The model relates the measured Δ and Ψ as a function of λ to the optical properties of the sensor surface ($Ti/TiO_2/SiO_2$), the adsorbed films (SLB and oligonucleotide layer), and the surrounding solution. The semi-infinite bulk solution was treated as a transparent Cauchy medium, with a refractive index $n_{sol}(\lambda) = A_{sol} + B_{sol}/\lambda^2$. For the surrounding buffer solution, A_{sol} = 1.325 and B_{sol} = 0.00322 μm^2

were used[158]. The optical properties of the opaque Ti layer were determined from data acquired in air and in the presence of bulk solution by fitting $n_{\mathrm{Ti}}(\lambda)$ and $k_{\mathrm{Ti}}(\lambda)$ over the accessible wavelength range using a B-spline algorithm implemented in CompleteEASE. Simultaneously, thicknesses of the two additional oxide layers ($d_{\mathrm{TiO_2}}$) and ($d_{\mathrm{SiO_2}}$) were fitted assuming them as Cauchy films with tabulated optical constants ($n_{\mathrm{TiO_2}}$ from CompleteEASE and $n_{\mathrm{SiO_2}}$ from Biolin Scientific). The solvated SLB and oligonucleotide films were treated as separate layers, which we assumed to be transparent and homogeneous (Cauchy medium), with a given thickness (d), a wavelength-dependent refractive index ($n(\lambda) = A + B/\lambda^2$), and a negligible extinction coefficient ($k = 0$). d and A were treated as fitting parameters, assuming $B = B_{\mathrm{sol}}$. The χ^2 value for the best fit was typically below 2, indicating a good fit. The adsorbed oligonucleotide mass per unit area (Γ) was determined using de Feijter's equation[159, 160],

$$\Gamma = d \cdot \frac{A - A_{\mathrm{sol}}}{\mathrm{d}n/\mathrm{d}c} \tag{3.1}$$

with the refractive index increment of $\mathrm{d}n/\mathrm{d}c = 0.17\ \mathrm{cm^3/g}$ [161].

3.3. RESULTS AND DISCUSSION

3.3.1. BEHAVIOR OF DIFFERENT ANCHOR TYPES

We measured the lipid-bilayer anchoring strengths of the different hydrophobic anchoring groups, Ch, C_{18} and $(C_{18})_2$ using QCM-D. A supported lipid bilayer (SLB) was formed by exposing a cleaned, silica-coated quartz crystal to a flowing suspension of small unilamelar vesicles made of DOPC lipids, while monitoring the frequency and dissipation changes of the sensor. The QCM-D response was as is expected for the formation of a DOPC SLB, see Fig. 3.2 and Refs. [125, 162]. The adsorption of the vesicles to the sensor surface is visible as a decreasing frequency and an increasing dissipation. In a second stage, the vesicles rupture and spread, signaled by an increasing frequency and decreasing dissipation. A DOPC SLB of appropriate quality is characterized by a final frequency change of $\Delta f = -25 \pm 1$ Hz and a dissipation, $\Delta D \leq 0.5 \cdot 10^{-6}$. The vesicles remaining in the bulk solution were removed by rinsing with buffer (with $CaCl_2$). Before the inflow of oligonucleotide suspension, the SLB was rinsed with buffer without $CaCl_2$ for 15 min.

We first verified that the oligonucleotide binding/unbinding is not affected by unwanted non-specific interactions. For this purpose, the QCM-D responses of unmodified oligonucleotides in contact with an SLB and of cholesterol modified oligonucleotides in contact with a bare silica coated sensor were measured. During both measurements no significant responses were detected, implying that the oligonucleotides do not exhibit any non-specific interactions with the SLB nor with the underlying silica substrate, see Fig. 3.3. Exploratory measurements of the binding and unbinding of ss-Long-Ch to a SLB, indicated, however, that inter-DNA interactions on the surface can affect the DNA (un)binding, see Fig. 3.4. At 1 μM bulk concentrations, DINAMelt predicts a melting temperature (T_{m}) of roughly 0 °C for two partially hybridized ss-Long-Ch oligonucleotides. However, if one considers a surface density of 2 pmol/cm^2 and a layer thickness of 10 nm (estimated from combined QCM-D and SE measurements presented in section: 3.3.3), the effective oligonucleotide concentration at the surface is roughly 2000 times the bulk concentration. At 2 mM concentration, a melting temperature of about 30 °C is pre-

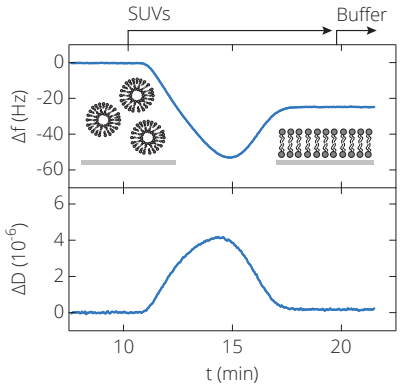

Figure 3.2: Formation of a supported lipid bilayer (SLB) on a silicon oxide substrate. A SLB is formed by exposing a clean silicon oxide coated sensor crystal to suspended SUVs and monitoring the crystals' Δf and ΔD responses in time. The arrows from left to right indicate the start and duration of sample administration and buffer rinsing respectively. A uniform SLB is characterized by $\Delta f \sim$ -25 Hz and $\Delta D \leq 0.5{\cdot}10^{-6}$.

dicted. During the QCM-D measurements, inter-DNA interactions could hence occur. To minimize such interactions, we performed the measurements on single stranded DNA using a sequence of only thymine nucleotides.

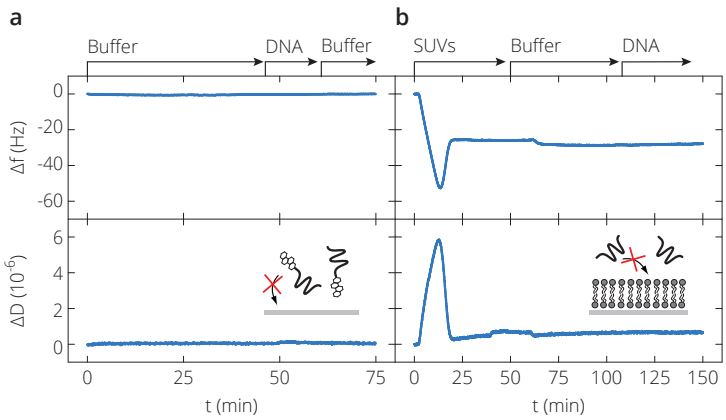

Figure 3.3: QCM-D measurements on the adsorption and desorption of (a) cholesterol modified oligonucleotides (ss-Long-Ch) to a bare silica coated QCM-D sensor and (b) unmodified oligonucleotides (ss-Long (no anchor)) to a SLB. The arrows indicate the start and duration of sample administration or buffer rinsing, as indicated.

Fig. 3.5a shows the QCM-D responses measured upon the introduction of the constructs ss-Long-T_{only} modified with Ch, C_{18} or $(C_{18})_2$ to a SLB. The resulting strong shifts in the resonance frequency Δf and in the dissipation ΔD provide evidence for the successful formation of a soft and hydrated DNA film in all three cases. Interestingly, in Fig. 3.5a the adsorption kinetics for the different anchor types is substantially different.

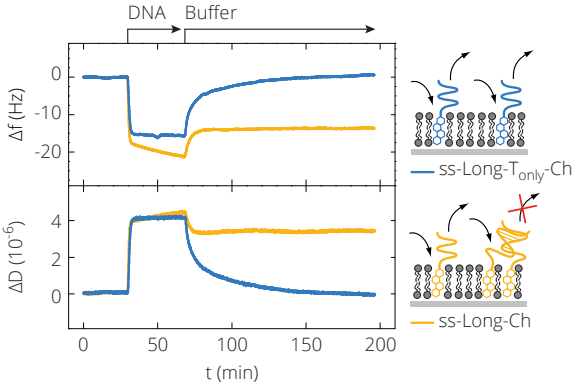

Figure 3.4: Comparison between the QCM-D measurements on the adsorption and desorption to a SLB of Ch modified oligonucleotides with the sequence ss-Long or ss-Long-T_{only}. The arrows from left to right indicate the start and duration of sample administration and buffer rinsing, respectively. As can be seen in the plots, the incomplete unbinding of the ss-Long-Ch upon rinsing suggests the occurrence of interactions other than those between the hydrophobic anchors and the SLB. We hypothesize that, due to a high surface density at equilibrium binding, the ss-Long-Ch anchored to the SLB can interact with neighboring oligonucleotides. The interacting oligonucleotides form constructs that are anchored to the bilayer by more than one anchor which stabilizes their incorporation into the SLB. The unbinding of ss-Long-T_{only}-Ch remains seemingly unperturbed, suggesting that the probability of inter-DNA interactions is sufficiently decreased.

The Ch anchor incorporates the oligonucleotides the fastest into the SLB, followed by C_{18} and finally $(C_{18})_2$.

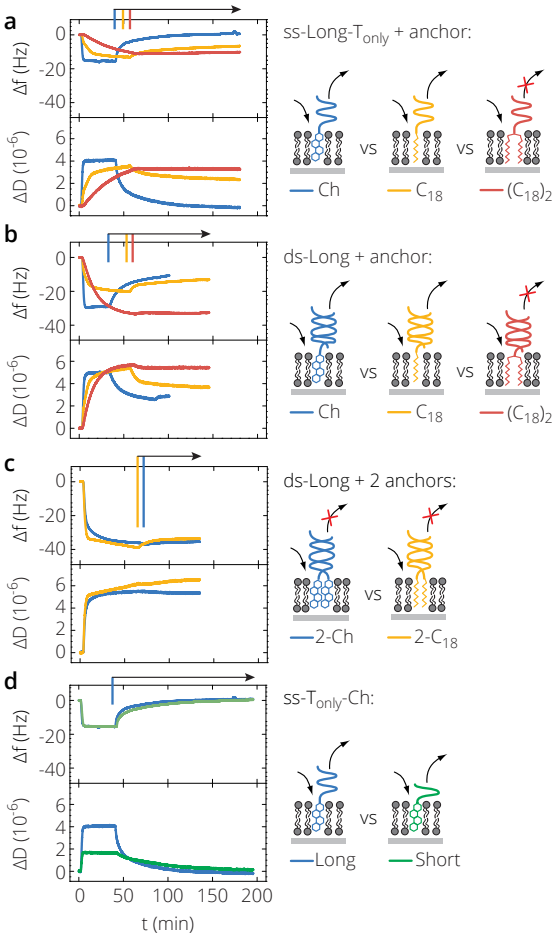

Figure 3.5: QCM-D measurements on the adsorption and desorption of different oligonucleotides modified with either Ch, C_{18} or $(C_{18})_2$ to a DOPC SLB. (a) The frequency Δf (top) and dissipation ΔD (bottom) changes upon exposure of a SLB to ss-Long-T_{only} conjugated with either Ch, C_{18} or $(C_{18})_2$ plotted as a function of time. (b) The plots of Δf (top) and ΔD (bottom) upon exposure of a SLB to double stranded complexes carrying one anchor. (c) The plots of Δf (top) and ΔD (bottom) upon exposure of a SLB to double stranded complexes carrying two anchors. (d) Plots of Δf (top) and ΔD (bottom) upon exposure of a SLB to ss-Long-T_{only}-Ch or ss-Short-T_{only}-Ch. Note that the graph of ss-Long-Ch is the same as in (a). In all measurements the oligonucleotides were injected at t = 0 until rinsing with buffer was initiated, which is indicated by the arrows.

To further explore the origin of the distinct kinetics we repeated the QCM-D measurements on the samples depicted in Fig. 3.6a at increased flow rates of 100 and 200 μl/min. Under conditions of mass-transport limited binding, and considering the geometry of the liquid chamber (i.e. laminar flow in a slit), the adsorption rate would be expected to be linearly proportional to the cube root of the flow rate [163]. In contrast, no dependence on the flow rate would be expected if the binding process were (kinetically) limited by the insertion step into the SLB. To quantify the adsorption rates in our experiments, we numerically computed the derivative of Δf by calculating the slopes at each point in time (see for an example Fig. 3.6a, bottom graph) and plotted its minimum as a function of $\sqrt[3]{Q}$, see Fig. 3.6b. Next the data points were fitted with a line through the origin. The good agreement of the linear fits with the maximum absolute rates of frequency shifts depicted in Fig. 3.6b (R^2~1) shows that the maximum adsorption rates of the oligonucleotides are linearly proportional to $\sqrt[3]{Q}$ independent of anchor type. This suggests that the rate limiting step during adsorption is the transport (by convection and diffusion) of the constructs to the SLB.

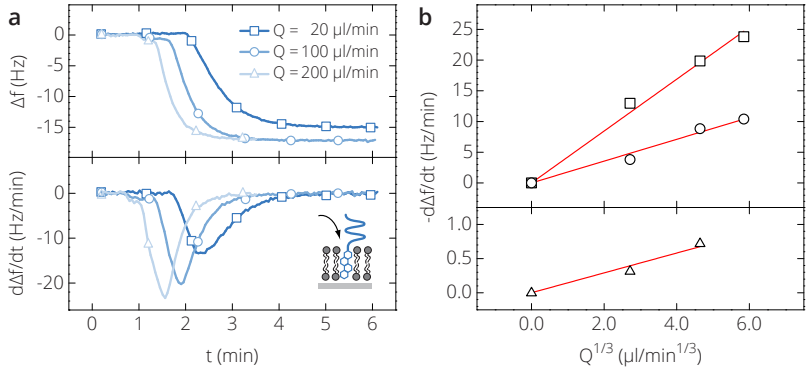

Figure 3.6: The flow rate dependence of the adsorption of Ch, C_{18} and $(C_{18})_2$ conjugated oligonucleotides to a DOPC SLB. (a) The frequency changes Δf (top) and their computed derivatives (bottom) during the adsorption of ss-Long-T_{only}-Ch to a SLB at different flow rates (Q) plotted as a function of time. (b) The minima of the computed derivatives shown in (a) and of the other anchors plotted as a function of $\sqrt[3]{Q}$. The plotted minima were fitted to a linear model with fixed origin at (0,0). The quality of the fits are determined by evaluating the corresponding R^2 and are found to be 0.996, 0.99 and 0.98 for Ch, C_{18} and $(C_{18})_2$, respectively.

As the hydrodynamic sizes of the three hydrophobically terminated oligonucleotides are similar, their respective mass transport to the surface at equal flow rate is expected to be the same, provided that the concentration of molecules available in the solution is comparable [163]. As the total oligonucleotide concentration in the measurements of Fig. 3.5a was kept constant, the distinct adsorption kinetics of the differently hydrophobically modified oligonucleotides may appear surprising. However, due to their amphiphilic character, the modified oligonucleotides could self-assemble into micelles in the bulk solution. The micelles would lower the concentration of free oligonucleotides in solution and would hence impede adsorption to the SLB. Rough determinations of the critical micelle concentration (CMC) show that Ch and C_{18} modified oligonucleotides form micelles above ~10 μM, whereas the $(C_{18})_2$ anchor has a CMC of ~1 μM (cf. Fig. 3.7).

Given a solution concentration of 1 μM in our QCM-D experiments, the $(C_{18})_2$ conjugated oligonucleotides may indeed form micelles that influence the adsorption process.

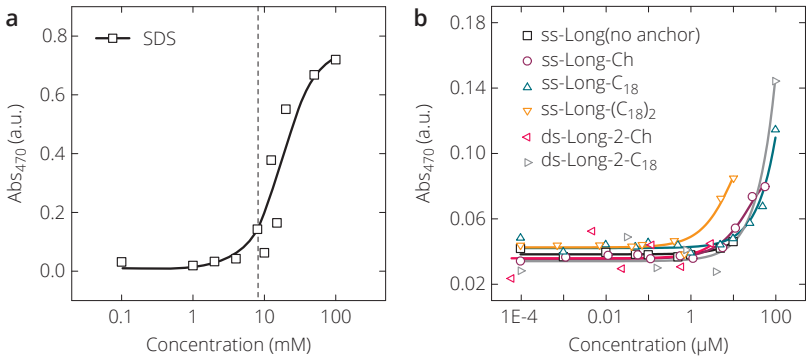

Figure 3.7: Detecting the CMC for hydrophobically modified oligonucleotides using UV-Vis spectroscopy. (a) Measured absorptions at 470 nm of differently concentrated SDS suspensions mixed with PAN/Hexane and ultrapure water. The solid black line is a guide for the eyes and the dashed black line indicates the CMC of SDS published in literature [164]. (b) Measured adsorptions at 470 nm of different concentrations of the oligonucleotides ss-Long'(no anchor), ss-Long-T_{only} conjugated to Ch, C_{18} or $(C_{18})_2$, and ds-Long conjugated to two Ch or C_{18} anchors in a solution of PAN/Hexane and buffer. The solid lines are guides for the eyes.

When the oligonucleotide solution was replaced by pure buffer, the frequency and dissipation responses of the sample with the Ch modified oligonucleotides were seen to return to their original level, thereby demonstrating complete desorption of the oligonucleotides from the SLB (Fig. 3.5a). Regarding figure 3.5d, the reversible binding of single anchored/single stranded was not strongly affected by the oligonucleotide length, as both ss-Long-Ch and ss-Short-Ch desorbed at roughly similar rates upon rinsing. The C_{18} conjugated strands also desorb from the SLB during rinsing, yet do not seem to come off completely within the time scale probed in the experiment. This effect could be caused by fast rebinding of the oligonucleotides to the SLB [163]. The $(C_{18})_2$ modified oligonucleotides on the other hand remain fully anchored during rinsing, which suggests that the second alkyl chain makes the hydrophobic interaction with the SLB strong enough to beat the gain in translational and conformational entropy when the oligonucleotides are freely suspended in solution.

3.3.2. DOUBLE VERSUS SINGLE ANCHORS

Having seen that the $(C_{18})_2$ conjugated oligonucleotides, which have two hydrophobic tails, bind essentially irreversibly to the SLB, we studied the impact of a second anchor on the anchoring stability of the other constructs. To this end, we hybridized two complementary oligonucleotides, ss-Long and ss-Long' (see Table 3.1) resulting in double stranded complexes of which both strands bear a hydrophobic moiety. Firstly, we investigated how the structure difference between single and double stranded oligonucleotides with a single anchor affects their adsorption and desorption to the SLB. For that purpose we hybridized ss-Long and ss-Long'(no anchor), creating double helices that bear only one anchor, and monitored the QCM-D responses upon interaction with a SLB. One

can see in Fig. 3.5b that the single anchored/double stranded complexes either conjugated to Ch or C_{18} adsorb to the SLB in a qualitatively similar manner as their single anchored/single stranded counterparts. They reach maximum binding at comparable rates and desorb during rinsing. Only the absolute frequency and dissipation values at maximum binding are different, indicating that the layers of oligonucleotides on the SLB are indeed differently organized. We further see that the desorption is incomplete. A possible explanation for this could be that there is a certain amount of unhybridized oligonucleotides, which could bind to other single stranded neighbors in a process that has been described in Section 3.3.1. We also measured the QCM-D responses of the ds-Long-1-$(C_{18})_2$. Here, we again see that the single anchored/double stranded complex behaves qualitatively similar as its single stranded analog, although showing larger frequency and dissipation changes.

After confirming that double-stranded oligonucleotides display qualitatively similar behavior, we measured the adsorption kinetics and stability of double stranded oligonucleotides carrying two anchors (Fig. 3.5c). We find that the QCM-D responses upon rinsing with buffer show no substantial unbinding of either of the complexes, demonstrating that terminally equipping oligonucleotides with two hydrophobic moieties grants a stable binding to a SLB. Furthermore, we find that the adsorption of the double-anchored/double stranded complexes either bearing two Ch or two C_{18} groups is initially fast but gradually slows down. We hypothesize that the binding is initially mass-transport limited and then increasingly limited by surface crowding which slows down access of oligonucleotides from the solution to the surface.

3.3.3. OLIGONUCLEOTIDE ORGANIZATION ON THE SURFACE

When the Δf and ΔD responses corresponding to the binding and unbinding of the Ch, C_{18} and $(C_{18})_2$ conjugated oligonucleotides to a SLB are plotted parametrically it can be seen that the three curves largely overlap (see Fig. 3.8a). The fact that the $\Delta f/\Delta D$ relations are so similar implies that the three oligonucleotide layers are similarly organized. This observation is further supported by the quantities obtained from QCM-D modeling on Δf and ΔD using the information from all overtones. From the values listed in Table 3.2 it becomes clear that the three oligonucleotide layers at the end of the incubation (Fig. 3.5a) are characterized by comparable thicknesses (d $\approx$ 10.5 nm) and viscoelastic properties ($G_0' \approx 0.05$ MPa, $G_0'' \approx 0.12$ MPa, where $G'(f) = G_0' \cdot (f/f_0)^{\alpha'}$ and $G''(f) = G_0'' \cdot (f/f_0)^{\alpha''}$ and $f_0 = 15$ MHz).

In order to relate the QCM-D frequency shifts induced by the anchorage of the hydrophobically terminated oligonucleotides to a SLB to DNA areal mass densities, we performed simultaneous QCM-D/SE measurements. Results of the measurement of the adsorption of ss-Long-T_{only}-C_{18} to an SLB are shown in Fig. 3.4b and c. Strong Δf and Γ changes directly upon injection of the oligonucleotides indicate the formation of an oligonucleotide layer on top of the SLB. In the inset, we plotted Δf vs Γ parametrically to demonstrate that Γ is approximately linearly proportional to Δf with a slope of 0.14 pmol·cm^{-2}·Hz^{-1}. This slope is subsequently used to convert Δf to Γ in all other QCM-D measurements on this particular oligonucleotide. Furthermore, because the overlapping curves in Fig. 3.8a suggest that the ss-Long-T_{only} oligonucleotides organize similarly on the SLB independent of the anchor, the same slope can also be used to obtain the grafting

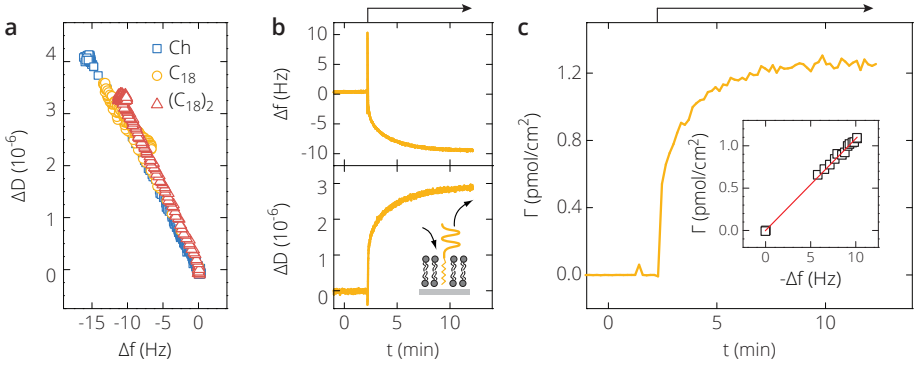

Figure 3.8: Determining the densities of the Ch, C_{18} and $(C_{18})_2$ conjugated oligonucleotides anchored to a DOPC SLB. (a) Parametric plots of ΔD as a function of Δf of the data depicted in Fig. 3.2a. (b) Plots of Δf (top) and ΔD (bottom) as a function of time corresponding to the binding of ss-Long-T_{only}-C_{18} to a SLB. Simultaneously, the surface density Γ was measured with SE as depicted in (c). The inset shows a parametric plot of Δf versus Γ, fitted to a linear model (red line) with a slope of -0.14 pmol·cm^{-2}·Hz^{-1}. The arrows in (b) and (c) indicate the start and duration of injection.

densities of the Ch and $(C_{18})_2$ anchored ss-Long-T_{only} oligonucleotides. We note that the calibration curve in Fig. 3.8c (inset) is applicable for the seventh overtone only. Equivalent calibration curves for other overtones can of course be established. They do all show a roughly linear dependence of Γ on Δf but result in different conversion factors. The DNA surface density and the affinity of the anchor with the SLB, however, do not depend on the choice of overtone.

Using the obtained grafting densities and by assuming a homogeneous distribution of hexagonally packed oligonucleotides in the SLB, we estimated the mean distance between neighboring anchors points,

$$s = \sqrt{\frac{2}{\sqrt{3}} \cdot \frac{1}{N_A \cdot \Gamma}} \tag{3.2}$$

where N_A is the Avogadro constant and Γ is the surface density in mol·cm^{-2}. The prefactor $\frac{2}{\sqrt{3}}$ represents an assumed hexagonally packed organization of the objects. The Γ and s of the oligonucleotide layers mediated by Ch, C_{18} and $(C_{18})_2$ are listed in Table 3.2. One can see that the spacing between the anchors in the case of Ch, C_{18} and $(C_{18})_2$ is similar to the thickness of the oligonucleotide layer. The thickness and spacing compare well with the equilibrium end-to-end distance $R_{ee} = \sqrt{2 b_{nt} l_p k_{nt}}$ of ~13 nm of a worm-like chain of $k_{nt} = 59$ nucleotides of size $b_{nt} \approx 0.63$ nm and with a persistence length $l_p \approx 2.4$ nm [165].

Similarly, we determined the oligonucleotide organization of the double stranded/double anchored ds-Long-2-Ch depicted in Fig. 3.5c at the moment just before rinsing. After modeling the QCM-D data and having determined the Δf-to-Γ conversion factor with combined QCM-D and SE (Fig. 3.9), we obtained a layer thickness of ~19 nm and an average oligonucleotide spacing of ~10 nm (Table3.2). Hence, the ds-Long-2-Ch complexes form a layer which is twice as thick as compared to the single stranded oligonu-

cleotides, but with a comparable oligonucleotide spacing. A double stranded oligonucleotide of k_{bp} = 47 basepairs, when assumed as a semi-flexible rod has in solution an estimated end-to-end distance R_{ee}(= $b_{bp}k_{bp}$) of ~16 nm with a distance between basepairs b_{bp} of 0.34 nm. The ds-Long complex also has a 12 nucleotide overhang ($R_{ee} \approx$ 6 nm) which means that the total $R_{ee} \approx$ 22 nm, which is very comparable to the layer thickness as determined with QCM-D, hence the oligonucleotides anchored to the SLB are likely to be close-to-fully stretched and orientated perpendicular to the surface. Yet, regarding the estimated spacing and given a diameter of the double stranded complexes of ~2.0 nm there may be a certain amount of oligonucleotides that flex at their spacer, leaving them differently orientated with respect to the SLB.

Lastly, we investigated how the anchoring density is affected by the length of the oligonucleotides by performing QCM-D/ SE measurements on the binding of Ch modified ss-Short-T_{only} oligonucleotides to a SLB (Fig. 3.9a). We determined the layer thickness of the films with QCM-D modeling to be ~3 nm which is a factor three thinner than the layer of the longer oligonucleotides, see Table 3.2. After determining the Δf-to-Γ relation (Fig. 3.9b) we found a spacing of ~5 nm between individual oligonucleotides. A comparable measurement on hydrophobically modified oligonucleotides to a DOPC lipid bilayer has been done by Woller et al [166]. They studied the anchoring of oligonucleotides functionalized with a single porphyrin anchor positioned at a fixed nucleotide position and report for 39-mer single stranded oligonucleotides a surface area of 40 nm^2 per strand at saturated binding which is equal to a spacing of ~6.3 nm. This spacing lies in between the values we find for our short (12-mer) and long (59-mer) oligonucleotides. The fact that the estimated spacing between the anchoring groups for Ch modified ss-Short-T_{only} is nearly twice as large as the thickness of the oligonucleotide film indicates that the DNA is not closely packed. Hence, of all the constructs measured in this study the anchoring process of the short oligonucleotide is expected to be the least affected by steric interactions with neighboring oligonucleotides. This, in combination with the complete reversibility of the binding upon rinsing and the good solubility makes the short oligonucleotide a suitable candidate for quantifying the affinity of the Ch anchor toward the SLB. To this end, we performed a QCM-D titration measurement in which we sequentially administered increasing concentrations of oligonucleotides to a SLB, see Fig. 3.10. We fitted the frequency shifts at equilibrium binding for each concentration to a Langmuir isotherm,

$$\Delta f_{eq}(c) = \frac{\Delta f_{max} \cdot c}{K_D + c} \tag{3.3}$$

where c is the concentration of ss-Short-T_{only}-Ch in the bulk suspension and Δf_{max} is the maximally induced frequency change expected at saturation. In this way we obtained a K_D of ~80 nM, which is of the same order of magnitude as the 17 nM reported by Pfeiffer et al. [116], who performed similar titration measurements on strands comprising twenty nucleotides at 100 mM NaCl.

Table 3.2: **Layer properties of different oligonucleotides anchored to a DOPC SLB through different anchors.**

sequence/anchor	d (nm)[a]	G_0' (MPa)[a]	α'[a]	G_0"(MPa)[a]	α"[a]	Γ (pmol/cm^2)[b]	s (nm)[b]
ss-Long-Ch	11.0 ± 0.8	0.05 ± 0.004	0.26 ± 0.04	0.12 ± 0.002	0.94 ± 0.02	2.1 ± 0.07	9.9 ± 0.15
ss-Long-C_{18}	9.3 ± 2.8	0.04 ± 0.02	0.35 ± 0.04	0.11 ± 0.01	0.95 ± 0.02	1.7 ± 0.13	11.0 ± 0.4
ss-Long-$(C_{18})_2$	8.4 ± 0.9	0.04 ± 0.01	0.38 ± 0.04	0.11 ± 0.004	0.95 ± 0.01	1.5 ± 0.21	12.0 ± 0.9
ds-Long-2-Ch	19.2 ± 5.7	0.03 ± 0.02	0.51 ± 0.06	0.15 ± 0.02	0.93 ± 0.03	2.2 ± 0.05	9.6 ± 0.1
ss-Short-Ch	3.2 ± 0.2	0.47 ± 0.02	0.17 ± 0.04	0.19 ± 0.06	1.02 ± 0.20	7.5 ± 0.35	5.1 ± 0.1

[a] d, G_0', G_0" are respectively the thickness and the storage and loss moduli determined with QCM-D. α' and α" are the power law exponents that describe the frequency dependencies of G' and G", respectively. G_0' and G_0" at f_0 = 15 MHz, α' and α" for f = 15-65 MHz.
[b] Γ and s are respectively the molar surface density and the average anchor spacing (assuming packing in a hexagonal lattice) determined with SE. The values and error bars display the mean and standard deviation obtained from averaging over at least four measurements.

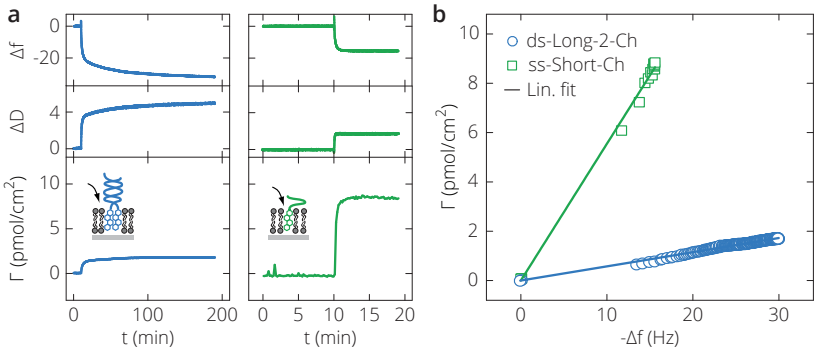

Figure 3.9: Determining the layer organization of ds-Long-2-Ch and ss-Short-Ch. (a) From the top to bottom the graphs present Δf, ΔD and Γ as a function of time of the binding of ds-Long-2-Ch (left) and ss-Short-Ch (right) to a SLB. The arrows indicate the start and duration of binding of the oligonucleotides. (b) Parametric plots of the measured Δf and Γ presented in (a). The slopes of the fits are -0.06 and -0.60 pmol·cm^{-2}·Hz^{-1} for ds-Long-2-Ch and ss-Short-Ch, respectively. Note that the calibration curves are applicable for the seventh overtone only, as also mentioned in the main text.

3.4. CONCLUSION AND PERSPECTIVES

Oligonucleotides can be anchored to lipid bilayers through diverse hydrophobic modifications. Here, we have investigated the binding characteristics of three frequently used anchors to a DOPC supported lipid bilayer (SLB) with the surface sensitive techniques QCM-D and SE.

We find that the choice of anchor type is crucial for the stable binding of oligonucleotides to a DOPC SLB. Oligonucleotides conjugated to a single cholesterol (Ch) or stearyl (C_{18}) anchor were found to bind reversibly to the SLB, desorbing again upon rinsing with pure buffer. The anchoring can be enhanced by conjugating single stranded oligonucleotides to a di-stearyl ((C_{18})$_2$) anchor, or by hybridizing two Ch or C_{18} bearing oligonucleotides into double stranded complexes.

We further find that the different anchors display different adsorption kinetics. For all the anchors, the binding is limited by the transport of molecules to the substrate. However, some of the hydrophobically modified oligonucleotides may form micelles at the concentrations employed, especially the (C_{18})$_2$ anchor. Hence, it is likely that the difference in binding kinetics is caused by differences in the effective concentration of free oligonucleotides, as a result of micelle formation.

Lastly, concerning the organization of the oligonucleotides, we find that the 'long' single stranded/single anchored oligonucleotides form an equilibrium film of densely packed strands, independent of whether the binding is reversible or not. At the same bulk concentration, the double stranded/double anchored constructs, which also bind irreversibly to the SLB, form a less densely packed film. However, the lack of equilibrium binding indicates a coverage-dependent reorganization of the DNA that we attribute to the more rigid character of the double stranded helices.

We find that the length and the conformational flexibility (i.e. single vs. double stranded DNA) does not have an appreciable effect on binding stability over the length

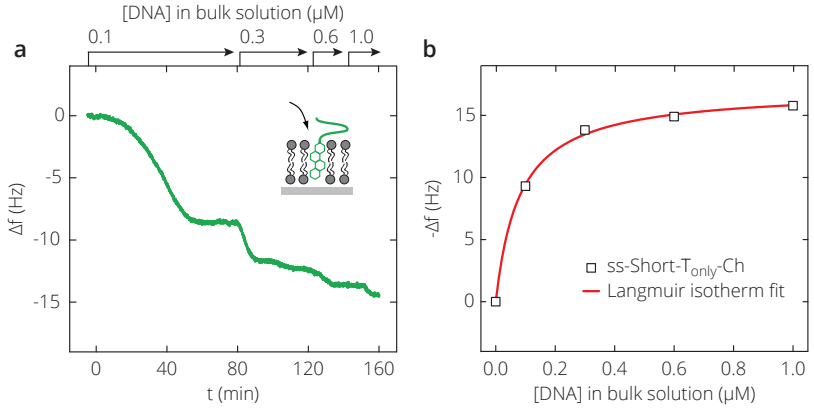

Figure 3.10: Anchorage of a cholesterol conjugated oligonucleotide containing 12 bases (ss-Short-T_{only}-Ch) to a DOPC SLB. (a) Titration curve, determined by QCM-D for the binding of ss-Short-T_{only}-Ch to a SLB. The arrows indicate start and duration of incubation with the indicated oligonucleotide concentrations to the SLB. (b) Frequency shifts (approximately proportional to adsorbed amounts) for ss-Short-T_{only}-Ch at equilibrium with a fit by a Langmuir isotherm (solid red line).

range that was covered in our experiments and that was also typically used by others. In future studies, it will be interesting to investigate if the conformational flexibility of the oligonucleotides does affect the anchoring stability for very long DNA chains. In particular, a decrease in binding stability would be expected as flexibility and length increase, because of the entropic penalty related to the reduced conformational space of anchored DNA.

To conclude, the presented results on the anchoring kinetics and stability of hydrophobically modified oligonucleotides incorporated into a DOPC lipid bilayer as well as the organization of the extending oligonucleotides provide essential information for optimizing applications that require efficiently anchored, surface mobile oligonucleotides. Our results on a simple yet well-defined DOPC membrane model system should serve as a valuable reference for future work on more complex lipid membranes.

We would like to acknowledge Ralf Richter and Galina Dubacheva for facilitating and collaborating on the QCM-D and SE measurements. We thank John Randolph of Glen Research for the synthesis of the stearyl conjugated oligonucleotides and Florian Huber for a critical reading of the manuscript.

4

SOLID COLLOIDS WITH SURFACE-MOBILE DNA LINKERS

Surface functionalization with bio-inspired binding groups is increasingly used to steer nano- and micro-scale self-assembly processes, with complementary DNA 'sticky ends' as one of the most notable examples. The fabrication of well-organized structures is complicated, however, by the sharp association/dissociation transitions and the slow rearrangement kinetics intrinsic to collections of discrete, surface-immobilized binding groups and aggravated by natural nonuniformities in the surface coating. In this chapter, we demonstrate a novel system of solid microparticles functionalized with specific binding groups - in this case DNA linkers - that are fully mobile along the particle surface. These colloids display qualitatively new behavior and circumvent many of the commonly encountered issues. Importantly, the association/dissociation transition, and thereby the temperature window for equilibrium self-assembly, is much broader. We further find that the linkers are uniformly distributed above the DNA melting temperature, while visibly accumulating at the inter-particle contacts below this temperature. The unique combination of binding group mobility with non-deformability, monodispersity and facile manipulation of solid particles should have a profound impact on DNA-mediated and other bio-inspired self-assembly approaches. Moreover, our highly tunable experimental system enables detailed model investigations that will also deepen our fundamental understanding of other systems with surface-mobile binding groups, for instance biological ligand-receptor interactions.

The content of this chapter has been published as: S. A. J. van der Meulen, M. E. Leunissen, *J. Am. Chem. Soc.* **135**, 15129–34 (2013).

4.1. INTRODUCTION

Over the past two decades, the programmability of the behavior of nano-/micro-scale particle suspensions has been dramatically improved, in particular through the use of highly specific non-covalent binding groups that are immobilized on the particle surface. Many of these binding groups are biologically inspired molecular recognition motifs, for instance taking the form of naturally occurring peptides [167–170] or synthetic DNA sticky ends [1, 2, 4, 5, 61, 63, 79, 171]. The latter are especially promising, because they offer a large variety of user-defined nucleotide sequences and fine thermal control of the binding strength. Using DNA-coated particles, a number of groups recently obtained ordered crystals [4, 5, 63, 79] and self-assembled "colloidal molecules" [171]. However, the fabrication of such well-organized structures typically requires extensive fine-tuning and annealing of the system. One of the challenges lies in the sharp association/dissociation transition of the particles when one crosses the melting temperature of the DNA linkers[1, 11, 64, 65, 81, 82]. The temperature window for equilibrium self-assembly thus is easy to miss, leading to "hit & stick" type aggregation without further structural rearrangements. It was also shown that the particles generally have difficulty rolling around each other [172, 173], which may dramatically slow the annealing process, as compared to colloids with a continuous interaction potential, e.g. of electrostatic origin.[23, 174, 175] The intrinsic self-assembly challenges posed by collections of discrete, surface-immobilized binding groups are further aggravated by surface heterogeneities, such as roughness [63] or natural non-uniformities in the coating [11], as well as unwanted non-specific interactions. Here, we present a novel system of solid colloids functionalized with specific (DNA) binding groups that are fully mobile along the particle surface, which alleviates many of the aforementioned problems and provides access to profoundly new behavior.

4.2. MATERIALS AND METHODS

4.2.1. PARTICLE FUNCTIONALIZATION

We functionalized silica micro-particles with mobile DNA linkers by first integrating the hydrophobically modified linkers into the lipid bilayer of small unilamellar vesicles (SUVs, Fig. 4.1a). To this end, the phospholipids 1,2-dioleoyl-*sn*-glycero-3-phosphocholine (DOPC, Avanti) or 1,2-dipalmitoyl-*sn*-glycero-3-phosphocholine (DPPC, Avanti) and 1, 2-dipalmitoyl-*sn*-glycero-3-phosphoethanolamine-N-[methoxy-(polyethylene glycol)--2000] (DPPE-PEG_{2000}, Avanti) were mixed in 40:1 molar ratio in chloroform. The chloroform was evaporated by a gentle stream of nitrogen and two hours of vacuum desiccation, whereafter the lipids were rehydrated for at least 30 min in 10 mM HEPES/50 mM NaCl (pH 7.4) at a concentration of 2 mg/mL. The lipid mixture was then extruded 21 times through two stacked polycarbonate filters of 30 nm pore size (Avanti). The resulting SUVs were incubated for 15 min with 2-5 μM solutions of cholesterol- conjugated DNA linkers.

We used two different DNA linkers (S and S', Eurogentec) with 11 base long complementary sticky ends and fluorescently labeled with, respectively, FAM-6 and Cy3 (Fig. 4.1 d). The sticky ends were connected to a 47 base pair long double-stranded "backbone" construct with two cholesterol-TEG groups at the opposing end. We prehybridized the

backbone by cooling from 90 to 22 °C at a rate of 1.5 °C/min in 10 mM HEPES/150 mM NaCl (pH 7.4) at an overall concentration of 5 μM (NanoDrop 2000) and with a 50% excess of the "nonsticky" strand. Surfactant-free suspensions of 0.5 wt % nonporous, nonfunctionalized silica microparticles with a diameter of either 1.30, 2.06 (Microparticles GmbH), or 3.56 μm (Bangs Laboratories) and with coefficients of variability of respectively 2.9, 2.2 and 8.7% were exposed to an equal volume of the DNA- functionalized SUV solution for 15 min at 50 °C (Figure 1B). Excess SUVs were removed by pelletizing (30 s at 50 rcf) and resuspending three times in 10 mM HEPES/50 mM NaCl (pH 7.4). The final linker density on the particles was estimated from the DNA:SUV:particle ratio.

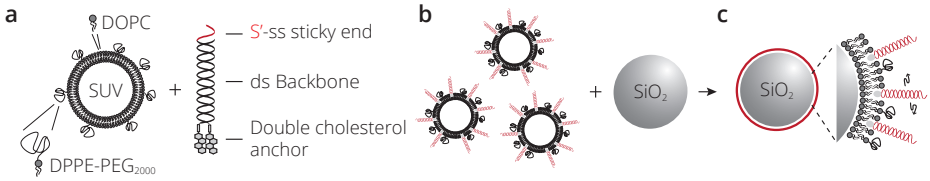

d

Backbone:

```
Cholesterol-TEG-5'- TTTATCGCTACCCTTCGCACAGTCAATCTAGAGAGCCCTGCCTTACGA -3'-sticky end
                    ||||||||||||||||||||||||||||||||||||||||||||||||||
Cholesterol-TEG-3'- TTTTAGCGATGGGAAGCGTGTCAGTTAGATCTCTCGGGACGGAATGC  -5'
```

Sticky-ends:

```
S :   Backbone-5'- GTAGAAGTAGG -3'-FAM6
                   ||||||||||||
S':          Cy3-3'- CATCTTCATCC -5'-Backbone
```

Figure 4.1: Lipid-bilayer-coated microparticles functionalized with laterally mobile DNA binding groups. Experimental functionalization scheme. DOPC:DPPE-PEG2000 SUVs are first mixed with double-cholesterol-conjugated DNA linkers (a) and then with silica microparticles (b), leading to the formation of a DNA-functionalized lipid bilayer that envelopes the particles (c). (d) Base pair sequences of the complementary DNA linkers.

4.2.2. MICROSCOPY SETUP AND IMAGE ANALYSIS

We used a custommade sample cell for our various microscopy studies. These sample cells were prepared by cleaning glass coverslips and objective slides by sonication in, subsequently, 2% Hellmanex and Milli-Q. The cleaned coverslips were exposed to UV-ozone for 30 min in a preheated UV-ozone cleaner (ProCleaner). Slivers of coverslips were used as spacers to create three side-by-side channels with a nominal volume of 10 μL each. Slides, spacers, and coverslips were bonded together with optical adhesive (NOA68, Norland), which was also used to seal the channels. Fluids could still be exchanged through 1 mm diameter predrilled holes in the objective slides. The channels were first passivated for 30 min with 5 mg/mL casein solution (casein sodium salt from bovine milk, Sigma Aldrich), after which the channels were rinsed with copious amounts of 10 mM HEPES/50 mM NaCl (pH 7.4). The DNA-functionalized particle suspensions were then administered to the channels, where they sedimented to effectively form a twodimensional system. The channels were oriented such that the particles sedimented to the surface of the coverslip, which facilitated bright-field, confocal, and TIRF microscopy. For our quantitative association/dissociation studies, the sample cells were

mounted on a custom-made stage setup on a Nikon Eclipse Ti-E light microscope, which enabled fine temperature control while imaging in transmission mode. At each temperature of interest we recorded five independent images and determined the singlet fraction by common video microscopy methods. Our analysis method did not distinguish between pairs of bound particles and singlets that just happened to be very near each other in our still images. We corrected for this systematic error with a simple 2D simulation of "hard spheres" at the same overall concentration as the experiment.

4.2.3. QCM-D

Quartz Crystal Microbalance with Dissipation Monitoring (QCM-D) measures changes in resonance frequency, Δf, and dissipation, ΔD, of a sensor crystal upon interaction of (soft) matter with its surface. The QCM-D response is sensitive to the mass (including coupled water) and the mechanical properties of the surface-bound layer. Using this technique, we monitored the cholesterol-modified DNA adsorption to lipid bilayers in situ with sub-second time resolution. A buffer solution of 150 mM NaCl, and 10 mM HEPES, pH 7.4, in ultrapure water was used to prepare lipid vesicles and to dilute DNA stock solutions. 2 mM $CaCl_2$ was added during the incubation step that lead to the formation of a supported lipid bilayer. Lyophilized dioleoylphosphatidylcholine (DOPC) was purchased from Avanti Polar Lipids (Alabaster, AL, USA). Lipids were mixed in chloroform, dried, re-suspended in buffer and homogenized as previously described by Richter et al. [176] Small unilamellar vesicles (SUVs) were obtained by sonication (30 min) with a tip sonicator (Branson, USA), operated in pulsed mode at 30% duty cycle with refrigeration, followed by centrifugation in an Eppendorf centrifuge (30 min at 14,000g at 4°C) to remove titanium particles. SUV suspensions were stored at 4°C under nitrogen. Concentrations and mixing ratios were estimated from the dry masses of employed lipid material and before use vesicle suspensions were diluted to 50 μg/ml. QCM-D measurements were performed with a Q-Sense E4 system (Q-Sense AB, Västra Frölunda, Sweden). The system was operated in flow mode with a rate of typically 20 μl/min, using a syringe pump (KD Scientific, Holliston, MA, USA). Before starting the measurement both the system and the sample solutions were equilibrated to the desired temperature (here, either 23 or 55°C). Δf and ΔD were measured at 6 overtones (n = 3, 5, …, 13, corresponding to resonance frequencies of $f_n \approx 15, 25, \ldots, 65$ MHz) simultaneously. Changes in dissipation and normalized frequency, $\Delta f = \Delta f_n/n$, of the seventh overtone are presented.

4.3. RESULTS AND DISCUSSION

4.3.1. PARTICLE FUNCTIONALIZATION

We created a system of solid particles with surface-mobile binding groups by coating silica microspheres with a fluid lipid bilayer and hydrophobically anchored DNA linkers (Fig. 4.1 and section 4.2.1). The single-stranded complementary DNA sticky ends (S and S') were fluorescently labeled and were connected to a ~16 nm long double-stranded backbone construct with two cholesterol groups at the opposing end (Fig. 4.1d). The hydrophobic cholesterol anchors inserted spontaneously into the lipid bilayers of a preformed suspension of small unilamellar vesicles (SUV), leaving the sticky ends pointing outward. Subsequently, a process of vesicle rupture and fusion [54, 55] led to the forma-

tion of a uniform DNA-functionalized lipid bilayer around the silica microparticles. We verified the stability of the double cholesterol anchoring of the linkers in the temperature range used for our microscopy studies with quartz crystal microbalance (QCM-D) measurements on solid supported lipid bilayers of similar composition as those on the particles (Fig. 4.2 and section 4.2.3). In these measurements, we first let the DNA linkers adsorb to the lipid bilayer and then tried to desorb them again by prolonged rinsing with pure buffer. In agreement with the earlier results of Pfeiffer et al.,[116] we found that the second cholesterol group greatly strengthens the coupling to the lipid bilayer, as compared to a single cholesterol anchor, and makes the linker attachment essentially irreversible. Importantly, the DNA functionalized lipid bilayer largely determines the particle interactions, independent of the material of the particle core. To further suppress the unwanted nonspecific interactions that frequently plague colloid science, we introduced some additional short-ranged steric repulsion by including a small amount of PEG-ylated lipids (Flory radius ~3.8 nm), analogous to common practices for giant unilameller vesicles. Although the PEG-ylated lipids are mobile, their expulsion from the interparticle contact zone is counteracted by the lateral osmotic pressure of the PEG-ylated lipid reservoir on the rest of the particle. The resulting PEG distribution provides the steric repulsion and, as a result, we found that in suspensions of a single particle type (S or S' functionalized) most beads were stably dispersed as singlets.

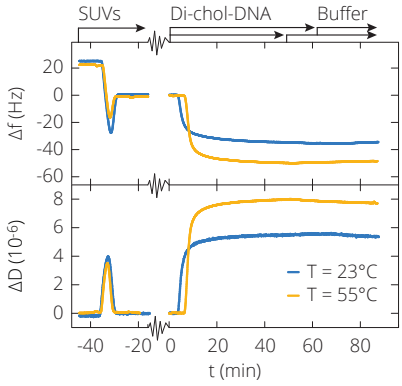

Figure 4.2: QCM-D measurements of the lipid bilayer anchoring of double-cholesterol functionalized DNA linkers at different temperatures. QCM-D response of the formation of a lipid bilayer and the subsequent adsorption of double-cholesterol modified DNA at T = 23 and 55 °C. The start and duration of the incubation with different samples is indicated (arrows). The time in between bilayer formation and the addition of DNA correspond to a buffer wash and is not shown because of clarity reasons. Pronounced changes in frequency and dissipation upon exposure to 1 μM double-cholesterol-DNA solution reflect the formation of a flexible and hydrated DNA coating on top of the lipid bilayer. The minimal change in the frequency and dissipation signals during the subsequent rinsing with pure buffer indicates that the cholesterol modified DNA linkers are stably coupled to the lipid bilayer at both high and low temperature.

4.3.2. BINDING GROUP MOBILITY

A crucial aspect of our new colloidal system is the lateral mobility of the cholesterol-anchored DNA linkers along the lipid-coated particle surface. The main phospholipid

component is DOPC, which has a melting point of ~-20°C. The lipid bilayer around the microparticles should thus be in the liquid phase and the DNA linkers should diffuse around freely, while remaining anchored to the particles. To probe the mobility of the DNA linkers, we conducted comparative fluorescence recovery after photo-bleaching (FRAP) studies. DOPC-coated microparticles functionalized with fluorescently labeled S' DNA linkers were made to stick to the bottom of a nonpassivated sample cell. We then bleached them on one side with a 500 ms high-intensity laser pulse (λ_{ex} = 561 nm), while the fluorescence emission was monitored in TIRF mode (Fig. 4.3, red-colored micrographs and curve). For comparison we conducted the same experiment on DPPC-coated microparticles (Fig. 4.3, blue-colored micrographs and curve). DPPC has a transition temperature of ~40 °C, so at room temperature exists in a gel phase and is therefore expected to inhibit the diffusion of the embedded DNA linkers.

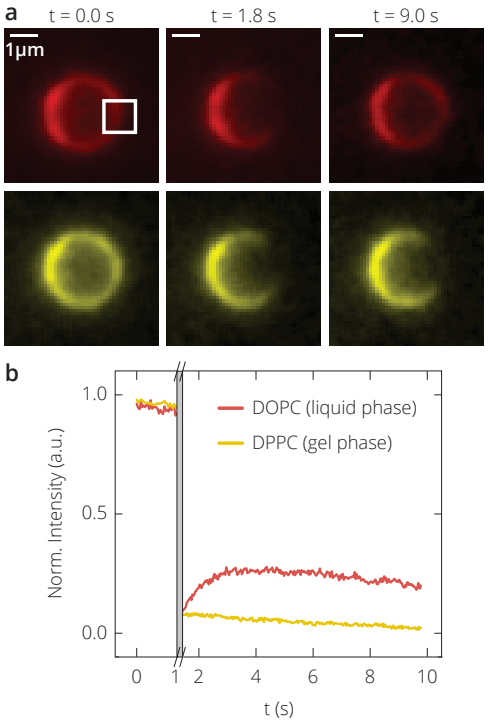

Figure 4.3: FRAP measurement of the lateral mobility of the lipid bilayer-anchored DNA linkers on the particles. (a) Fluorescent micrographs of the emission of Cy3- labeled DNA linkers (S') embedded in a lipid bilayer comprising DOPC (red) or DPPC (yellow) on a 3.56 μm diameter particle, before and after a partial bleach at t = 1.7 s (shaded bar in b). (b) Plot of the normalized mean pixel intensity of the bleached area (white square in a) versus time. The error bars represent the standard deviation in the averaged measurements of five particles.

The partial recovery of the fluorescence signal from the bleached area as seen for the DOPC-coated beads proves that the DNA linkers are indeed mobile, as unbleached and bleached linkers redistribute around the particle. The fluorescence intensity does not return to the initial prebleach level, because the irreversible bleaching of the DNA

linkers on a major part of the particle effectively dilutes the overall dye concentration. The time scale of the recovery is on the same order of magnitude as what was found by Gopalakrishnan et al.,[177] who probed the diffusivity of fluorescently labeled lipids in bilayers on silica particles. No significant recovery is seen for the DPPC-coated microparticles, showing that the gel phase that the DPPC lipids adopt indeed slows down the DNA-linker-motion completely.

The unique combination of binding group mobility with the monodispersity and nondeformability of solid colloids bridges the existing gap between hard nano/ microparticles with (covalently coupled) immobile binding groups and soft, "floppy" objects with mobile binding groups. Examples of the latter are DNA-functionalized lipid vesicles [97, 147, 178] and possibly oil-in-water droplets, [107] which both experience a strong deformation of their contact zone upon bond formation (for the oil droplets it is not known, however, whether the DNA linkers are actually mobile). Importantly, the pronounced surface-mobility of the DNA linkers in our system also implies that their distribution around individual particles is intrinsically uniform, without requiring any special efforts during the particle functionalization, something that is not necessarily true for the coupling of immobile binding groups.

4.3.3. MOBILE-DNA-MEDIATED INTERACTIONS

We studied the association/dissociation behavior of our mobile-DNA-coated colloids by mixing equal amounts of S- and S'-functionalized 1.30 μm diameter particles in a passivated sample cell (see Section 4.2.2). At 25 °C the particles formed extensive clusters, which dissociated when the temperature was raised to 55 °C (Fig. 4.4a-d). The dissociation into individual particles is clearly demonstrated by the time-averaged micrographs, in which the highly mobile singlets have a blurry appearance, while the less mobile particles inside clusters remain clearly distinguishable. This temperature-dependent association/dissociation behavior could be cycled back and forth many times. The clusters that formed at low temperature displayed an alternating order of the red- and green-fluorescently-labeled complementary particles (Fig. 4.4c). The specificity and the temperature-dependence of the interactions indicate that these are indeed mediated by the reversible hybridization of the complementary DNA linkers and that unwanted nonspecific interactions are suppressed.

In the confocal micrograph of Fig. 4.4c, one can also see that the contact points between the complementary particles inside clusters appear brighter, in this case with a yellow color due to overlap of the red and green fluorescent signals. Interestingly, in a system of S- and S'-functionalized 3.56 μm diameter particles that were randomly jammed together at a density where all translational freedom of the particles was eliminated – so that they also stayed in contact at elevated temperatures, independent of the state of DNA linker binding – the bright spots only appeared at low temperature and were absent at 55 °C (Fig. 4.4e,f). To verify that this was not an imaging artifact due to the overlapping signals from the two fluorescence channels, we performed experiments with complementary particle mixtures in which only one of the DNA linker types (S) was fluorescently labeled (Fig. 4.5). Also in these experiments we observed a nonuniform distribution of the fluorescence intensity around the particles at 25 °C, with the more intense fluorescent spots of the S linkers coinciding with the contact points between complementary

particles. Apparently, the DNA linkers distribute uniformly around the particles above the sticky end melting temperature (Fig. 4.4f), but they collect in the interparticle contact zones upon bond formation below this temperature (Fig. 4.4e and Fig. 4.5), a direct and remarkable consequence of the surface mobility of the binding groups.

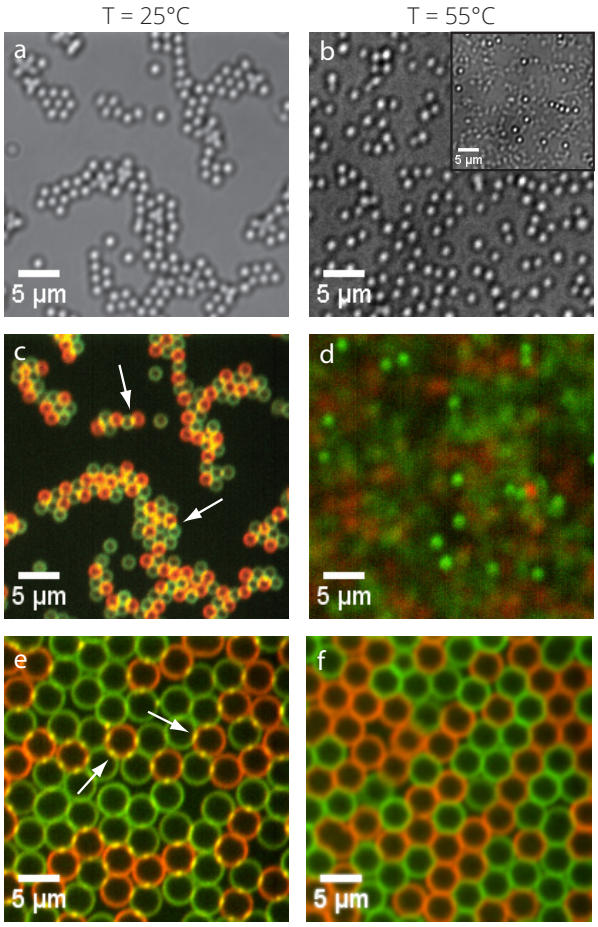

Figure 4.4: Temperature-dependent behavior of 1:1 microparticle mixtures functionalized with complementary mobile DNA linkers. (a, b) Bright-field snapshots of freely suspended 1.30 μm diameter S- and S'-functionalized particles at 25 °C (a) and 55 °C (b). The inset is a time average of 100 frames. (c and d) Time averages of 100 confocal micrographs corresponding to panels a and b, with S shown in green and S' in red. (e and f) Time averages of 100 confocal images at 25 °C (e) and 55 °C (f) of a high-density fully jammed random packing of 3.56 μm diameter particles with no remaining translational freedom to self-organize or diffuse away (the field of view drifted somewhat between the low- and high-temperature recordings, though). The white arrows in panels c and e indicate examples of the bright fluorescent spots that appear at low temperature at the complementary particle contacts, due to a locally enhanced linker concentration. The occasional bright spot between two particles of the same color is the result of a small number of fluorescent DNA-functionalized SUVs from our particle preparation procedure having been left behind in the suspension.

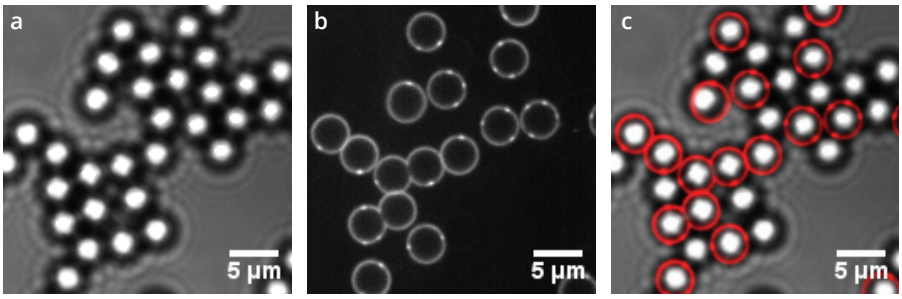

Figure 4.5: Single-dye fluorescence intensity increase at the contact points between particles carrying complementary mobile DNA linkers. (a) A time average of 100 brightfield images shows both the S and S' functionalized particles (3.56 μm diameter) interacting with each other at 25 °C, whereas the averaged confocal fluoresence image of the same field of view (b) only shows the particles functionalized with the fluorescently labeled S linkers. The S' linkers on the other particles were not fluorescently labeled and are hence invisible in this image. (c) Composite image of 100 time-averaged bright-field snapshots (in gray) and 100 time-averaged confocal fluorescence snapshots (in red) of 3.56 μm diameter S- and S'-functionalized particles interacting with each other at 25°C. Only the S linkers were fluorescently labeled and appear as red shells around their host particles, while the S'-functionalized particles are only visible in bright-field mode.

4.3.4. ASSOCIATION/DISSOCIATION TRANSITION

We quantified the association/dissociation behavior by recording the fraction of unbound particles, or "singlet fraction", as a function of the temperature for four different DNA linker densities on 1.30μm diameter particles (Fig. 4.6 and section 4.2). We let 1:1 mixtures of the S- and S'-functionalized particles associate for 15 min at 30 °C and then increased the temperature to 60 °C in steps of 2°C, with a 15 min waiting time per step. We used these 15 min equilibration intervals to ensure that at the start of the measurement all particles were clustered and to avoid possible kinetic effects due to redistribution of the linkers on the particle surface. The equilibrium linker distribution depends on a combination of factors, including the number of contacts with neighboring particles, and nonequilibrium effects could occur if the speed of linker redistribution is slow compared to other relevant processes in the system. From our FRAP measurements we find that linker diffusion takes on the order of seconds/μm^2. This should be compared with a heating rate of minutes/°C and the characteristic association time of the particles. The latter depends on the particle concentration and size (through their diffusivity) and is on the order of several tens of seconds for micrometer-sized particles. Our experimental system thus had ample time to reach equilibrium in each temperature step, which is also confirmed by the fact that faster ramps of 1 °C/min gave essentially the same results.

As expected for DNA-mediated particle interactions, the dissociation curves in Fig. 4.6 systematically shift to lower temperatures as the mobile linker density decreases, thus demonstrating good control over the particle functionalization and their association behavior. There is an important difference with the dissociation curves of particles with immobile linkers, though. To illustrate this, we performed a similar experiment with 1.05 μm diameter Dynabeads (MyOne Streptavidin C1,Molecular Probes), functionalized with the same sticky ends through a surface-immobile biotin-streptavidin coupling, as described before.[10, 64] From Fig. 4.5, it is clear that at similar overall linker densities on the particles, the dissociation transitions of our mobile-DNA-coated colloids are

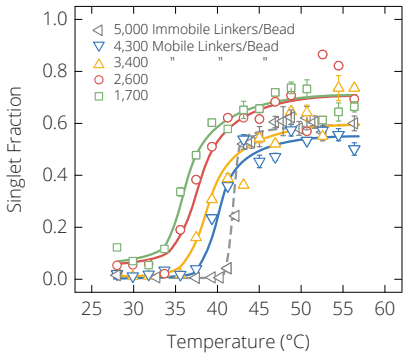

Figure 4.6: Temperature-induced dissociation transition for microparticles with different DNA linker densities. Shown is the particle singlet fraction as a function of the temperature in 1:1 mixtures of 1.30 μm diameter particles with mobile S and S' linkers (solid lines) and of 1.05 μm diameter Dynabeads with immobile S and S' linkers (dashed line). The lines are drawn as a guide to the eye. The error bars represent the standard deviation from five independent images at each temperature.

much broader (width 6.5 ± 1.7 °C) than the transitions observed for the immobile-DNA-coated particles, which are extremely sharp (~1-2°C, as is usual for these linker densities [64]). A detailed comparison with the more elaborate immobile-DNA coated colloid data of Wu et al. [179] leads to the same conclusion. Assuming an interparticle binding distance of roughly the DNA linker length, [11] it follows from geometrical considerations that at our lowest and highest mobile linker densities (1700 and 4300 linkers/bead) there are, respectively, about 12 and 30 linkers in the contact zone within reach of the linkers on the partner particle, that is, if we neglect the accumulation of linkers in the contact zone upon bond formation (Fig. 4.4e). These lower-limit estimates roughly correspond to immobile-DNA-coated colloid systems with sticky end fractions χ = 0.1-0.15 in ref [179]. There it was found that the transition width is 1.5°C for χ = 0.1 and 1.2°C for χ = 0.2, with even sharper transitions as the number of linkers in the contact zone increases further. Due to the somewhat different buffer conditions (73 versus 50 mM NaCl in our experiments) we cannot directly compare the dissociation temperature at 50% singlets (T_m), but the strongly different width of the curves does support the conclusion that the broad transitions are a distinctive property of our mobile-DNA-coated colloids. A couple of theoretical studies on other types of systems also suggest that binding group (im)mobility leads to qualitatively different equilibrium interactions, [180, 181] but a simple conceptual understanding of the broad transitions is still lacking. It is important to realize, though, that the equilibrium interactions are no less predictable or user-tunable for particles with mobile binding groups than they are for immobile binding groups. One only needs to account for the fact that the equilibrium distribution of mobile linkers is not strictly uniform but the direct result of other system parameters that could be included in an appropriate model (for instance, building on the analytical theories of refs [68] and [114]).

The less dramatic dissociation transition that we observe for our mobile-DNA-coated colloids provides a much larger temperature window for equilibrium self-assembly and

should thus facilitate the formation of well-organized structures. Moreover, even if we cool quickly to temperatures below the equilibrium self-assembly window–where the bonds are very strong–we find that the mobile-DNA-coated particle clusters are much more compact and ordered than the typically fractal-like low-temperature aggregates of immobile-DNA-coated colloids, as is exemplified by an increase of the average number of nearest neighbors from 2.6±1.0 to 3.4±1.2 in parts a and b of Fig. 4.7, respectively. Ramping the temperature down more slowly, from 52 to 25°C in 3 h, still gives slightly better structures, raising the average number of nearest neighbors to 4.2±1.3 (Fig. 4.7c), but even without any fine-tuning or annealing one can get good self-organization results. It is noteworthy that when the temperature is increased, the clusters of mobile-DNA-coated particles develop a "floppy" character while the particles are still connected, instead of "shattering" in a sudden transition from a tightly bound to a fully unbound state the way immobile-DNA-coated colloids do (compare Supplementary Movies S1 and S2, which is provided in the Supporting Information of ref. [69]). We speculate that these observations are due to a collective mobility of the bonds in the contact zone that allows particles to more easily roll around each other and rearrange, besides the mobility of individual linkers when they are not bound.

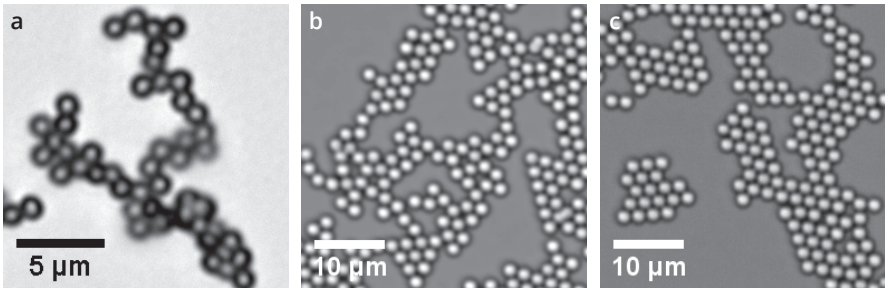

Figure 4.7: Self-organization of complementary microparticle mixtures functionalized with either immobile or mobile DNA linkers. 1:1 mixtures of S- and S'-functionalized particles were cooled quickly from a fully dissociated state at 52°C to a fully associated state at 25°C in 15 min. The bright-field snapshots show the resulting structures for (a) 1.0μm diameter particles with immobile DNA linkers and (b) 2.0 μm diameter particles with mobile DNA linkers. (c) The same sample as in panel b after redissociating and slowly cooling from 52 to 25°C in 3 h.

4.4. CONCLUSION

We have demonstrated a novel system of hard, nondeformable particles that interact specifically and reversibly through DNA binding groups that are fully mobile along the particle surface. These colloids display qualitatively new behavior, including a much broader association/dissociation transition than is common for colloids with immobile binding groups. The observed accumulation of linkers at the interparticle contacts suggests that the binding group mobility could also enable other types of new behavior, for instance in the form of "selflimited" association processes [95, 182–184]. And, whereas the current focus mostly was on equilibrated systems, one could also obtain time-dependent properties that depend on the flux of binding groups along the particle surface. This

could be done by tuning the different time scales in the system, in particular through the particle size, the linker coverage, and the rate of temperature change. The facile manipulation of the solid particles and the temperature-tunable binding strength of the easy-to-image fluorescent DNA linkers enable detailed quantitative investigations. Moreover, the particle functionalization uses no harsh coupling chemistries and requires only commercially available components, and the DNA linkers could even be used to attach other types of binding groups. We therefore expect this new model system to be broadly applicable and to deepen our fundamental understanding of a range of bioinspired self-assembly approaches and of other systems with surface-mobile binding groups, for instance, biological ligand-receptor interactions.

We thank Ralf Richter and Galina Dubacheva for facilitating and collaborating on the QCM-D measurements, the group of Daan Frenkel –especially Bortolo M. Mognetti and Patrick Varilly – for useful discussions, the AMOLF technical support for equipping our microscope setup with temperature control functionality, and Huib J. Bakker for a critical reading of the manuscript.

5

TOWARDS MULTI-BOND FORCE MEASUREMENTS

Mediating the self-assembly of micro-particles into secondary structures using DNA linkages has shown to be a promising strategy for steering the self-assembly towards complex, functional particle-based materials. In order to control the structures into which the micro-particles assemble, it is essential to accurately tune the interaction strengths induced by the complementary DNA base-pair interactions. In this context, it has recently been shown with simulations that a fine balance between repulsive and attractive interactions in combination with the possibility for the DNA molecules to diffuse over the surface of the particles, can lead to crystal structures with a wide variety of order parameters. In this chapter we show the development and first results of force measurements designed to quantify the interaction strengths between silica surfaces decorated with surface-mobile DNA linkers under various conditions. Two complementary techniques are described that both rely on optical tweezers to accurately apply forces to connected micro-particles. The first is based on a combination of a high-numerical-aperture optical trap with high-resolution, reflection interference contrast microscopy (RICM) and fast video image processing. RICM provides nanoscale resolution of the 3D bead position on short to long time scales (milliseconds to minutes), which is required to measure the force at which the optical trap pulls on a DNA-coated particle when it detaches from a DNA-coated flat substrate. We are still developing this technique and here we present the efforts that so far went into building this instrument. The second technique is based on two optical traps of which one can be automatically steered to bring two DNA carrying beads in close contact after which they are pulled apart. The setup used for this technique was readily available and here we present the first, preliminary results on the interaction strengths between two bound particles by surface-mobile DNA bridges.

5.1. INTRODUCTION

In biology as well as in synthetic self-assembly systems it is essential that the basic constituents that built up the intended final structure can recognize their correct binding partners even in a typically crowded micro environment. This is achieved by the possibility of the molecular building blocks to continuously bind and unbind with each other so as to dynamically probe their surroundings and find the best fitting partner. How well two molecules fit is defined by their chemical and physical properties and the conditions of the medium they are in. Better understanding of how these molecular characteristics control the interactions will be beneficial for the development of more advanced self-assembly processes and better targeted medicine.

One of the most desired current objectives in nano medicine is to be able to distinguish specific diseased cells from other healthy cells within their natural environment. Acquiring the capability to pinpoint a specific type of cell would allow one to target it with manipulative drugs while leaving surrounding tissues unaffected. This would for example be useful for directing certain cytotoxic moieties to tumor cells. Currently, a popular method to establish such selectivity, is to detect a tumor associated antigen and target it with a high-affinity, monovalent, cell-binding agent. This would be a perfect strategy if it were not for the fact that so far no antigen has been discovered that is solely expressed by tumor cells. Thus, other healthy cells that display the same antigen will be harmed as well. To enhance the success-rate of the current cancer treatments, this strategy therefore needs to be improved [185, 186].

Physiologically, cells not only express different types of receptors to sense their environment, they also tune their spatial arrangement [187]. By concentrating receptors at specific sites or distributing them evenly over their surface, cells are not only sensitive to the *presence* of a specific molecule, but they can also tune the sensitivity to the molecule's concentration. For example, leukocytes are only attracted by cells if they display multivalent arrays of glycosaminoglycans whose formation is controlled by the presence of chemokines. If the surface density of glycosaminoglycans is too scarce, no leukocyte will bind [188].

Tumor cells can respond differently to certain cues than healthy cells. For this purpose, the orchestration of the complex ensemble of molecules on their surface needs to be different. This has been acknowledged by Carlson *et al.*, who exploited a well-studied immune response known for inducing a barrier to xenotransplantation. An important player in this process is galactosyl-(1-3)galactose (α-Gal) carbohydrate epitope which is abundantly expressed on the surface of nearly all mammalian and bacterial cells. However, because of the absence of functional glycosyltransferase, no α-Gal is displayed on human cells. Instead, humans and other species lacking glycosyltransferase, generate high levels of antibodies (anti-Gal IgG & IgM) driving the acute rejection of xenotransplanted organs. What is interesting for the scope of this study is that the bivalent anti-Gal IgG and decavalent anti-Gal IgM interact only weakly with a single α-Gal epitope but bind with higher functional affinity to multivalent arrays of the carbohydrate. This selectivity for surface receptor density was utilized to target tumor cells based on their high expression of $\alpha_v\beta_3$ integrins. Using a synthesized bifunctional compound to render $\alpha_v\beta_3$ presenting cells with α-Gal, Carlson *et al.* succeeded in selectively targeting and killing tumor cells while leaving 'healthy cells' untouched (Fig. 5.1). Using the same

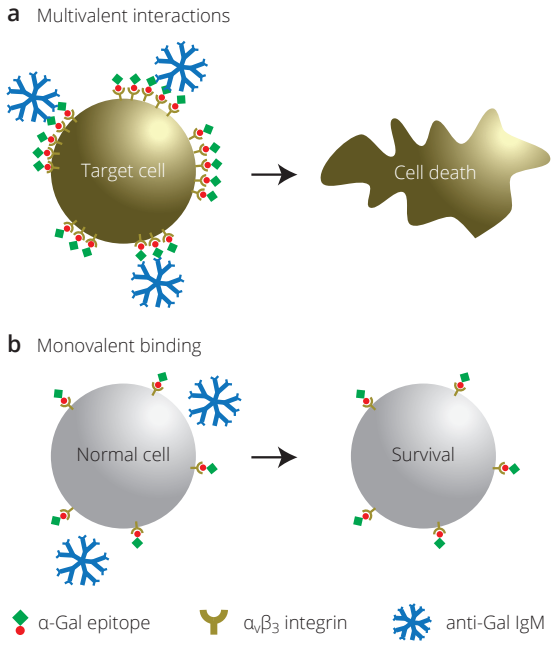

Figure 5.1: Schematic representation of how multivalent interactions can target cells based on the coverage of specific surface moieties. Carlson *et al.* developed a bifunctional conjugate containing a nonpeptidic RGD mimetic and the α-Gal epitope [189]. The RGD mimetic binds with high affinity to $\alpha_v\beta_3$ integrin. Exposing cells with this conjugate therefore renders their surface with α-Gal. a) Cells in which the $\alpha_v\beta_3$ integrin is up regulated automatically also display a high number of α-Gal and hence become targets for anti-Gal antibodies resulting in cell death. b) Cells with low levels of $\alpha_v\beta_3$ stay immune for the antibodies and remain unaffected.

multivalency principle, Davis *et al.* successfully targeted cancer cells with nanoparticles based on their over-expression of human-transferring-protein receptors [190]. In addition, several theoretical studies have been performed to explain the substantial difference in binding affinity between certain multivalent systems and their monovalent counterparts [182, 191–198]. In particular, Martinez-Veracoechea *et al.* formulated a generic explanation, that allowed them to present a basic set of rules for the design of guest particles that selectively target surfaces with a concentration of receptors greater than a critical value [199]. Although their predictions could be reproduced with Monte Carlo simulations, direct experimental realization of super-selective particles has still not been accomplished. Encouraging results have been obtained by Dubacheva *et al.* who observed superselectivity in the multivalent binding of hyaluronic acid (HA) polymers modified with various number of β-cyclodextrin to ferrocene presenting self-assembled monolayers (SAMs) [200]. The demonstration of pronounced superselectivity together with the great degree of tunability renders their system very helpful in understanding multivalent interactions in biological systems.

A potential application for multivalent, mobile interactions which is more in line with the scope of this thesis, may be found in colloidal self-assembly. Recent theoretical work has indicated that colloids coated with mobile interactions can crystallize into crystals

with a low coordination number and open structure without the need for patches as was previously thought [17]. The theoretical predictions in this work rely on certain descriptions for the interactions between the particles. Our work could provide the experimental tools to elucidate to what extent these descriptions hold. For this purpose, we have developed a model system comprising the interactions between two solid objects mediated by short, surface-mobile DNA bridges. The two opposing solid supports are in this case either two micro-particle or a micro-particle and a coverslip surface. The surface mobility of the DNA strands is achieved by integrating them by one end into a lipid bilayer with which the solid surfaces are coated. By varying the linker density, the maximal number of possible bonds, i.e. the valency, is tuned.

In this chapter we demonstrate two methods with which the binding selectivity can be assessed via the strength of the multivalent DNA bridges. The first is based on a combination of a high-numerical-aperture optical trap with high-resolution, reflection interference contrast microscopy (RICM) and fast video image processing. RICM provides nanoscale resolution of the 3D bead position on short to long time scales (milliseconds to minutes), which is required to measure the force at which the optical trap pulls on the particle when it detaches. We are still developing this technique and here we present the efforts that so far went into building this instrument.

The second technique is based on two optical traps of which one can be automatically steered to bring two DNA carrying beads in close contact after which they are pulled apart.

The setup used for this technique was readily available and here we present the first, preliminary results. As our model system of micro-particles coated with mobile DNA strands relies on the anchoring of DNA into a lipid bilayer, we first investigated if the anchoring at certain conditions could be disrupted by applying a force. For this we used a slightly modified system in which cholesterol bearing DNA strands were strongly coupled to one bead through a streptavidin-biotin coupling. A second bead, coated with a supported lipid bilayer, provided the anchoring sites for the cholesterol groups on the former bead to bind with. By bringing these beads into close proximity and subsequently pulling them apart, the likelihood of binding and unbinding was assessed at varying densities of cholesterol-bearing DNA strands.

Similar experiments were finally conducted to measure the force required to break two particles held together by mobile DNA linkers. Like with the anchoring-strength experiment, we varied the density of DNA linkers e of the rupture force to unravel the dependence of rupture force on the number of linkers participating in the bond. Although limited by the narrow force range permitted by the instrument, the obtained force spectra do already indicate the expected increasing rupture force as a function of the number of linkers. These first results demonstrate the usability of our model system, thereby providing the encouragement for future measurements to unravel the actual underlying relation between binding strength and linker density.

5.2. THEORETICAL BACKGROUND

In the field of dynamic force spectroscopy a lot of effort has been put in providing a theoretical framework that describes the interaction strengths of bonds between single or multiple molecular bonds. This theoretical understanding finds its roots in the work per-

formed by Bell and later Evans who analyzed the failure of single-molecule bonds under stress [118, 201]. In their model they approach the binding and unbinding of a molecular bond as a transition reaction which can be written as,

$$A + B \underset{k_u^0}{\overset{k_b^0}{\rightleftharpoons}} C, \tag{5.1}$$

in which the molecules A and B form complex C and k_b^0 and k_u^0 are the intrinsic rates for the binding and unbinding of the complex. In the absence of an external force, such a bond can be described in terms of a free-energy landscape extending over the reaction coordinate x, i.e. the separation distance between the molecules A and B. A typical free-energy curve of a weak bond is given in Fig. 5.2a.

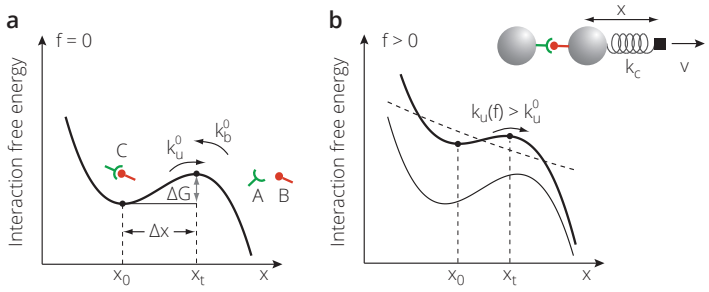

Figure 5.2: Schematic representation of a typical free energy landscape governing the weak interaction between two biomolecules A and B. a) The free energy surface with a minimum-to-barrier distance $\Delta x = x_t - x_0$, the activation energy ΔG and intrinsic binding and unbinding rates, k_u^0 and k_b^0 in the absence of an externally applied force. b) By applying a force, f (dashed line), to the molecular bond, the Bell model assumes that the free energy surface tilts thereby decreasing ΔG and Δx. As a consequence, the off-rate, $k_u(f)$, surpasses the intrinsic off-rate, k_u^0. The free-energy surface in the absence of force is indicated by the thin line, while the new situation at a non-zero force is represented by the thick line.

The local minimum, x_0 indicates the most favorable position of the bond. In order to break the bond, work has to be applied so as to overcome the potential barrier located at x_t. A bond is indicated as weak if the magnitude of the energy difference between the local minimum and the barrier, the activation energy ΔG, is on the order of $n k_B T$, where n ranges roughly between 1 and 50, k_B is Boltzmann's constant and T the absolute temperature. In this case, there is still a measurable timescale on which these bonds rupture spontaneously.

The rupture probability can be influenced by applying a force to the bond. This is achieved by coupling both molecules A and B to a mechanical force transducer, of which a simplified schematic representation is given in Fig. 5.2b. According to Bell, applying a force tilts the free energy curve so that ΔG decreases and the likelihood of bond-breaking increases, see Fig. 5.2b. Based on concepts obtained from kinetic theory of the strength of solids, Bell assumed that the force-dependent off-rate k_u scales with the exponential of the applied force f according to the formula:

$$k_u(f) = k_u^0 e^{f x_t / k_B T} \tag{5.2}$$

This model has been widely used to explore the kinetics of many different molecular transitions of bonds found in nature. It allowed for the determination of the intrinsic off-rate, k_u^0 and distance between the free-energy minimum and the transition state, $\Delta x = x_t - x_0$. By employing a constant pulling speed v so that the applied force grows linearly with time t, as $f(t) = rt$ with $r = k_c v$ and k_c being the spring constant of the force transducer, the mean rupture force is predicted to scale proportionally to the natural logarithm of the loading rate,

$$\langle f \rangle = \frac{k_B T}{x_t} \ln\left(\frac{r x_t}{k_u^0 k_B T}\right) \tag{5.3}$$

Eq. (5.3) indicates that the rupture force, measured at various loading rates, when plotted as a function of the natural logarithm of the loading rate should fall onto a straight line. This approach has been the standard for many experiments in which a plethora of different molecular interactions have been explored with a large range of different techniques.

However, it soon appeared that the force vs loading rate relation of many systems does not fit to the $f \sim \ln r$ prediction. With the assumption that under an applied force the on-rate, k_b, quickly vanishes, these observations were ascribed to a succession of multiple energy barriers along the rupture pathway [202]. Friddle et al., recently took the challenging task to reassess a large part of the available force spectra and recognized that the existence of multiple energy barriers is somewhat unnatural [203]. In addition, they stress that a large part of the publications that utilized the multiple-barrier approach, report distances from the energy minimum at binding to the "inner" barrier orders of magnitude below 1 Å. These seemingly counter-intuitive observations motivated them to develop a model that circumvents the need for additional complexities in the unbinding pathway. Their model builds further on previous analyses which included either the rebinding possibility at slow loading rate or the fluctuations of rebinding interactions within a cluster of bonds [118, 191, 204–211]. In both cases, the relation between the force and loading rate displays an equilibrium regime which is characterized by a constant nonzero force and a kinetic regime characterized by a weak loading dependence, $f \sim \ln r$. As their model demonstrated an accurate interpolation between these two regimes for both single- and multi-bond cases, we apply their analysis to predict the outcome that we can expect for our system of colloids with multiple, mobile linkers.

In what follows, we summarize the expressions derived by Friddle et al. that we consider to be relevant for us [203, 212]. They illustrate their approach using an adapted representation of the free-energy surface as is shown in Fig. 5.3.

The process of unbinding under load is considered as an intermolecular potential $U(x)$ plus a harmonic spring $V(x,t) = 1/2 k_c (x - vt)^2$. For simplicity, both the bound state of $U(x)$ and the initial minimum of $V(x, t = 0)$ are located at $x_0 = 0$, see Fig. 5.3a. Then, the combined energy landscape $E(x,t) = U(x) + V(x,t)$ ensures that at time $t = 0$ there is an impenetrable barrier to bond rupture. If the bonds are rigidly connected to the force probes, the lifetime of the bound state remains essentially infinite until the probe potential is translated far enough to create a second free-energy minimum, Fig. 5.3b. This feature is fundamentally different from the previous model; it essentially means that a harmonic potential ensures that a bond can rupture only if the applied force exceeds a certain minimum value. When the translation of the harmonic potential is slow enough

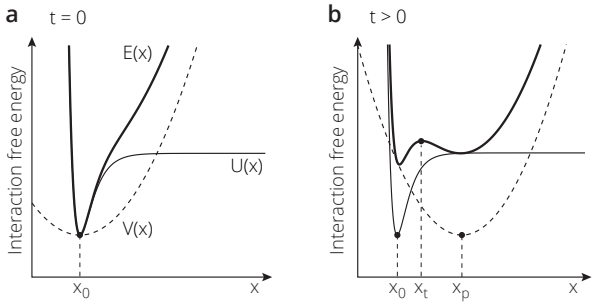

Figure 5.3: Schematic representation of Friddle's interpretation of the free-energy landscape governing the weak interaction between two biomolecules A and B [212]. a) The energy landscape, $E(x)$ (thick line) of a combination of a intermolecular potential $U(x)$ (thin line) and an external harmonic potential $V(t)$ (dashed line) positioned at $t = 0$ at the free-energy minimum of the bond, x_0. $U(x)$ is here represented by a Morse potential. b) The change in the combined energy landscape upon translating the external harmonic potential from x_0 to x_p.

it furthermore implies that rebinding processes become significant. At too high loading rates the two approaches merge as the applied forces exceeds the minimum required force very quickly so that rebinding becomes negligible.

Assuming that the time scale of intra-well relaxation is faster than any other time scales of the system, the difference between the internal energy between the bound and unbound states can then be described as,

$$\Delta U = U_0 - V(0, vt = x_p) = U_0 - \frac{f^2}{2k_c}, \tag{5.4}$$

where U_0 is the internal energy of intermolecular bond and x_p is the position of the harmonic potential. For the average rupture transition to occur, the total free energy change must be zero, $\Delta U - T\Delta S = 0$, where ΔS is the entropy difference between the bound and unbound states. Incorporating this in Eq. (5.4) gives the equilibrium force required to rupture the bond,

$$f_{eq} = \sqrt{2k_c(U_0 - T\Delta S)} = \sqrt{2k_c\Delta G_0}, \tag{5.5}$$

where $\Delta G_0 = k_B T \ln\left(k_b^0/k_u^0\right)$, is the equilibrium free energy change between the bound and the unbound state.

For the multibond case, Friddle et al., built upon a continuum approach that represents such a system by the following differential equation [118, 191, 208, 211],

$$r\frac{dN_b}{df} = -N_b k_u(f/N_b) + (N_t - N_b)k_a, \tag{5.6}$$

where r is the loading rate, N_b is the number of parallel bonds of the N_t total bonds that are allowed to independently unbind and rebind, k_a is the constant rebinding rate of an individual molecule acting over a short distance from its retracted position while the overall cluster remains bound and $k_u(f)$ is the unbinding rate. As with the single

bond situation, two regimes appear. At slow loading rates fluctuations in the number of closed bonds are relatively fast and the system establishes a meta-stable number of bonds, $N(f) = N_t/(1 + k_u(f/N)/k_a)$. The stability of the cluster is lost when the force exceeds the equilibrium force,

$$f_{\mathrm{eq}} = N f_\beta W\big[\exp\big(\beta \Delta G_{\mathrm{ba}} - 1\big)\big], \tag{5.7}$$

where $f_\beta = k_{\mathrm{B}}T/x_{\mathrm{t}}$, $W(x)$ is the Lambert W-function, which is defined as the solution for W to the equation $We^W = x$, and $\exp(\beta\Delta G_{\mathrm{ba}}) = k_{\mathrm{a}}/k_{\mathrm{u}}^0$ defines the equilibrium free energy $\Delta G_{\mathrm{ba}} = \Delta G_{\mathrm{a}} - \Delta G_{\mathrm{b}}$ of the closed bond ΔG_{b} relative to an open bond ΔG_{a} within the bound cluster.

In our system, colloids bind together via the hybridization of single or multiple combinations of two complementary oligonucleotides each comprising eleven nucleotides. Such bonds derive their stability from a variety of small free energy changes associated to hydrogen bond interactions. In our experiments we tried to measure both the interactions between one pair of sticky ends as well as between multiple parallel pairs. These interactions are probed using two optical traps that exhibit a Hookean response on the trapped particles upon displacement. So far we performed the force spectroscopy measurements at only one loading rate, which is why we solely estimate the expected rupture forces using Eqs. (5.5) and (5.7) to be able to put our preliminary results in perspective. This comparison is presented in section 5.5.

5.3. OPTICAL TWEEZER TECHNIQUES

In this study, two potential methods to probe the force required to rupture the interactions between multiple, laterally mobile DNA sticky ends are presented. Both these methods rely on the manipulation of microparticles with optical tweezers (see Fig. 5.4a and b). In the first method, which we refer to as the axial pulling method, a bead functionalized with mobile oligonucleotides is brought close to a planar supported lipid bilayer carrying the complementary strands. After a specified time, the bead is pulled away from the substrate to detect whether a bond has been made and to measure the force required to break it. The trap displacement required to break the bond and the corresponding force is measured by reflection interference contrast microscopy (RICM).

For the second method, which we refer to as the lateral pulling method, the foci of two optical traps are brought at equal height above the substrate a certain distance apart from each other, each trapping a particle carrying mobile oligonucleotides (see Fig. 5.4b). The two beads are consecutively brought close together, kept at close proximity for some time and pulled apart. A bond is detected when during the pulling phase both beads are slightly pulled away from their respective trap centers. The distance at which the beads are pulled away from their trap the moment the bond breaks reflects the rupture force.

Both techniques have their advantages and disadvantages. The axial pulling method allows for the determination of the separation of two surfaces at subnanometer precision. Being able to accurately measure the surface separation inherently means a higher precision in the rupture force. And although outside the scope of this thesis, the high accuracy also permits the registering of molecular transformations upon a mechanical force. A disadvantage of this particular technique is that the calibration of the stiffness of the trap has to be done using image analysis, which is limited by the maximum capturing

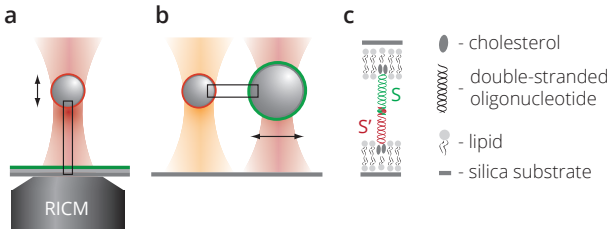

Figure 5.4: Schematics of the two presented methods to measure the rupture forces between multiple, mobile DNA strands. (a) The axial pulling method. (b) The lateral pulling method. The arrows in both panels (a) and (b) indicate the direction along which the optical traps are moved. (c) Composition of the areas outlined by the rectangular frames in (a) and (b).

rate of the camera. Although the world of ultrafast cameras is rapidly growing, the sensitive, fast cameras suitable for RICM are expensive and often still limited to frame-rates of only several kHz, leaving high frequency events unaccessible. As a consequence, optical traps with a high stiffness cannot be reliably calibrated.

High frequency calibration is possible with the lateral pulling method as it relies on quadrant photon diodes (QPDs) that are capable of reaching acquisition frequencies of hundreds of kHz.

A disadvantage both techniques suffer from is the capability to perform only one measurement at a time. This low experimental efficiency defines an experimental time in the order of days before sufficient statistics can be collected, while rare events become even hardly detectable.

5.3.1. AXIAL PULLING METHOD: RICM

Reflection Interference Contrast Microscopy (RICM) is a technique that allows fast and accurate tracking of the 3D motion of microspheres. For this purpose, a bead is illuminated through the objective of an inverted optical microscope and imaged with reflected light. A schematic representation of the setup can be found in Fig. 5.5a.

In short, monochromatic light is directed through a linear polarizer and deflected by a polarizing beam splitter into a quarter-wave-plate-containing objective. The circularly polarized light incidents the sample and the light that gets reflected is collected by the objective to become linearly polarized by the quarter-wave plate again. Due to the reflection however, the polarization is rotated 90° and hence trespasses the polarizing beam splitter and subsequent analyzer and gets focused on the camera sensor. This sequence of polarizers tremendously minimizes the detection of internal reflections while maximizing the intensity of the imaging light.

In our experiments the incident light rays are reflected by a micro-particle, which due to its symmetrical and curved shape form the well-known Newton rings as shown in Fig. 5.7a. For the rings to be formed, the components of the light reflected from the coverglass-buffer interface and the underside of the microsphere must be mutually coherent and collected by the objective. Only the mutually coherent rays of reflected light that cross in the object plane contribute to the interference pattern imaged by the objective. This creates a 3D interference pattern local to the object. Due to the high-NA

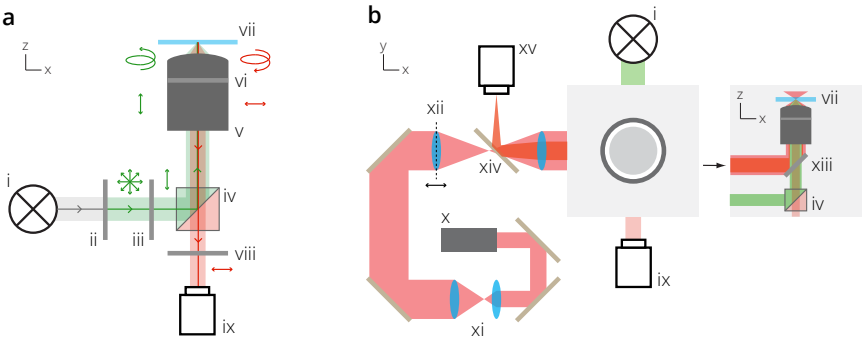

Figure 5.5: Detailed schematic of the main microscope components required for RICM imaging in combination with an optical trap. (a) Quasi-monochromatic light, generated by a mercury lamp (i) (Nikon intensilight) is directed through a 546 nm (± 12.5 nm) interference filter (ii) and focused in the back-focal plane of the objective to achieve Köhler epi-illumination. This light is filtered by a linear polarizer (iii) and guided with a polarizing beam splitter (iv) (Edmund Optics) into the objective (v) (Antiflex EC "Plan-Neofluar" 63x/1.25 Oil, Zeiss). A quarter-wave plate built inside the objective (vi) changes the light to circular polarization where after it illuminates the sample (vii). Part of the light that gets reflected by the sample is collected by the objective and passes through the polarizing beam splitter through an analyzer (viii) onto the sensor of the sCMOS (PCO.edge 5.5) camera (ix).
(b) A 1064 nm laser (IPG YLM-5-1064-LP) (x), is guided by two mirrors into the beam expanding telescope (xi). The expanded beam is subsequently guided into a steerable telescope (xii) that can steer the focus of the trap in x, y and z directions by a manually controllable stage. This steerable telescope lens is additionally placed on top of a piezo stage for automatic control of the trap depth. After being coupled into the objective by a dichroic mirror which reflects 1064 nm light while transmitting lower wavelengths (xiii), the incoming beam is focused into the sample (vii). A 50/50 beam splitter (xiv) is placed in the light path for projecting the beam when reflected back from the sample onto a CCD camera (Hamamatsu) (xv), which facilitates the positioning of the beam onto the camera image and analyzing its shape. For clarity the positions of the mercury lamp (i), polarizing beam splitter (iv) and the sCMOS camera (ix) depicted in (a) are also included.

(1.25) oil-immersion objective, the focus has a very small focal depth, hence only a 2D slice of the 3D interference pattern is visualized. Thus, the pattern of the Newton rings depends on the object plane of focus. Typically, one will adjust the focus to produce an interference pattern that contains the highest contrast. However, the position of this high-contrast plane changes with the distance of the bead with the substrate, which compromises the height measurement. Therefore, to circumvent issues generated by continuously changing the focal plane, the measurements were conducted with the microscope's focus fixed at the coverslip-bilayer interface. Maintaining the focus on the coverslip/medium interface is achieved by utilizing a strict autofocussing protocol developed by Heinrich et al. and also described by Wong et al. [213, 214]. The protocol is based on maintaining the z-position of the stage where the contrast of the image with the area outside the image is highest. For this purpose the position of the aperture is adjusted so that one edge of the aperture is imaged by the camera. During the course of a measurement, the variance of the pixel intensities in a small rectangular area covering a portion of the pixels in- and out-side the aperture image is continuously monitored. Using a piezo-stage (Mad City Labs, Nano-OP50-M) that controls the z-position of the stage

with ~0.1 nm steps, the stage is controlled to find and keep close to the position where the measured variance is ~95% of its maximum.

Using image recognition software, the center and the phase of the minimums and maximums of the ring patterns are determined to asses the lateral and axial position of the particle. High-speed tracking of the lateral bead position is achieved by implementing a series of algorithms developed by Wong et al [214]. Briefly, the center location is refined by *(i)* weighted center-finding of intersecting intensity gradients; and *(ii)* normalized cross-correlation of the pattern with horizontally or vertically flipped mirror images of itself (see Fig. 5.7a-f).

Once the bead center is known, the intensity profile is analyzed to determine the bead height and radius. Because we focus the objective at the plane of the coverslip/ buffer interface, its interference pattern dominates the detected intensity distribution. Therefore, to enhance the signal to noise ratio of the signal coming from the particle, the radial pattern is circularly averaged (Fig. 5.7g&h).

To extract the particle height, we correlate the averaged radial profile with a model that is based on geometrical optics first proposed by Readler et al., 1992 [215] and further improved by Heinrich et al., 2001 [213]. The model accounts for the fact that the illumination of the mercury lamp has only temporal coherence. For an interference event between two rays to be detected by the camera, the rays must originate from common incoming rays. Fig. 5.6 illustrates that the interference pattern is generated only by the rays that reflect from the microsphere under normal incidence. From geometric principles, the optical path difference in the schematic of Fig. 5.6b, is defined as

$$\Lambda(r) = 2n\sqrt{r^2 + (h+R)^2} - R \tag{5.8}$$

From Eq. (5.8) the phase difference is given by

$$\begin{aligned} \Delta(r) &= \frac{2\pi\Lambda(r)}{\lambda} + \delta \\ &= \frac{4\pi n\sqrt{r^2 + (h+R)^2} - R}{\lambda} + \pi \end{aligned} \tag{5.9}$$

where r is the radial distance from the axis of symmetry, R is the radius of the particle, and h is the height at which the particle is floating above the substrate. The value of the refractive index $n \approx 1.34$ for the buffer solution and the wavelength was $\lambda = 546$ nm. A phase shift of $\delta = \pi$ is introduced to account for the reflection at the high index glass surface of the microsphere.

Extrema of the cosine of the phase shift $\Delta(r)$ determine the positions of the fringes in the Newton-ring pattern. Due to the dependence of the reflected intensity on the incoming angles through Fresnel coefficients, which is convolved with the diffraction-limited transfer function of the microscope, the mapped interference pattern is additionally modulated. As recognized previously, this can be approximated by superposing Gaussian contrast functions on the ideal radial intensity profile,

$$I(r) = A_1 e^{-b_1 r^2} + A_2 e^{-b_2 r^2} \cos(\Delta(r)) \tag{5.10}$$

where $A_{1,2}$ and $b_{1,2}$ are empirical fitting parameters. In our experiments, the height of a particle above a lipid bilayer coated substrate is determined by fitting the radially aver-

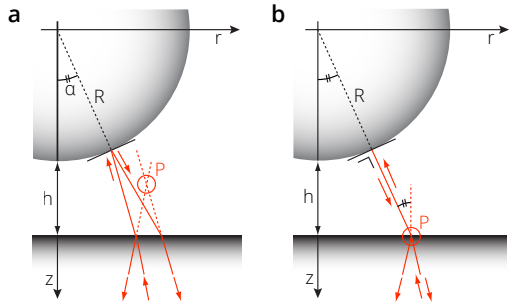

Figure 5.6: Illustration explaining the geometric principles of the model used to determine the height from the Newton ring pattern obtained from the captured RICM image of a particle floating right above a substrate. (a) Illustration showing how an incoming light beam is reflected when it hits the particle's surface in an angle other than normal to the surface. The location of self-interference for the reflected rays is imaged above the substrate at focus position P. (b) An example of the course of a light ray that approaches the particle under normal incidence, causing the reflecting ray to hit the substrate at the same spot as where it originated from and hence the location of self-interference is imaged at the substrate/buffer interface (P).

aged intensity profile as depicted in Fig. 5.7h, to Eq. (5.10). Typical fit results of a trapped bead kept at different heights are shown in Fig. 5.7i.

Due to the substantial processing time the image analysis is performed off line. This means that the images are first taken and stored after which they are fed to a Matlab routine that repeats all the described processes of finding the particle center, computing the radial profile and fitting for each individual image and stores the obtained x, y and z coordinates as well as the other fitting parameters and residuals. This enabled us to automatically analyze several thousands of images in the order of several minutes.

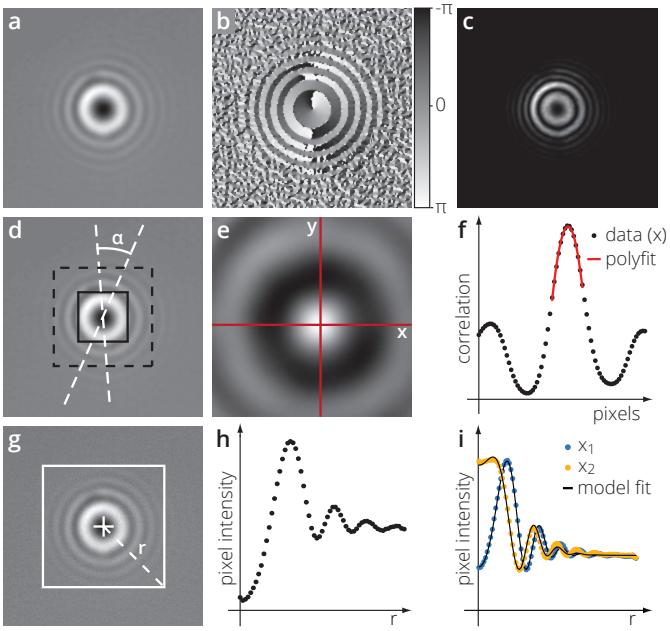

Figure 5.7: The RICM pattern analysis procedure. To determine the lateral and axial position of a microparticle above a planar surface, the radial pattern imaged with RICM needs to be analyzed. This is achieved by first localizing the center of the ring pattern followed by circularly averaging the pixel intensities a distance r from the center. The center is localized by conducting a sequence of image processing steps. First, the center is approximated by computing intersecting gradients. For a radially symmetric feature, the vast majority of intensity gradients point either towards or away from its center. The gradient lines are obtained by convolving the Gaussian blurred image (a) with a Sobel gradient operator and storing the direction (b) and squared magnitude (c) at each pixel. The intersection of two gradient lines are accepted when both magnitudes are greater than a certain threshold and the angle (α) between them is greater than 30° (d). In parallel, the cumulative sums are computed, which are needed to calculate the center of the radially symmetric pattern as given by the weighted 2D average position of all suitable gradient intersections. The averages are weighted by the sine of the intersecting angle. The precision of the center of the bead is further improved by cross correlating the area indicated by the black box in (d) with a diagonally mirrored version of itself. Performing the cross correlation for an area around the ring pattern (the dashed box in d) gives a map of the level of correlation (e) and the coordinates of its maximum correspond to the center of the concentric Newton ring-pattern. To achieve subpixel resolution, a low-order polynomial is fit to a small range of cross-correlation data around the center and the location of the maximum of the fitting curve is computed (f). Finally, the intensity profiles over all radial directions around the center (g) are averaged and the resulting 1D radial profile (h) is fitted to the fitting function described in the text in order to retrieve the height of the particle. (i) Resulting radial profiles and fits obtained from placing the telescope lens, which defines the focus of the trapping laser beam and hence the height of a trapped bead, at two positions $x_1 = 0.0\mu$m and $x_2 = 78.5\mu$m. The retrieved corresponding heights, h_1 and h_2, were 31.3 and 78.5 nm respectively. See section 5.3.2 for an explanation on how lens displacements affect the height of the trapped particle.

5.3.2. AXIAL PULLING METHOD: CALIBRATION

In addition to the optics required for RICM, an additional sequence of optics is built around the microscope to focus a 1064 nm laser into the sample in order to trap a microparticle. Details of the arrangement of the optical parts are schematically shown in Fig. 5.5b. With the piezo stage to which the telescope lens is attached and which is connected to the software we can control the focus depth of the optical trap and hence the particle height with nanometer precision. How the manipulation of the piezo stage results in a displacement of the trap focus is illustrated in Fig. 5.8. Moving the telescope

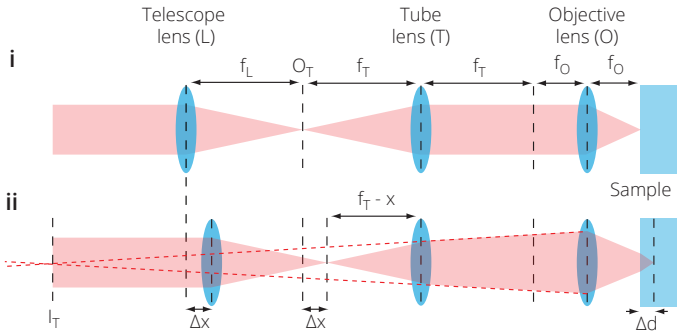

Figure 5.8: Schematic illustrating the relation between the displacement of the telescope lens to the final displacement of the focus of the optical trap in the sample. In the image, two situations (i and ii) are compared in which the telescope lens (L) in ii is moved by a distance Δx with respect to the situation in i. The quantitative relation between the attributed Δx and the final displacement of the trap Δd is obtained using the lens equations and the focal lengths of all contributing lenses. The focal lengths of the telescope, tube and objective lenses are annotated by f_L, f_T and f_O respectively. O_T is the object of the tube lens and I_T indicates the position of the virtual image created by moving the telescope lens. To obtain the correct Δd one should also take into account the extra refraction enforced by the different refractive indices of the glass substrate and the buffer solution of the sample. The exact relation is explained in more detail in the main text.

lens forward by a distance Δx results in an equal displacement of the object plane of the tube lens, thereby creating a virtual image before the object. This virtual image relocates the object for the objective lens. With,

$$\frac{1}{f_T} = \frac{1}{O_T} + \frac{1}{I_T} \Rightarrow \frac{1}{I_T} = \frac{1}{f_T} - \frac{1}{O_T} = \frac{1}{f_T} - \frac{1}{f_T - \Delta x} = \frac{-\Delta x}{f_T^2(1 - \frac{\Delta x}{f_T})}$$
$$I_T = \frac{f_T^2(1 - \frac{\Delta x}{f_T})}{-\Delta x} \tag{5.11}$$

the object for the objective lens becomes,

$$O_O = f_O + f_T - I_T = f_O + f_T + \frac{f_T^2\left(1 - \frac{\Delta x}{f_T}\right)}{\Delta x} \tag{5.12}$$

Notice the sign change which is due to object and image being on the same side of the lens. Then from eqs. (5.11) and (5.12) and the relation,

$$\frac{1}{f_O} = \frac{1}{O_O} + \frac{1}{I_O} \Rightarrow \frac{1}{I_O} = \frac{1}{f_O + \Delta d} \tag{5.13}$$

we obtain

$$\Delta d = \frac{f_O^2}{f_T^2}\Delta x \tag{5.14}$$

Due to refraction at the glass/water interface, the true beam focus moves only by $\Delta\tilde{d} = (n_w/n_g)\Delta d$. From Eq. (5.14), the known focal lengths of the tube and objective lenses of respectively 200.0 and 2.6 mm and the refractive indices of water and the Menzel® glass coverslip of 1.33 and 1.52 respectively, a telescope lens displacement of 1.0 μm is expected to exert a trap displacement of 0.15 nm. The range of the piezo stage is limited to 320 μm hence we can move a particle over a height difference of ~47 nm. Considering the measured height difference at the extremities of the range of the piezo stage as shown in Fig. 5.7i, $\Delta h = 78.5 - 31.3 = 47.2$nm, the theoretically calculated displacement accurately predicts the experimentally attainable value.

How reproducible the expected focus displacement is, is determined by repeatedly moving the telescope lens from maximum to minimum displacement while trapping a 3.56 μm particle at a laser power of 0.8W and monitoring its motion relative to the underlying coverslip. The resulting heights during such a ramp are plotted in Fig. 5.9. The

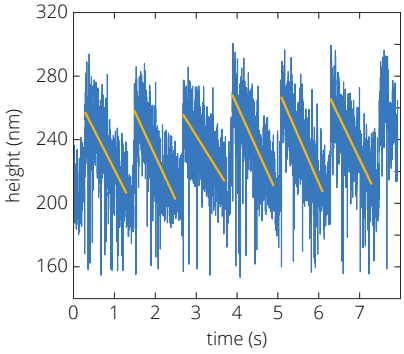

Figure 5.9: The height of a trapped particle, $\varnothing = 3.56\mu$m, upon repeatedly moving the focus of the trap in z direction. At the start of each ramp, the lens was positioned at 320 μm where the particle was held for 100 ms. Then the lens was moved to 0 μm at a constant speed of 320 μm/s, kept there for 100 ms, and instantly moved back to 320 μm again. The ramp could not be simultaneously started with the recording, hence the recording was started and stopped while the ramp was continuously repeated. Each applied linear motion is fitted to a linear fit (orange lines) to extract the speed of the particle's height displacement.

absolute maximum displacement attainable is deduced from the slopes of the linear fits that cover the parts of the curve during which the lens was moving. The mean slope is equal to -52.7 ± 5.7 nm/s, hence the maximum expected displacement of 47.2 nm can be reproduced.

Next to the automatic displacement of the trapped particle, the stiffness of the trap has to be determined. Because of the RICM functionality this can be done in x, y and z directions. The stiffness calibration is done by recording RICM images of the Brownian motion of a trapped bead at maximum attainable frame-rate of 1000 Hz at different laser powers [216]. Then the obtained x, y and z displacements are expressed in terms of their frequency components from which a power spectrum is computed. Each obtained

spectrum is binned and is fit to the Lorentzian, Eq. (5.15), which yields the trap spring constant k_c in N/μm in x, y and z directions.

$$P(f) \equiv |x^2(f)| = \frac{k_B T}{2\pi^2 \gamma (f^2 + f_c^2)} \tag{5.15}$$

where γ is the friction coefficient defined as

$$\gamma = 6\pi\eta R \tag{5.16}$$

and where D represents the bead's diffusion constant, η the dynamic viscosity, k_B the Boltzmann constant, T the absolute temperature, f the frequency and k_c the trap stiffness. The radial cutoff frequency of the system f_c is defined as the frequency at which $P(f)$ is one-half its maximal value

$$f_c = \frac{k_c}{2\pi\gamma}, \tag{5.17}$$

where k_c is the trap stiffness.

It is known that sampling Brownian motion with a camera is distorted by two important effects [216, 217]. The first is due to the finite sampling time of the camera, meaning that it collects data over finite integration times, thereby averaging events that happen in between time points. This time averaging is often referred to as video image blur and adds errors in the position of the tracked particle and also causes systematic biases when quantifying fluctuations. The second effect is aliasing, which results in a contribution to the frequencies of the measured spectrum by signal frequency components that are higher than the sampling frequency. This principle is known as back-folding, and although it does not affect the integrated power of the spectrum, it does change its shape and therefore the cutoff frequency of the system. Assuming that the integration window of the camera is rectangular the measured power spectra are corrected for both described effects by applying the correction steps described by TeVelthuis et al. after which the real power spectra are retrieved [216].

In Fig. 5.10a a typical power-spectrum of the fluctuations in z of a 3.56 μm diameter particle trapped by the laser at an input laser power of 0.1 W is plotted. The powerspectrum is fitted to Eq. (5.15) and from the obtained f_c, the stiffness of the trap, k is calculated. Fig. 5.10b shows the stiffnesses of the trap at a range of laser powers, which verifies the linear relation between the input laser power and k_c.

5.3.3. LATERAL PULLING METHOD: SETUP

A schematic of the used setup is given in Fig. 5.11. All the components in the setup are build around a Nikon Eclipse Ti inverted microscope. Two optical traps are coupled into the microscope each with their own wavelength, a 1064nm and a 808nm trap. In the optical path of the 1064 nm laser there are two Acousto Optical Deflectors (AOD's) positioned, one for either x or y deflections. These deflectors are controlled by custom-made software, making the 1064nm trap fully steerable from the software, within an area of 25μm×25μm. After the light beams of both lasers have passed through the sample they are split by a dichromatic mirror, directing each beam to their corresponding Quadrant Photo Diode (QPD). Both QPD's measure X, Y and Sum signals, where X=(I+III)−(II+IV),

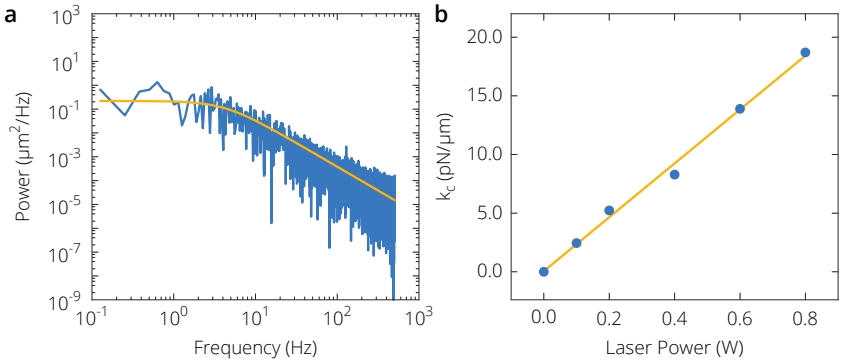

Figure 5.10: Determining the stiffness of an optical trap. (a) Typical powerspectrum (blue line) of the motion in x direction of a micro-particle ($\varnothing = 3.56\mu$m) trapped by the 808 nm laser at a power of 100 mW (input settings). The spectrum is fitted to Eq.(5.15) (orange line) to extract the corner frequency, f_c, and the corresponding stiffness, k_c, which are in this graph equal to 4.2 Hz and 2.4 pN/μm respectively. (b) The stiffnesses of the 808 nm laser at different input powers probed with the same micro-particle as in (a). The obtained are linearly proportional to the laser power with slope 0.02 and zero offset.

and Y=(I+II)−(III+IV), and Sum=I+II+III+IV, see Fig. 5.11 for the symbol explanation. The X and Y signals are normalized to compensate for fluctuations in light intensity, by dividing the signal by the Sum. The resulting values range from -1 to +1 where only the sub range -0.5 to +0.5 is considered to be linear. To visualize and record a sample, a camera (Photometrics Coolsnap HQ^2) is attached as well. The camera is also used to calibrate the AOD's.

5.3.4. LATERAL PULLING METHOD: CALIBRATION

Each time before a measurement is started a sequence of calibration steps was performed. First the positions of both lasers are centered with respect to the camera image. This is achieved by trapping a bead with one of the lasers and positioning it in the center of the camera image by manually adjusting the x,y position of the corresponding telescope lens. Then the AODs are calibrated by steering a bead that is trapped in the 1064 nm laser over a specified grid and recording the applied steering voltage and the actual bead position on the camera image. A Hough Circle Transformation is applied to detect the bead's center from the camera images. From the constructed map the AOD voltages are linked to positions in the sample. When the AOD voltage-to-μm conversion is known, the 1064 nm laser is set to 4.5V in the x direction which corresponds to ~5.5 μm. In both lasers a bead is trapped and the z-positions of the focus points of both lasers are leveled by based on the positions of two equally sized particles. To minimize hydrodynamic drag effects occurring near the substrate surface, the beads are brought roughly 35 μm above the substrate of the sample cell. The stiffness of both laser traps is determined by analyzing the power spectrum of the displacements of the trapped particle by measuring its corresponding QPD signal for a few seconds at a rate of 200 kHz. For this, both laser beams are aligned such that the laser spots are circular and that all the light is projected on the center of the QPD sensors. Each obtained spectrum is binned and the average of

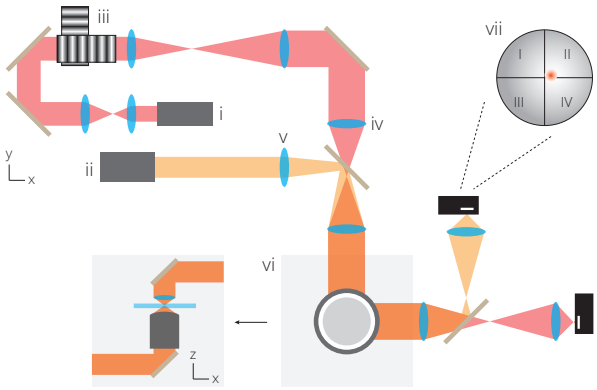

Figure 5.11: Schematic of the laser setup for the simultaneous trapping of two micro-particles by two independent lasers. A 1064 nm (i) and a 808 nm laser (ii) are directed via reflecting mirrors and beam expanders into the x and y AOD's (iii). Through two corresponding telescope lenses (iv,v) which allow for the manual manipulation of the beam focus position, the beams are coupled into the objective (vi). The objective lens focuses both light beams in the sample after which the transmitted light is guided onto two separate QPD sensors (vii). Each of the QPD sensors is divided into four quarters (I, II, III and IV) that allow for the quantification of any x, y deflections that the laser underwent upon passing through the sample, as is explained in the main text.

multiple spectra (≥ 10) is fit to the slightly modified Lorentzian as presented by Eq. (5.15),

$$P(f) \equiv |x^2(f)| = \frac{p^2 k_B T}{2\pi^2 \gamma (f^2 + f_c^2)} \tag{5.18}$$

By describing a trapped particle's position $x(t)$ in terms of its frequency components, a Lorentzian fit to the power spectrum yields the trap spring constant, k_c (Eq. (5.17)), and the sensitivity, p in m/V of the QPD in the x direction.

5.3.5. LATERAL PULLING METHOD: MEASUREMENT ROUTINE

For each measurement a pair of differently-sized beads was trapped by the two lasers, where the smallest bead was always trapped in the stationary 808 nm laser. In Fig. 5.12 the deflections of both trapped particles in a typical measurement are plotted. A measurement starts with an 'equilibration' phase during which the particles are held far apart. This is followed by an 'approach' phase during which the particle trapped in the 1064 nm laser is moved towards the stationary particle. Then the particles are kept at close proximity for 30 seconds ('dwell' phase) to allow for an interaction to take place after which they are separated again. The recorded deflection signal obtained during this sequence of events is corrected by subtracting the offset defined by the mean signal during the equilibration phase and linear drift from the original signal and is subsequently filtered using a Savitzky-Golay filter with a window length equal to 50 miliseconds and a polynomial order of 3, to increase the signal to noise ratio which enables the rupture event detection described later on.

Firstly, it can be seen that considerable deflections are recorded in the y direction even when we displace the particle in the 1064 nm laser solely in the x direction. This

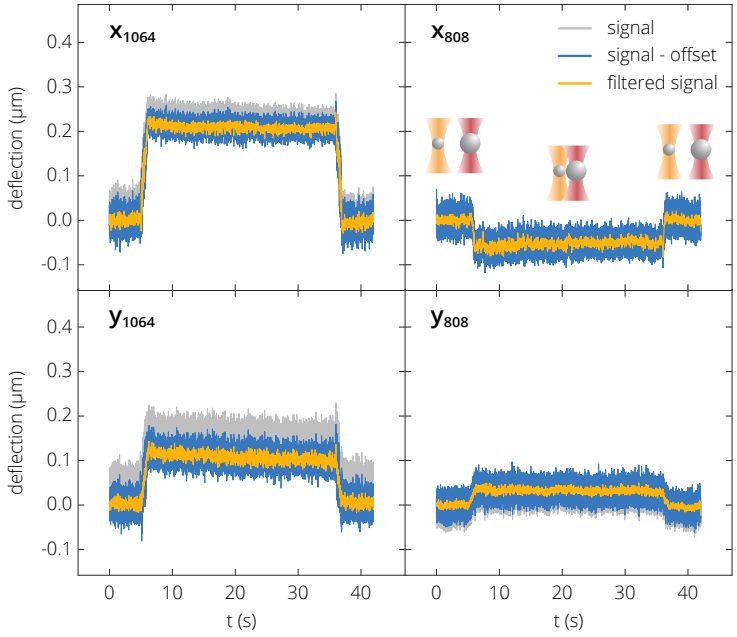

Figure 5.12: Particle deflections in x and y corresponding to either a particle trapped by the 808 or 1064 nm laser during the course of a typical measurement. No binding event was detected during this particular experiment.

is probably due to the imperfect AOD-controlled motion of the laser focus and the fact that the opposing particles are not perfectly aligned. From here on we only consider the deflections recorded in x.

Furthermore, notice the significant deflection shifts from the baseline during the approach and retract phases on both QPDs even when there are no molecular links between the beads. Plotting the mean deflections of the 808 nm laser measured during the dwell phase at different trap separations revealed that these shifts are a result from the overlapping trap potentials at small separations (see Fig. 5.13). Here, the separation is defined as the initial position of the center of the 1064 nm laser minus the induced displacement. Below a certain trap separation both beads start experiencing a pulling force from the other trap, indicated by a negative deflection of the 808 nm laser. The magnitude of this deflection keeps declining upon decreasing the trap separation until the beads collide and start pushing each other back towards their respective trap centers indicated by a recovering deflection signal.

Similar behavior is expected to occur for the deflections of the bead trapped by the 1064 nm laser. However, the actual responses of the bead trapped in the 1064 nm laser were obscured by two effects as can be seen in Fig. 5.14. The first effect is caused by the movement of the laser. During the movement of the laser, the shape of the beam profile slightly changes due to small differences in how the laser is aimed on the different optical parts of the microscope which leads to slight changes in the position where the laser

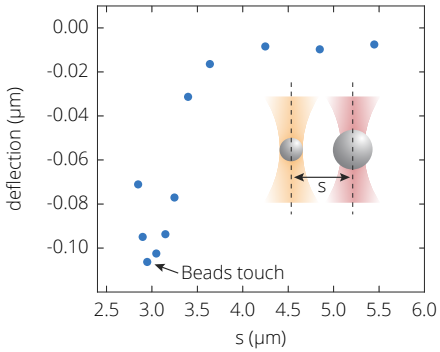

Figure 5.13: Relation between the mean deflections of a micro-particle trapped in the 808 nm laser and the separation with the second 1064 nm trap.

beam hits the QPD sensor. The relation between the imposed response and the velocity of the applied trap motion is obtained by performing linear ramps at different speeds with the 808 nm laser turned off. The slopes of the deflection change at different speeds were fitted to a linear model whose slope is used as the coefficient that relates the linear distortion to the trap speed. After each measurement the assumed linear distortion is computed by using the determined coefficient and applied trap speed and is subtracted from the signal.

Secondly, in Fig. 5.14 it can be seen that the deflection signal is modulated with an oscillation with a period between 0.1 and 0.2 seconds and an amplitude of ~0.05 μm. By measuring the laser power right after the laser exits every component in the setup while continuously displacing the laser focus we observed that the modulation occurs after the light exits the AODs. We believe that the imposed oscillation is caused by the light creating a resonance in the AODs, whose frequency is set by the AOD dimensions and can hence not be avoided.

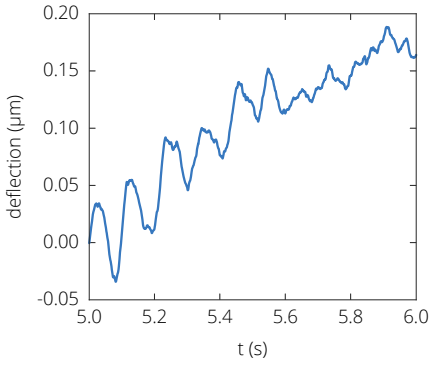

Figure 5.14: Zoomed part of the 1064nm response upon moving the laser focus in x-direction at a speed of 2.4 μm/s.

When during the dwell phase a bond of measurable strength has formed, the absolute deflections start increasing until the bond ruptures or until one bead is pulled into the other trap. The calibrated and filtered QPD response of the 808 nm laser in x direction during a binding and rupturing event is exemplified in Fig. 5.15.

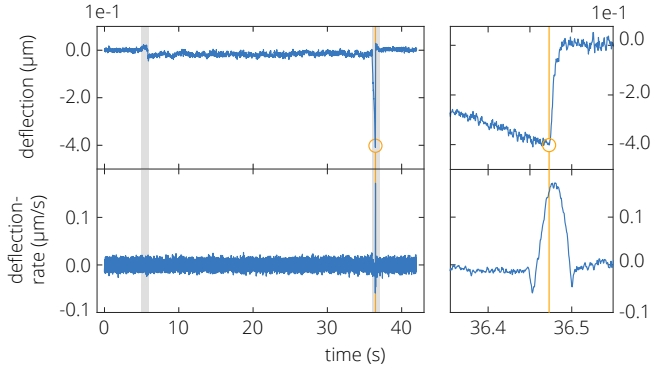

Figure 5.15: Example deflections of the 808 nm laser upon a binding and rupturing event (top) and its corresponding computed derivative (bottom). The shaded areas depict the approach and retract phases respectively. The moment the bond breaks is indicated with the orange circle. The right graph is a zoomed part of the retraction phase.

The moment at which the bond breaks is detected by computing the derivative of the filtered signal and determining where its maximum is located. This value corresponds to the maximum slope and does therefore not correspond exactly to when the bond breaks. To determine the actual breaking moment we scan the QPD responses of the filtered signal back in time from the moment of maximum slope until a value is reached that is within 95% of the minimum deflection. The deflection measured at that time point is multiplied with the stiffness of the trap as determined for each pair of particles, corresponding to the rupture force.

To distinguish between an actual rupture event and an event during which one bead is pulled into the other trap, we use the magnitude of the standard deviation of the signal right after a pull event. When a bond ruptures, both beads return to their equilibrium positions in their respective traps, hence the standard deviation of the signal is similar to the signal during the equilibration phase at the start of the measurement. Due to the lower stiffness of the 808 nm laser and the smaller particle trapped inside it, an unbreakable bond always results in the particle trapped by the 808 nm laser being pulled into the 1064 nm laser. An empty laser trap shows a deflection signal with a significantly reduced standard deviation. Distortions as a result of for example a third bead entering the trap or the rare event of the bead trapped in the 1064 nm jumping into the 808 nm laser, are detected in a similar way and are subsequently removed from the data set. The outlined detection protocol is put together in a Python program, allowing for the automatic analysis of many consecutive measurements.

5.4. MATERIALS AND METHODS

5.4.1. PARTICLE FUNCTIONALIZATION WITH IMMOBILE DNA

To measure the anchoring strength of cholesterol-modified DNA strands in a lipid bilayer, we slightly modified our main model system. For this, one micro-particle was functionalized with cholesterol bearing DNA strands through a biotin-streptavidin bond, while a second particle was surrounded with a lipid bilayer. The system is schematically illustrated in Fig. 5.16.

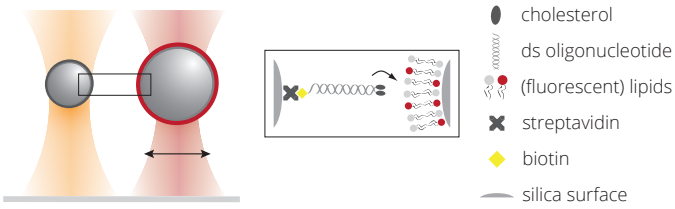

Figure 5.16: A sketch of the experimental setup for assessing the strength of the oligonucleotide-bilayer coupling. The composition of the area outlined by the rectangular frame is schematically illustrated in the center image.

For this purpose, silica microparticles coated with streptavidin ($\varnothing$ = 2.12μm, microparticles.de) were functionalized with biotinylated oligonucleotides based on the method described by Dreyfus et al [64]. Each DNA strand consisted of a 59 nucleotide long oligomer (Eurogentec, Belgium), attached via a tri-ethylene-glycol (TEG) spacer to a 3' biotin group. The opposing 5' end was coupled through the same TEG spacer to a cholesterol group. The strand was hybridized with a 47 nucleotide long complementary strand bearing a cholesterol on its 3' end to establish a double anchor construct. The hybridization was done at an overall concentration of 6.5 μM in 10 mM HEPES/150 mM NaCl buffer (pH 7.4) by slowly cooling from 90 to 22°C.

Different surface coverages were obtained by diluting the total number of functional DNA strands (S) with a certain amount of inert strands (N) which lacked the cholesterol modification. The streptavidin coated silica particles were functionalized with N and S DNA in the ratio $\chi = n_S/(n_S + n_N)$ where n_S and n_N are, respectively, the number of S and N DNA strands per bead. In each case the total number of oligonucleotides that were added to the beads was kept constant at a level ensuring a 100 times excess number of strands with respect to the available total bead surface area. For this purpose 5 μl of bead suspension was mixed with 10 μl of a DNA solution at 6.5 μM concentration and 85 μl buffer, followed by a 30 minute incubation at 55°C which is below the melting temperature of the double stranded tether which is ~80°C at 1 μM. This procedure has been shown to ensure a reproducible, sufficient DNA-functionalization [10]. To remove excess and non-specifically adsorbed DNA we centrifuged (2000g, 25 seconds) and resuspended the particles in 100 μl 10 mM HEPES/50 mM NaCl buffer. The incubation/rinsing procedure was repeated twice.

5.4.2. VESICLE PREPARATION

For the preparation of small unilamellar vesicles (SUVs), the phospholipids 1,2-dioleoyl-*sn*-glycero-3-phosphocholine (DOPC, Avanti), 1-palmitoyl-2-oleoyl-sn-glycero-3-phospho-L-serine (POPS, Avanti) and 1,2- dipalmitoyl-*sn*-glycero-3-phospho-ethanolamine-N-[methoxy-(polyethylene glycol)-2000] (DPPE-PEG_{2000}, Avanti) were mixed in a 190 : 10 : 1 molar ratio in chloroform. For visualizing and confirming the fluidity of the SLB, 0.5 mol % 1,2-dioleoyl-sn-glycero-3-phosphoethanolamine-N-(lissamine rhodamine B sulfonyl) (TRITC, avanti) was added to the lipid mixture. The chloroform was evaporated by a gentle stream of nitrogen and two hours of vacuum desiccation, whereafter the lipids were rehydrated for at least 30 min in 10 mM HEPES/150 mM NaCl (pH 7.4) at a concentration of 2 mg/mL. Small unilamellar vesicles (SUVs) were formed by sonication (45 min) with a tip sonicator (Branson, USA), operated in pulsed mode at 25% duty cycle with refrigeration, followed by centrifugation in an Eppendorf centrifuge (30 min at 20,000 *g* at 4°C) to remove any titanium particles that may possibly be present. SUV suspensions were stored at 4°C.

5.4.3. PARTICLE FUNCTIONALIZATION WITH MOBILE DNA

Silica microparticles were functionalized with lipids and cholesterol modified oligonucleotides using the method described by van der Meulen *et al.*[69]. The two main DNA strands consisted each of a 59 nucleotide long oligomer (Eurogentec, Belgium), attached via a tri-ethylene-glycol (TEG) spacer to a 5' cholesterol group. The final 11 nucleotides at the opposing 3' end were complementary so as to form the sticky ends and are from now on referred to as S and S'. Like for the immobile DNA case, both S and S' were hybridized with a 47 nucleotide long complementary strand bearing a cholesterol on its 3' end to establish a double anchor construct. Different ratios of functional and inert DNA were mixed in 9 μl 10 mM HEPES/150 mM NaCl buffer (*p*H 7.4) and 10 μl SUV suspension. The vesicle/DNA mixture was incubated for 30 minutes at room temperature to allow for the DNA to anchor into the vesicle lipid bilayers. Then 10 μl of bead suspension (SiO_2, 1 mg/ml) was added. The suspension was incubated for 5 minutes, after which 70 μl 10 mM HEPES/150 mM NaCl buffer was added. To get rid of excess and non-specifically adsorbed lipids and DNA the bead suspension was centrifuged (1000g, 30 seconds) and resuspended 5 times in 100 μl 10 mM HEPES/20 mM NaCl / F127(0.5 wt%) buffer. Before use, the particle suspensions were diluted an additional 50 times.

5.4.4. SUPPORTED LIPID BILAYER FORMATION

For the axial pulling experiments custom-made sample cells were used. These sample cells were prepared by cleaning glass coverslips and objective slides by sonication in, subsequently, 2% Hellmanex and Milli-Q. The coverslips were further cleaned in an acid Piranha solution. For this purpose, 100 ml MilliQ was heated to 75°C after which 20 ml concentrated ammonium hydroxide was mixed with the solution. Under continuous stirring with a magnetic stirrer, 20 ml H_2O_2 was added and the solution was heated until 75°C. Once the solution started boiling, the coverslips were submersed and kept in the solution for 10 min. Aftherwards, the coverslips were rinsed by sonication in fresh MilliQ solution. Slivers of parafilm were used as spacers to create three side-by-side channels with a nominal volume of 10 μL each, whereafter slides, coverslips and spacers were

bonded together by shortly heating the assembly until the parafilm melts. The entire construct was sealed with preheated VALAP (Vaseline:Lanoline:Parafine (1:1:1), melting point: 70-80°C). Fluids could still be exchanged through 1 mm diameter predrilled holes in the objective slides. Finally, a SLB was formed by injecting 10 μl SUV suspension (1 mg/ml) to a channel and incubating for 15 minutes after which the SLB was rinsed three times with 200 μl buffer (10 mM HEPES/150 mM NaCl). Prior to the addition of the microparticles, the SLB was rinsed twice with 200 μl buffer containing less salt (10 mM HEPES/50 mM NaCl, pH 7.4).

5.4.5. SUBSTRATE PASSIVATION

For the lateral pulling experiments similar sample chambers were used as for the axial pulling experiments but without the drilled holes. After cleaning the coverslips and objective slides with HellmanexII, the coverslips were exposed to UV/ozone for 30 minutes and to hexamethyldisilazane vapor (HMDS, Sigma-Aldrich) for 15 minutes to render the surface hydrophobic. Channels were made using parafilm slivers to glue the hydrophobic coverslip to a cleaned objective slide and the channels were pre-filled with 10 mM HEPES/ 20 mM NaCl/ F127 (0.5 wt%) buffer (*p*H 7.4) after which the particle suspension was added. The channels were finally sealed with pre-heated liquid VALAP.

5.5. RESULTS AND DISCUSSION

We have developed a model system consisting of micro-particles coated with mobile DNA strands with which we aim to measure the interaction strength between multiple diffusive weak bonds. Here, we present the results that we obtained by conducting the measurement protocol associated with the lateral pulling method as described in section 5.3.5.

5.5.1. ANCHOR STABILITY

Since our model system relies on the hydrophobic anchoring of the interacting oligonucleotides to a lipid bilayer it is essential that while pulling on two linked particles, the hydrophobic anchors do not detach due to the applied force. Therefore, we performed pulling measurements on pairs of beads of which one was solely coated with a lipid bilayer and the other was functionalized with cholesterol exposing oligonucleotides that were coupled to the particle's surface by a biotin-streptavidin link. A schematic of the measurement is provided in Fig. 5.16.

For these experiments the sample composition was slightly different as compared to the conditions during the acquisition of specific oligonucleotide interactions. The NaCl concentration was adjusted to 50 mM instead of 20 mM and the negatively charged POPS lipids were left out of the lipid mixture. We changed these conditions because under the former conditions no binding events were measured. We speculate that the lack of binding events was a consequence of the long-range repulsion between the bilayer and the cholesterol-bearing oligonucleotides due to an imposed kinetic barrier too high for the cholesterol to reach the bilayer. At the increased NaCl concentration and without any negatively charged POPS lipids, binding events were detected. To assess the strength of the anchoring of a single cholesterol-bilayer coupling, we gradually diluted the density

of cholesterol-bearing oligonucleotides by mixing it with increasing amounts of oligonucleotides without the cholesterol modification. The different ratios χ of functional to non-functional oligonucleotides that we tested at are 1.0, 0.05, 0.01, 0.005 and 0.001. From basic geometry principles, we can estimate the number of bonds that can form between two particles using [64],

$$N_b = 2\pi\chi\rho R_p^2 \frac{L - h/2}{R_p + L} \approx 315\chi \tag{5.19}$$

Here, ρ is the total oligonucleotide coverage (6.4×10^3 strands/μm^2), R_p the particle radius (1.06 μm), L the length of the oligonucleotides construct (~15 nm), and $h \approx L$ the distance between the particle surfaces. Hence, going from $\chi = 1.0$ to 0.001 encompasses an expected range of possible bonds between ~100 and 0.1, thereby gradually increasing the likelihood of assessing a single bond. For each experiment we ensured that the particles touched during the dwell phase by bringing the beads at a distance where the deflections progressed through a minimum deflection, which is an indication for the beads pushing each other back towards their trap centers as mentioned in section 5.3.4.

In the majority of binding events that we observed the stiffness of our weakest trap appeared too limited for the bonds to break. As a consequence, an insufficient number of rupture forces were measured to be statistically meaningful and therefore no force distributions are presented. What we do present is the binding and unbinding probabilities as a function of χ, as plotted in Fig. 5.17. The probability of binding is defined as the number of binding occurrences divided by the total number of trials. The number of times the detected bonds could subsequently be pulled apart defines the unbinding probability. For each density at least ten trials with different beads were conducted.

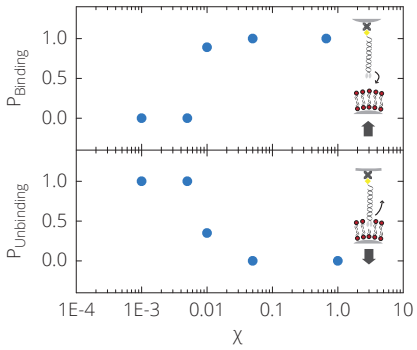

Figure 5.17: Anchoring strength of double cholesterol-bearing oligonucleotides into lipid bilayers. The anchoring strength is represented by the probability of binding and unbinding as a function of the density of anchor bearing oligonucleotides χ.

From the graph it becomes clear that at and above a χ of 0.01 the binding events suddenly become highly probable. Moreover, the detected binding events appeared to have a non-zero unbinding probability only at a χ of 0.01. At higher ratios no unbinding events were observed. Due to the small number of rupture events and hence the lack of

a properly quantified rupture force, we can only explain our observations based on previously reported off rates for the binding of double cholesterol bearing oligonucleotides to a lipid bilayer in equilibrium [116]. According to these measurements, the off-rate in the absence of force, k_u^0, can be expected to be on the order of 10×10^{-5} s^{-1}.

Following the methods discussed in section 5.2, we model the binding process as a Brownian particle trapped in a one-dimensional binding potential $U(x)$, with the reaction coordinate x describing the distance between the cholesterol molecule and the surrounding lipids in the bilayer. At the preferred orientation of the cholesterol within the bilayer ($x = 0$), $U(x)$ should have a stable minimum which is surrounded by a region of attraction that spreads until a certain coordinate x_t outside which the cholesterol-bilayer coupling is considered broken. Using Eq. (5.5), we can estimate the required minimum force to break a *single* cholesterol-bilayer coupling using the optical trap. If we fill in the estimated values for $k_u^0 = 10 \times 10^{-5}$ s^{-1}, $k_b^0 = 100$ Hz, $k_c = 2 \times 10^{-5}$ N/m and $T = 300$ K, we find an equilibrium force, f_{eq} ~1.5 pN. This force-magnitude is very close to the thermal force scale, $f_\beta = k_B T / x_t = 4.1$ pN, assuming a barrier location $x_t = 1$ nm, corresponding to the thickness of one bilayer leaflet. That the equilibrium rupture force is below the thermal force scale implies that the anchoring is thermodynamically unstable, meaning that the anchors should detach spontaneously without the need for an external force. This is however, opposite to the equilibrium binding properties measured previously, which indicated no significant unbinding on the timescale of hours [116, 117].

For *multiple* bonds, we estimate the equilibrium rupture force using Eq. (5.7). Assuming the constant rebinding rate of an individual molecule acting while the total cluster of bonds remains bound, $k_a = 10 k_u^0$, the rupturing of a cluster of $N = 2$ bonds requires an equilibrium force of 10 pN. In the slow-loading regime, the equilibrium force is assumed to be linearly proportional to the number of bonds in the cluster, hence a total number of 6 bonds would already require a force that is beyond the force range of 30 pN permitted by our setup.

The estimated equilibrium forces for both single and multiple cholesterol-bilayer couplings roughly correspond to the binding and unbinding probabilities as plotted in Fig. 5.17. Binding events are seen for $\chi = 0.01 - 1.0$ which correspond to a number of bonds in the order of 1-300. Moreover, only at $\chi = 0.01$ (~1 bond) have we measured unbinding events while at $\chi \geq 0.05$ (~5 or more bonds) all binding events appeared irreversible. Given a maximum applicable force of ~30 pN, the measured binding and unbinding probabilities are not unreasonable.

5.5.2. INTERACTIONS BETWEEN MULTIPLE 'STICKY' ENDS

Despite the possible interesting aspects of investigating the strength of the hydrophobic anchoring of short oligonucleotides in lipid bilayers, the actual purpose of this study is to measure the interactions between multiple, diffusing, short complementary oligonucleotides. To this end, we measured the force required to pull two particles apart that are bridged together by a varying number of complementary oligonucleotides embedded in the lipid bilayers by which each bead is encapsulated. The single stranded oligonucleotide extensions are referred to as 'sticky ends', whose specific sequences are given in chapter 4.

A crucial requirement of this approach is that we are able to control the density of

linking molecules on the particles' surface. For this we compared fluorescence intensities of particles decorated with different ratios of functional to non-functional oligonucleotides χ equal to 1.0, 0.5 and 0.25, using confocal microscopy.

Equal ratios of particles with either FAM6-labeled (S) or Cy3-labeled S' oligonucleotides were mixed and imaged using 488 nm and 561 nm excitation lasers and corresponding photo multiplier tube detectors. Using image segmentation tools implemented in a Python script, we quantified the mean pixel intensity per detected feature. We analyzed multiple images per ratio taken at different areas in the sample to finally compute the normalized histograms presented in Fig. 5.18.

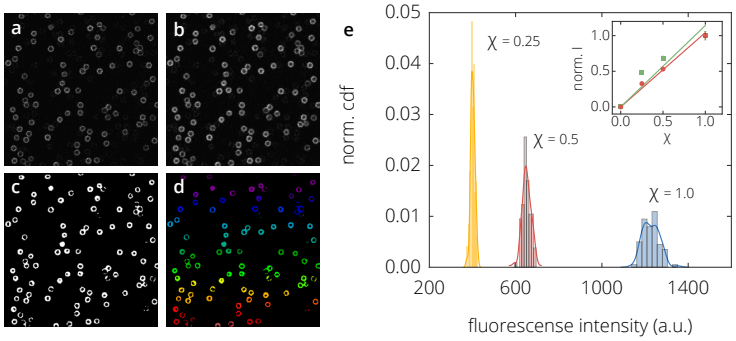

Figure 5.18: The relative fluorescence intensity of microparticles functionalized with different ratios of fluorescent and non-fluorescent mobile oligonucleotides. Confocal micrographs were processed by a sequence of standard image segmentation algorithms provided by Python. a) Original image of the fluorescence intensity detected with the 561 nm channel b) The original image was smoothed with a Guassian blur. c) Using Otsu filtering the images were converted into a binary image. d) Features comprising pixels that were connected according to a squared connectivity structure were grouped into individual features . e) The mean pixel intensity of the features detected with the 561 nm detector of multiple time series taken at five different regions in the sample were computed and plotted in an histogram. The lines are computed using a Kernel density estimator. (Inset) Plot of the mean pixel intensity measured with both the 488 nm (circles) and 561 nm (squares) detectors for each χ, normalized to the mean pixel intensity for $\chi = 1.0$, as a function of χ. The data is fitted to a linear fit with zero offset (lines), giving slopes of 1.04 for the red channel and 1.14 green channel and corresponding χ^2_{res} values of 2.3×10^{-5} and 2.3×10^{-3}.

The average intensities measured for both channels appeared to be linearly proportional to χ with slopes close to 1.0. This indicates that the final oligonucleotide density on the particles correspond closely to the ratios that were mixed during the preparation. Being able to control the oligonucleotide surface density makes our model system suitable for our goal of measuring the interaction strength as a function of oligonucleotide density. For this purpose, we applied the approach/retracting routine explained in section 5.3.5 for ratios χ of 0.0, 0.01, 0.1 and 1.0. The resulting forces measured using the 808 nm trap are presented in Fig. 5.19. The x axis is cutoff at 30 pN which is the upper limit attainable by our instrument, hence all the irreversible binding events for each χ collapse into one point in the plot connected by a dashed line.

For the interpretation of the measured forces we apply the same analysis as performed for the cholesterol-bilayer measurements, i.e. we use Eqs. (5.5), (5.7) to estimate the equilibrium rupture forces for single and multiple bonds respectively. For this we

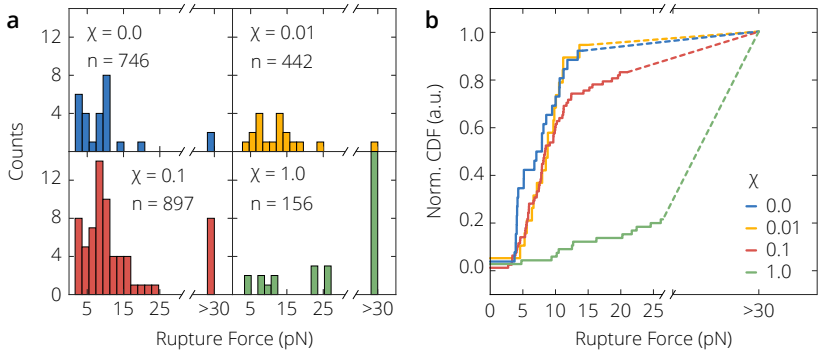

Figure 5.19: Rupture force distributions required to break single or multiple parallel bonds between complementary, diffusive sticky ends. a) Individual histograms of the rupture forces measured for χ = 0.0, 0.01, 0.1, and 1.0. The number of trials per χ are indicated by n. The number of events for a rupture force > 30 for χ = 1.0 originally reached 45, but was truncated for comparative purposes. b) Cumulative representation of the rupture forces presented in (a).

need a value for the activation energy, ΔG_0, that represents the binding of two sticky ends when they are both coupled to a separate particle. Leunissen et al., developed an analytical expression for the interaction potential between particles coated with single-stranded DNA sticky ends that are connected to the surface by short, stiff double stranded tethers. A very crude prediction from their model, is that the free-energy per bond, $\Delta G_{\text{tether}} = \Delta G^0_{\text{solution}} - T\Delta S_{\text{conf}}$, where $\Delta G^0_{\text{solution}}$ is the free-energy of the same bond when free in solution, T the absolute temperature and ΔS_{conf} is the entropic penalty resulting from the confinement of the bond between the two particle surfaces [11]. $\Delta G^0_{\text{solution}}$ can be calculated using the free-energy calculation method developed by Santa lucia et al. [218] which is implemented by the online tool called mfold (http://unafold.rna.albany.edu/). Entering the sequences of our sticky ends (see chapter 4) and the conditions corresponding to our experiments, we find $\Delta G^0_{\text{solution}} \approx -5 k_B T$. According to the study of Leunissen et al., the configurational entropy cost is approximately -10 $k_B T$, hence $\Delta G_{\text{tether}} \approx 5\ k_B T$. Combined with again a k_b = 100 Hz, Eq. (5.5) gives $f_{eq} \approx 0.9$ pN. This is substantially less than the thermal force scale, $f_\beta = k_B T / x_t \approx 4$ pN, assuming x_t = 1 nm, which means that the bond is thermodynamically unstable.

Regarding the non-zero forces measured at $\chi = 0$ and the approximate number of overlapping linkers at χ = 0.01 to be approaching 1, any rupture events between sticky end may be hidden among the non-specific binding events. The specific interactions become measurable when increasing the sticky end density to 0.1, indicated by a shift of the distribution to slightly higher forces as well as an increase in the number of unbreakable bonds. This change in the rupture force might be due to the breaking of multiple bonds. To estimate the equilibrium force for multiple bonds we use Eq. (5.7) again. Here we fill in for the $k^0_u = k^0_b / (\exp(\Delta G_0 / k_B T) = 15 \cdot 10^3\ \text{s}^{-1}$, where k^0_b = 100 Hz. Together with the remaining parameters already outlined above and $k_a = 10 k^0_u$, we obtain an equilibrium force, f_{eq}, equal to ~10 pN for N = 2 bonds. Assuming a linear scaling with the number of bonds in the slow loading regime, this implies that already with a few parallel bonds

the rupture force becomes too large for us to measure. Which is indicated by the number of unbreakable events at $\chi = 0.1$ and 1.0. In conclusion, though the measurements here clearly show that there is a relation between the rupture force and the number density of bonds, what this exact relation is remains to be measured. Yet, due to the limited accessible force range of our instrument and the rapidly increasing rupture force with the number of bonds, it is recommendable to change to an alternative measurement technique that enables probing at higher forces.

As already briefly pointed out, a considerable number of non-zero rupture forces for $\chi = 0$ were measured. The origin of these interactions remains elusive, yet it is not unlikely that it they were due to non-specific hydrophobic or electrostatic interactions between the DNA and the bilayer, which might occur when the beads are pushed very close together [219–221]. To reveal any existing relation between the separation at which the beads are brought together and the occurrence of a binding event, we evaluated the separation, s, between the two trapped particles during the course of an experiment as defined by

$$s(x) = x - r_1 - r_2 - \delta_1 - \delta_2 \tag{5.20}$$

where x is the position of the movable 1064 nm trap, r_1 and r_2 are the radii of both trapped particles and δ_1 and δ_2 the non-zero deflections induced by the overlapping trap potentials at close contact. Fig. 5.20a provides a schematic illustration of this definition. In practice the variables composing the separation yield high uncertainty levels, e.g. the

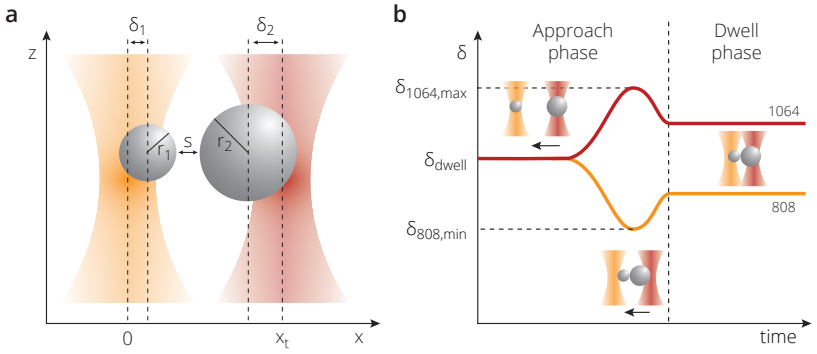

Figure 5.20: Schematic representation of the evolution of the deflection signal δ if two trapped beads are brought beyond touching separation. a) Illustration of how the particle-particle separation $s(x = x_t)$ is defined. b) Evolution of the deflection signals, δ, of both traps during the approach and dwell phase of a typical experiment. During the approach phase, the particle in the 1064 nm trap is moved towards the 808 nm trap. At a certain separation, the particles inside these traps are attracted by the opposing traps, represented by a changing δ. The moment the two particles touch but the traps are brought even closer together, the absolute values of δ decline again, as the particles are pushed back into their respective traps.

sample to sample variance in particle size and the day to day difference in trap alignment. More importantly, the definition assumes that both trap centers are positioned perfectly on the coordinates x_{808} and x_{1064}. As this positioning relies on the interpretation of camera images and manually adjusting the x and y positions of the telescope lenses, the positioning process introduces large uncertainties. These factors combined

generate a huge spread on the separation making it a unreliable representation for the actual separation. As we have seen in Fig. 5.13, once the two traps come in close enough proximity the trapped particles become slightly attracted by the opposing trap causing an increasing absolute deflection signal $|\delta|$. Decreasing the separation even further eventually causes the particles to sterically interact, effectively pushing them back towards their respective trap centers, represented by a decreasing $|\delta|$. How close the beads are together is therefore indicated by the imposed deflection at close separation. However, when the beads touch while their traps are still moving towards each other, the imposed deflection goes through a minimum, hence certain deflection values may indicate two different separations. As a consequence, just taking the level of deflection during the dwell phase is also an insufficient indicator for the separation. To obtain a more suitable indicator, we introduce the unit-less touch-ratio, β, which is defined as the dwell phase deflection divided by the minimum deflection measured during the approach phase δ_{min}.

In Fig. 5.21, the value of β obtained for each individual measurement is plotted, including those where no binding event occurred. The figure additionally displays whether a binding took place and whether this bond ruptured upon pulling. The binding events

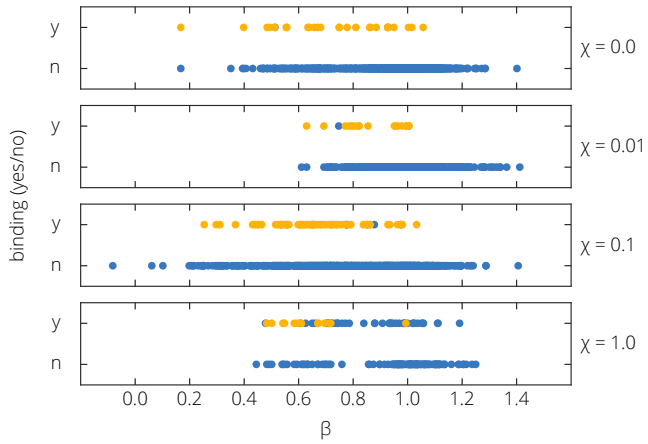

Figure 5.21: The binding and unbinding of two particles interacting through varying densities of diffusing DNA linkers, χ, as a function of the level of separation β. Each dot represents a single measurement. A binding event is plotted on the line annotated by 'y' in which the reversible events are indicated in yellow. Each graph represents the results obtained for $\chi = 0.0, 0.01, 0.1 \text{and} 1.0$.

predominantly occur at $\beta \leq 1.0$, which indicates that the beads should touch or be at least very close to touching before the sticky ends can interact and bind. Secondly, only at $\chi = 1.0$ a substantial number of binding events were measured at $\beta > 1.0$, of which there was only one reversible.

The binding events for the other densities are not correlated to a certain separation, they are extended over a wide β-range. Accordingly, as the only slight distance dependence is seen for $\chi = 1.0$, only at this particular ratio it can be said that the interactions are from specific DNA interactions. As the rupture events at lower ratios cannot be distinguished based on their separation level it cannot be excluded that we have been mea-

suring non-specific interactions in all those cases.

5.6. CONCLUSION

This chapter revolved around the role of multiple diffusive weak interactions in both biological and synthetic systems. Recently published studies pointed at utilizing multiple interactions to enhance the targeting of pathogens or tumor cells. We and others exemplified the beneficial effects of the diffusing characteristics for self-assembling colloids.

These studies are still at the brink of understanding the mechanism underlying processes mediated by multiple weak interactions. The development of a simple model-system in which the impact of different parameters like strength, mobility and density of the multiple bonds can be studied is therefore desired. In this chapter we presented such a model-system based on solid colloids covered with a lipid bilayer into which short double stranded oligonucleotides are embedded through a hydrophobic anchor. The ends of the surface mobile oligonucleotides constitute a short sequence of 11 nucleotides that is designed to be complementary to the ends of the oligonucleotides on a second set of particles. This generates an attraction that bridges two or multiple complementary particles together. The strength of the attraction can easily be adjusted by e.g. changing the length or sequence of the complementary ends, varying the surface density of the oligonucleotides or changing the diffusibility by adjusting the lipid composition.

Secondly we presented two techniques that can be utilized to probe the strength of the interactions, making them potentially suitable tools to unravel the influence of the aforementioned parameters. Both techniques relied on optical tweezers and we referred to them as the lateral and axial pulling methods. Since the development of the axial pulling method was not fully completed, we only explained the principles of the technique and showed the first results of the calibration measurements.

The setup for the lateral pulling method on the other hand was readily available and we have presented the first results of the force measurements. We were interested in the magnitude of the force that is required to rupture the bonds between two particles as a function of oligonucleotide density. We demonstrated that this density can be tuned by mixing functional with non-functional oligonucleotides (DNA strands that lack the complementary ends). The rupture-force measurements revealed that at high oligonucleotide density the force to rupture the majority of the binding events was too high for our setup to induce.

Lowering the relative density to 10% caused the binding occurrence to go down as well as the number of unbreakable bonds. Strikingly, going to 1% or even 0%, although the number of binding events dropped even further, the rupture forces required to break the low number of binding events appeared to be very similar to the rupture-forces measured at 10%. This raises the question what interactions we have actually been measuring.

The bead separations at which the beads were held to allow for an interaction, revealed no specific pattern, i.e. unbreakable bonds or the binding events measured at 0% density did not take place at specific separations. It has to be stressed that the noise level in the separation is very high due to the high uncertainty in the variables defining the separation. However, the noise levels are substantially reduced by the high number of repetitions per condition and still no structural pattern can be observed. Hence, for the

low density cases we cannot say with great certainty that the measured rupture forces actually came from dissociating oligonucleotide ends.

It can be concluded however, that the number of irreversible bonds increased upon increasing oligonucleotide density, which demonstrates the tunability of the model system. Therefore, the endeavor of measuring the rupture forces using our developed model system of colloids with surface mobile oligonucleotides is worth pursuing. Yet, for measuring the magnitude of the rupture force required for these unbreakable bonds one is advised to switch to other techniques. Existing methods that are more likely to be able to measure the high rupture forces are AFM, Acoustic force spectroscopy [222], magnetic tweezers or the centrifuge force microscope [223]. Alternatively, the strength of the individual bonds can be tuned down by lowering the number of complementary nucleotides, thereby reducing the rupture force of the combined multiple bonds.

In addition, it could be interesting to deduce the origin of the rupture forces measured at 0% density, which we now have simply attributed to non-specific interactions. We have already studied the effects of ionic strength and lipid composition to reduce their occurrence, yet the number of binding events could never be totally reduced to zero. Information on what causes these interactions would help to find conditions were the non specific attraction is reduced to a minimum and subsequently show whether the rupture forces measured at 1 and 10% densities are coming from DNA bonds.

We thank Gijsje H. Koenderink for facilitating the optical tweezer setup and the AMOLF technical support for implementing the required software adjustments.

6

CONCLUSION AND OUTLOOK

Inspired by the way cells interact with their surroundings through the use of surface-mobile receptors embedded in their membranes, we investigated the beneficial effects of such mobility on the self-assembly of micro-particles coated with DNA linkers. The mobility of the DNA linkers on the surface of the micro-particles is achieved by combining the ability to coat silica particles with a lipid bilayer and the coupling of DNA strands to lipid bilayers. We have shown thathe ability for the DNA linkers to diffuse over the particle's surface greatly enhances the self-assembly of the micro-particles into ordered structures.

In Chapter 3 we have seen that there are multiple options to link short DNA strands to a planar supported lipid bilayer (SLB). Some of these possibilities are unstable, meaning that the DNA strands will slowly withdraw from the SLB when the supply of molecules from solution is depleted. Much stronger binding can however be achieved when the DNA strands carry two hydrophobic moieties. This can be done by hybridizing two single oligonucleotides which both bear a hydrophobic anchor or by covalently coupling two anchor molecules and coupling the combination to a single oligonucleotide.

Enlightened by the measurements in Chapter 3, we moved on to measure the effect of the mobile DNA linkers on the particle aggregation. In Chapter 4 we have shown how to coat silica micro particles with a lipid bilayer which included the anchored oligonucleotides. We additionally demonstrated that the oligonucleotides were able to exert lateral diffusion along a particle's surface which consequently resulted in a homogeneous oligonucleotide coating. By performing the aforementioned melting experiment, we observed a considerable widening of the temperature window for equilibrium crystallization. In addition, we observed that the formation of close-packed crystals occurred only within several hours without the requirement for repeated temperature oscillations. We speculate that both the widening of the temperature window as well as the ability of the particles to move around each other when connected, enhances the ability for the particles to escape from any potential kinetic traps so that can more easily reach their equilibrium position in the structure. Hence, the crystallization of micro-particles can readily be improved by using surface mobile DNA linkers.

To obtain a more detailed view on the effect of the mobility of the DNA linkers, we developed a technique to accurately measure binding strengths between single molecules as described in Chapter 5. This technique is based on reflection interference contrast microscopy (RICM) in combination with an optical tweezer. With RICM it is possible to measure the distance between the surface of a particle with an underlying planar substrate with nanometer precision. By continuously registering this distance while moving the particle with the optical tweezer, the force required to dissociate a particle from the substrate can be measured. When a particle is coupled to the substrate and the trap is moved up, the distance between the particle and the center of the trap increases, which generates a force on the particle pulling the particle back into the trap. The particle will jump back to the center of the trap the moment the bond breaks which is represented by a sudden jump in the particle-substrate distance. The magnitude of the maximum distance right before the breaking of the bond multiplied with the calibrated stiffness of the trap equals the rupture force. The development of this setup is still in progress. However, we have been able to conduct equivalent measurements using an already available microscopy setup built around two parallel optical tweezers. The concept of the measurement was conceptually similar to the one explained above, except for the replacement of the planar substrate by a second particle. One particle was kept stationary by a stationary trap, while a second particle was move to and fro the other at constant speed. The displacements of both particles relative to their respective trap centers were registered by QPDs, and together with the pre-determined stiffnesses of both traps we were able to measure the force of two dissociating particles.

By repeating the measurement a large number of times for different surface densities of DNA linkers, we obtained the first insight into the relation between the rupture force and the number of linkers per particle. We have to stress that the number of datapoints that we have collected is still insufficient to establish a unified picture which is in part a consequence of the limited force range of our instrument. Nonetheless, our measurements, in combination with experiments and established theories published earlier, reveal a force spectrum that can be expected for our model system of mobile bonds.

The facilitation of micro-particle crystallization by the introduction of surface-mobile DNA linkers has motivated others to test our results with simulations [17]. In addition to the close packed crystals that we have observed, they also predict conditions at which the particle aggregates equilibrate to crystals with a maximum valency that is lower than the maximum number of neighboring particles of defined by the shapes of the micro-spheres (the maximum number of neighbors with our particles is six for two-dimensional structures and twelve for three-dimensional structures). Having a lower maximum of binding partners allows for the self-assembly of crystals with lower coordination numbers. An example of an arrangement that could possibly emerge is that of the structure resembling the arrangement of carbon atoms in diamond crystals. Being able to self-assemble micro-particles into diamond-like arrangements is of great interest in this field of research due to its promising application in photonic materials. The spacing between the particles in such crystals has namely been shown to posses a full bandgap and is therefore used to develop materials in which the light can be captured and controlled. Currently, it is only possible to make these structures on a small scale with expensive photolithography or etching tools. Being able to form such structures

spontaneously would make these structures a lot cheaper to make, hence it is worthwhile pursuing the research on our model system with surface-mobile DNA linkers.

The logical step to take in this research would be to carry on with the rupture force measurements. The collection of data could be considerably accelerated if one would switch to novel techniques developed recently enabling the simultaneous attenuation of multiple particles and application of a larger range of forces. Examples of such techniques are magnetic tweezers, acoustic force spectroscopy and centrifugal force spectroscopy [216, 222, 223]. Firstly, more data could be collected on the effect of different linker densities on the most probable rupture force. How the density of linkers relates to the most probably rupture force can then be fitted to the available models [181, 191, 199, 203].

Secondly, one could investigate the time dependence of the rupture force. By comparing the rupture forces for different periods of time at which the particles are allowed to interact, would reveal the dependence of the DNA mediated interactions on the diffusion of the linkers. This could then be repeated for other linker densities or at different bilayer viscosities.

Aside from continuing with the force measurements it would also be interesting to continue the development of self-assembled ordered structures. The aforementioned valency effect should be attainable by adding a sufficiently large repulsive interactions to the system. Whether these predictions are experimentally feasible would be an interesting project.

6.1. FLEXIBLE PARTICLE CHAINS

We also recognized the value of our new model system for the research of flexible colloidal chains. There is a separate field of research that is particularly interested in the packing of polymers on the nano/micro as well as on the macro scale [224–231]. A purpose for which these colloidal chains are investigated, is for example to model the folding of DNA in chromosomes contained in the cell nucleus. Also they could help to understand the difference in maximum packing density for chains as compared with unchained particles. In addition, these chains could be useful for creating new materials with useful electromagnetic or photonic properties [43, 232, 233]. We initiated a side project in which we started making chains of our particles using the technique proposed by Vutukuri et al., as schematically represented by Fig. 6.1 [229].

The experiment encompasses two electrodes positioned parallel in the suspension of particles roughly 3-4 mm apart. When an alternating current is applied on these electrodes at a frequency of 1 MHz and a voltage of 1-10 V, an electric field of sufficient magnitude for particle alignment is generated within the sample. Because silica has a dielectric constant that is different from that of the solvent, the electric field imposes a dipole moment on the particles which aligns with the direction of the electric field. The rapidly alternating AC current prevents the particles and ions in the solution from following the electric field. However, the oscillating direction of the induced dipole moments remains the same for all particles and hence drives the alignment of the particles into strings. In order to link the particles together when they are aligned, we used a palindromic, self-complementary sequence for the sticky ends that allow all particles to bind with each other. This particular sequence inherently carries additional variations at which the

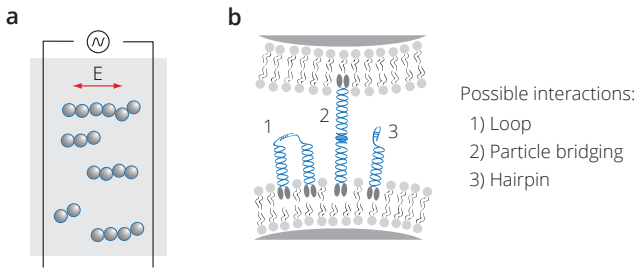

Figure 6.1: The assembly procedure of flexible particle chains. (a) Silica micro particles exert a dipole moment when exposed to an electric field. This dipole moment drives the alignment of the particle into chains. (b) The aligned particles are connected by palindromic sticky ends, which apart from particle bridging interactions can form loops and hairpin bonds as well.

sticky ends can form a bond. A bond can be formed between strands that are attached to the same surface and each sticky end can fold to bind with itself forming a so called hairpin. These additional binding options will compete with the desired particle-bridging interactions yet will not completely inhibit the coupling between particles. Turning the electric field off after having the particles aligned for several minutes, we monitored the motion of the particle chains. An example of the motion of such a chain is presented in the images in Fig. 6.2, which displays the configurations of the chain minutes after the electric field had been turned off.

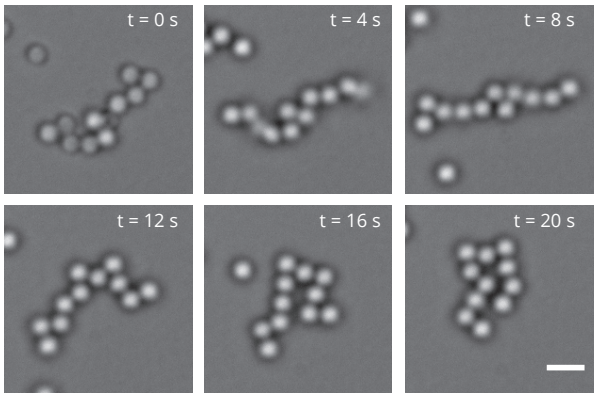

Figure 6.2: Flexible particle chain. Snapshot from a timeseries taken of a chain of particles ($r = 0.65\mu m$) connected by mobile DNA linkers at every 4 seconds. The white bar in the bottom right image represents 2.0 μm.

The large variation in particle chain configurations, indicates the high level of flexibility. To our knowledge, such flexibility has never been seen for particle chains before. After repeating the same procedure at different conditions we got the impression that this flexibility is controlled by the number of linkers forming the bonds. As can be seen

in Fig. 6.3, in which we formed chains with larger beads while adding the same concentration of DNA as compared to the smaller particles in Fig. 6.2, the chains are much stiffer. We hypothesize that the more linkers are mediating the bond, the lower the mobility and hence the lower the flexibility of the chain, but more measurements are needed before such can be concluded.

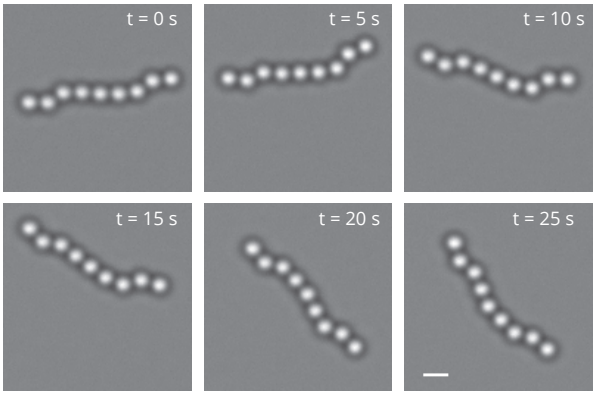

Figure 6.3: Stiff particle chain. Sanpshots from a timeseries taken of a chain of particles ($r = 1.03\mu m$) connected by mobile DNA linkers at every 5 seconds. The white bar in the bottom right image represents 3.0 μm.

When this project is continued, our hypothesis on the dependence of the flexibility of the chain on the linker density should be further verified. A quantitative approach that assesses the flexibility of a chain is by analyzing the persistence length of the chain. Since the individual particles are easily tracked one can compute the angular correlation between all the particles and hence calculate the persistence length from that.

Once we have sufficient control over the flexibility of the chains, we would be interested in how these chains would organize in confined spaces like droplets, resembling the folding of DNA in a cell's nucleus. Furthermore, we think it would be fascinating to exchange the silica particles with particles that can exert active Brownian motion. Such particles are obtained by covering one half of each particle with a platinum layer. When dispersed in a solution including hydrogen peroxide, the hydrogen peroxide will react with the platinum creating a driving force that propels the particles. We would be curious how the active Brownian motion of each individual particle affects the collective motion of a chain of particles.

We thank Alfons van Blaaderen and Rao Vutukuri for useful discussions and sharing their expertise on making linear particle chains.

BIBLIOGRAPHY

[1] Mirkin, C.; Letsinger, R.; Mucic, R.; Storhoff, J., A DNA-based method for rationally assembling nanoparticles into macroscopic materials. *Nature* **1996**, *382*, 607–609.

[2] Alivisatos, A.; Johnsson, K.; Peng, X.; Wilson, T.; Loweth, C.; Bruchez, M.; Schultz, P., Organization of 'nanocrystal molecules' using DNA. *Nature* **1996**, *382*, 609–611.

[3] Park, S. Y.; Lytton-Jean, A. K. R.; Lee, B.; Weigand, S.; Schatz, G. C.; Mirkin, C. a., DNA-programmable nanoparticle crystallization. *Nature* **2008**, *451*, 553–6.

[4] Nykypanchuk, D.; Maye, M. M.; van der Lelie, D.; Gang, O., DNA-guided crystallization of colloidal nanoparticles. *Nature* **2008**, *451*, 549–52.

[5] Macfarlane, R. J.; Lee, B.; Jones, M. R.; Harris, N.; Schatz, G. C.; Mirkin, C. A., Nanoparticle superlattice engineering with DNA. *Science* **2011**, *334*, 204–208.

[6] Chen, Q.; Yan, J.; Zhang, J.; Bae, S. C.; Granick, S., Janus and Multiblock Colloidal Particles Janus and Multiblock Colloidal Particles. *Langmuir* **2012**, *28*, 13555–13561.

[7] Auyeung, E.; Li, T. I. N. G.; Senesi, A. J.; Schmucker, A. L.; Pals, B. C.; de la Cruz, M. O.; Mirkin, C. A., DNA-mediated nanoparticle crystallization into Wulff polyhedra. *Nature* **2013**, *505*, 73–7.

[8] Zeravcic, Z.; Manoharan, V. N.; Brenner, M. P., Size limits of self-assembled colloidal structures made using specific interactions. *Proc. Natl. Acad. Sci. U.S.A.* **2014**, *111*, 15918–23.

[9] Schmatko, T.; Bozorgui, B.; Geerts, N.; Frenkel, D.; Eiser, E.; Poon, W. C. K., A finite-cluster phase in λ-DNA-coated colloids. *Soft Matter* **2007**, *3*, 703.

[10] Dreyfus, R.; Leunissen, M. E.; Sha, R.; Tkachenko, A.; Seeman, N. C.; Pine, D. J.; Chaikin, P. M., Aggregation-disaggregation transition of DNA-coated colloids: Experiments and theory. *Phys. Rev. E* **2010**, *81*, 1–10.

[11] Leunissen, M. E.; Frenkel, D., Numerical study of DNA-functionalized microparticles and nanoparticles: explicit pair potentials and their implications for phase behavior. *J. Chem. Phys.* **2011**, *134*, 084702.

[12] Michele, L. D.; Eiser, E., Developments in understanding and controlling self assembly of DNA-functionalized colloids. *Phys. Chem. Chem. Phys.* **2013**, *15*, 3115–29.

[13] Theodorakis; Fytas; Kahl; Dellago, Self-assembly of DNA-functionalized colloids. *Condens. Matter Phys.* **2015**, *18*, 22801.

[14] Angioletti-Uberti, S.; Mognetti, B. M.; Frenkel, D., Re-entrant melting as a design principle for DNA-coated colloids. *Nat. Mater.* **2012**, *11*, 518–22.

[15] Di Michele, L.; Varrato, F.; Kotar, J.; Nathan, S. H.; Foffi, G.; Eiser, E., Multistep kinetic self-assembly of DNA-coated colloids. *Nat. Comm.* **2013**, *4*, 2007.

[16] Halverson, J. D.; Tkachenko, A. V., DNA-programmed mesoscopic architecture. *Phys. Rev. E* **2013**, *87*, 1–7.

[17] Angioletti-Uberti, S.; Varilly, P.; Mognetti, B.; Frenkel, D., Mobile linkers on DNA-

coated colloids: valency without patches. *Phys. Rev. Lett.* **2014**, *113*, 1–5.
[18] Rogers, W. B.; Manoharan, V. N., Programming colloidal phase transitions with DNA strand displacement. *Science* **2015**, *347*, 639–642.
[19] Wang, Y.; Wang, Y.; Zheng, X.; Ducrot, É.; Yodh, J. S.; Weck, M.; Pine, D. J., Crystallization of DNA-coated colloids. *Nat. Comm.* **2015**, *6*, 7253.
[20] Langmuir, I., The Role of Attractive and Repulsive Forces in the Formation of Tactoids, Thixotropic Gels, Protein Crystals and Coacervates. *J. Chem. Phys.* **1938**, *6*, 873.
[21] Stanley, W. M., Isolation of a Crystalline Protein Possessing the Properties of Tobacco-Mosaic Virus. *Science* **1935**, *81*, 644–645.
[22] Pieranski, P., Colloidal crystals. *Contemp. Phys.* **1983**, *24*, 25–73.
[23] Leunissen, M. E.; Christova, C. G.; Hynninen, A.-P.; Royall, C. P.; Campbell, A. I.; Imhof, A.; Dijkstra, M.; van Roij, R.; van Blaaderen, A., Ionic colloidal crystals of oppositely charged particles. *Nature* **2005**, *437*, 235–40.
[24] Onsager, L., The effects of shape on the interaction of colloidal particles. *Ann. N. Y. Acad. Sci.* **1949**, *51*, 627–659.
[25] Sacanna, S.; Irvine, W. T. M.; Chaikin, P. M.; Pine, D. J., Lock and key colloids. *Nature* **2010**, *464*, 575–8.
[26] Chakrabarty, A.; Konya, A.; Wang, F.; Selinger, J. V.; Sun, K.; Wei, Q.-H., Brownian Motion of Boomerang Colloidal Particles. *Phys. Rev. Lett.* **2013**, *111*, 160603.
[27] Anders, G. V.; Klotsa, D.; Ahmed, N. K.; Engel, M.; Glotzer, S. C.; van Anders, G.; Klotsa, D.; Ahmed, N. K.; Engel, M.; Glotzer, S. C., Understanding shape entropy through local dense packing. *Proc. Natl. Acad. Sci. U.S.A.* **2014**, *111*, E4812–E4821.
[28] Bahng, J. H.; Yeom, B.; Wang, Y.; Tung, S. O.; Hoff, J. D.; Kotov, N., Anomalous dispersions of 'hedgehog' particles. *Nature* **2014**, *517*, 596–599.
[29] Frenkel, D., Order through disorder. *Nat. Mater.* **2015**, *14*, 9–12.
[30] Wolters, J. R.; Avvisati, G.; Hagemans, F.; Vissers, T.; Kraft, D. J.; Dijkstra, M.; Kegel, W. K., Self-assembly of "Mickey Mouse" shaped colloids into tube-like structures: experiments and simulations. *Soft Matter* **2015**, *11*, 1067–1077.
[31] Li, F.; Josephson, D. P.; Stein, A., Colloidal assembly: the road from particles to colloidal molecules and crystals. *Angew. Chem. Int. Ed.* **2011**, *50*, 360–88.
[32] Chen, J. H.; Seeman, N. C., Synthesis from DNA of a molecule with the connectivity of a cube. *Nature* **1991**, *350*, 631–3.
[33] Seeman, N., DNA components for molecular architecture. *Acc. Chem. Res.* **1997**, *4842*, 357–363.
[34] Winfree, E.; Liu, F.; Wenzler, L. a.; Seeman, N. C., Design and self-assembly of two-dimensional DNA crystals. *Nature* **1998**, *394*, 539–44.
[35] LaBean, T. H.; Li, H., Constructing novel materials with DNA. *Nano Today* **2007**, *2*, 26–35.
[36] Castro, C. E.; Kilchherr, F.; Kim, D.-n.; Shiao, E. L.; Wauer, T.; Wortmann, P.; Bathe, M.; Dietz, H., A primer to scaffolded DNA origami. *Nat. Methods* **2011**, *8*, 221–229.
[37] Woo, S.; Rothemund, P. W. K., Programmable molecular recognition based on the geometry of DNA nanostructures. *Nat. Chem.* **2011**, *3*, 620–7.
[38] Derr, N. D.; Goodman, B. S.; Jungmann, R.; Leschziner, a. E.; Shih, W. M.; Reck-Peterson, S. L., Tug-of-war in motor protein ensembles revealed with a pro-

grammable DNA origami scaffold. *Science* **2012**, *338*, 662–5.
[39] Ke, Y.; Ong, L. L.; Shih, W. M.; Yin, P., Three-Dimensional Structures Self-Assembled from DNA Bricks. *Science* **2012**, *338*, 1177–1183.
[40] Mashaghi, A.; Katan, A., A physicist's view of DNA. *De Physicus* **2013**, *24e*, 59–61.
[41] Jones, M. R.; Seeman, N. C.; Mirkin, C. a., Programmable materials and the nature of the DNA bond. *Science* **2015**, *347*, 1260901–1260901.
[42] Marras, A. E.; Zhou, L.; Su, H.-J.; Castro, C. E., Programmable motion of DNA origami mechanisms. *Proc. Natl. Acad. Sci. U.S.A.* **2015**, *112*, 713–718.
[43] Kuzyk, A.; Schreiber, R.; Fan, Z.; Pardatscher, G.; Roller, E.-M.; Högele, A.; Simmel, F. C.; Govorov, A. O.; Liedl, T., DNA-based Self-Assembly of Chiral Plasmonic Nanostructures with Tailored Optical Response. *Nature* **2011**, *483*, 311–314.
[44] Schreiber, R.; Do, J.; Roller, E.-M.; Zhang, T.; Schüller, V. J.; Nickels, P. C.; Feldmann, J.; Liedl, T., Hierarchical assembly of metal nanoparticles, quantum dots and organic dyes using DNA origami scaffolds. *Nat. Nanotechnol.* **2014**, *9*, 74–8.
[45] Langecker, M.; Arnaut, V.; Martin, T. G.; List, J.; Renner, S.; Mayer, M.; Dietz, H.; Simmel, F. C., Synthetic Lipid Membrane Channels Formed by Designed DNA Nanostructures. *Science* **2012**, *338*, 932–936.
[46] Alberts, B.; Bray, D.; Hopkins, K.; Johnson, A.; Lewis, J.; Raff, M.; Roberts, K.; And Walter, P., Essential Cell Biology, volume 231. 2nd edition (Garland Science, New York, 2004).
[47] Mueller, P.; Rudin, D. O.; Tien, H. T.; Wescott, W. C., Reconstitution of cell membrane structure in vitro and its transformation into an excitable system. *Nature* **1962**, *194*, 979–980.
[48] Lobatto, M. E.; Fuster, V.; Fayad, Z. a.; Mulder, W. J. M., Perspectives and opportunities for nanomedicine in the management of atherosclerosis. *Nat. Rev. Drug. Discov.* **2011**, *10*, 835–852.
[49] Miller, A. D., Lipid-based nanoparticles in cancer diagnosis and therapy. *J. Drug. Deliv.* **2013**, *2013*, 165981.
[50] Maglia, G.; Heron, A. J.; Hwang, W. L.; Holden, M. a.; Mikhailova, E.; Li, Q.; Cheley, S.; Bayley, H., Droplet networks with incorporated protein diodes show collective properties. *Nat. Nanotechnol.* **2009**, *4*, 437–440.
[51] Ang, P. K.; Jaiswal, M.; Haley, C.; Xuan, Y.; Wang, Y.; Sankaran, J.; Loh, K. P.; Li, A.; Lim, C. T.; Wohland, T., A Bioelectronic Platform Using a Graphene-Lipid Bilayer Interface. *ACS Nano* **2010**, *4*, 7387–7394.
[52] Khan, M. S.; Dosoky, N. S.; Williams, J. D., Engineering lipid bilayer membranes for protein studies. *Int. J. Mol. Sci.* **2013**, *14*, 21561–21597.
[53] Kiessling, V.; Yang, S.-T.; Tamm, L. K., Supported Lipid Bilayers as Models for Studying Membrane Domains, volume 75 (Elsevier Ltd, 2015).
[54] Baksh, M. M.; Jaros, M.; Groves, J. T., Detection of molecular interactions at membrane surfaces through colloid phase transitions. *Nature* **2004**, *427*, 139–41.
[55] Kong, Y.; Parthasarathy, R., Modulation of attractive colloidal interactions by lipid membrane-functionalization. *Soft Matter* **2009**, *5*, 2027.
[56] Bichenkov, E. E.; Budker, V. G.; Zarytova, V. F.; Ivanova, E. M., Interaction of Cholesterol-Modified Polynucleotide with Phosphatidylcholine Liposomes. *Biol. Membr.* **1988**, *5*, 735–742.

[57] Letsinger, R. L.; Zhang, G. R.; Sun, D. K.; Ikeuchi, T.; Sarin, P. S., Cholesteryl-conjugated oligonucleotides: synthesis, properties, and activity as inhibitors of replication of human immunodeficiency virus in cell culture. *Proc. Natl. Acad. Sci. U.S.A.* **1989**, *86*, 6553–6.

[58] Yoshina-Ishii, C.; Boxer, S. G., Arrays of mobile tethered vesicles on supported lipid bilayers. *J. Am. Chem. Soc* **2003**, *125*, 3696–7.

[59] Beales, P.; Vanderlick, T., Application of nucleic acid-lipid conjugates for the programmable organisation of liposomal modules. *Adv. Colloid Interface Sci.* **2014**, *207*, 290–305.

[60] Crocker, J. C., Golden handshake. *Nature* **2008**, *451*, 528–529.

[61] Geerts, N.; Eiser, E., DNA-functionalized colloids: Physical properties and applications. *Soft Matter* **2010**, *6*, 4647.

[62] Zhang, Y.; Lu, F.; Yager, K. G.; van der Lelie, D.; Gang, O., A general strategy for the DNA-mediated self-assembly of functional nanoparticles into heterogeneous systems. *Nat. Nanotechnol.* **2013**, *8*, 865–72.

[63] Kim, A. J.; Biancaniello, P. L.; Crocker, J. C., Engineering DNA-mediated colloidal crystallization. *Langmuir* **2006**, *22*, 1991–2001.

[64] Dreyfus, R.; Leunissen, M. E.; Sha, R.; Tkachenko, A. V.; Seeman, N. C.; Pine, D. J.; Chaikin, P. M., Simple Quantitative Model for the Reversible Association of DNA Coated Colloids. *Phys. Rev. Lett.* **2009**, *102*, 048301.

[65] Jin, R.; Wu, G.; Li, Z.; Mirkin, C.; Schatz, G., What controls the melting properties of DNA-linked gold nanoparticle assemblies? *J. Am. Chem. Soc* **2003**, *125*, 1643–1654.

[66] Leunissen, M. E.; Dreyfus, R.; Cheong, F. C.; Grier, D. G.; Sha, R.; Seeman, N. C.; Chaikin, P. M., Switchable self-protected attractions in DNA-functionalized colloids. *Nat. Mater.* **2009**, *8*, 590–5.

[67] Mognetti, B.; Varilly, P., Predicting DNA-mediated colloidal pair interactions. *Proc. Natl. Acad. Sci. U.S.A.* **2012**, *109*, E378–9.

[68] Varilly, P.; Angioletti-Uberti, S.; Mognetti, B. M.; Frenkel, D., A general theory of DNA-mediated and other valence-limited colloidal interactions. *J. Chem. Phys.* **2012**, *137*, 094108.

[69] van der Meulen, S. A. J.; Leunissen, M. E., Solid colloids with surface-mobile DNA linkers. *J. Am. Chem. Soc* **2013**, *135*, 15129–34.

[70] Smith, A.-S.; Sackmann, E., Progress in mimetic studies of cell adhesion and the mechanosensing. *ChemPhysChem* **2009**, *10*, 66–78.

[71] Nicolson, G. L., The Fluid-Mosaic Model of Membrane Structure: still relevant to understanding the structure, function and dynamics of biological membranes after more than 40 years. *Biochim. Biophys. Acta* **2014**, *1838*, 1451–66.

[72] Sackmann, E.; Smith, A., Physics of cell adhesion: some lessons from cell-mimetic systems. *Soft Matter* **2014**, *10*, 1644–1659.

[73] Walther, A.; Müller, A. H. E., Janus particles: synthesis, self-assembly, physical properties, and applications. *Chem. Rev.* **2013**, *113*, 5194–261.

[74] Halley, J. D.; Winkler, D. A., Consistent concepts of self-organization and self-assembly. *Complexity* **2008**, *14*, 10–17.

[75] Whitesides, G. M.; Grzybowski, B., Self-assembly at all scales. *Science* **2002**, *295*, 2418–21.

[76] Macfarlane, R. J.; O'Brien, M. N.; Petrosko, S. H.; Mirkin, C. A., Nucleic Acid-modified nanostructures as programmable atom equivalents: forging a new "table of elements". *Angew. Chem. Int. Ed.* **2013**, *52*, 5688–98.

[77] Ruzicka, B.; Zaccarelli, E., A fresh look at the Laponite phase diagram. *Soft Matter* **2011**, *7*, 1268.

[78] Rogers, W. B.; Crocker, J. C., Direct measurements of DNA-mediated colloidal interactions and their quantitative modeling. *Proc. Natl. Acad. Sci. U.S.A.* **2011**, *108*, 15687–15692.

[79] Casey, M. T.; Scarlett, R. T.; Benjamin Rogers, W.; Jenkins, I.; Sinno, T.; Crocker, J. C., Driving diffusionless transformations in colloidal crystals using DNA handshaking. *Nat. Comm.* **2012**, *3*, 1209.

[80] Rogers, W. B.; Sinno, T.; Crocker, J. C., Kinetics and non-exponential binding of DNA-coated colloids. *Soft Matter* **2013**, *9*, 6412.

[81] Lukatsky, D.; Frenkel, D., Phase Behavior and Selectivity of DNA-Linked Nanoparticle Assemblies. *Phys. Rev. Lett.* **2004**, *92*, 1–4.

[82] Leunissen, M. E.; Dreyfus, R.; Sha, R.; Seeman, N. C.; Chaikin, P. M., Quantitative study of the association thermodynamics and kinetics of DNA-coated particles for different functionalization schemes. *J. Am. Chem. Soc* **2010**, *132*, 1903–13.

[83] Anderson, V. J.; Lekkerkerker, H. N. W., Insigths into phase transition kinetics from colloid science. *Nature* **2002**, *416*, 811–815.

[84] McCarley, R.; Dunaway, D.; Willicut, R., Mobility of the alkanethiol-gold (111) interface studied by scanning probe microscopy. *Langmuir* **1993**, *9*, 2775–2777.

[85] Hostetler, M.; Templeton, A.; Murray, R., Dynamics of place-exchange reactions on monolayer-protected gold cluster molecules. *Langmuir* **1999**, 3782–3789.

[86] Jackson, A. M.; Myerson, J. W.; Stellacci, F., Spontaneous assembly of subnanometre-ordered domains in the ligand shell of monolayer-protected nanoparticles. *Nat. Mater.* **2004**, *3*, 330–6.

[87] Lee, D. W.; Banquy, X.; Kristiansen, K.; Kaufman, Y.; Boggs, J. M.; Israelachvili, J. N., Lipid domains control myelin basic protein adsorption and membrane interactions between model myelin lipid bilayers. *Proc. Natl. Acad. Sci. U.S.A.* **2014**, *111*, E768–75.

[88] Singer, S. J.; Nicolson, G. L., The fluid mosaic model of the structure of cell membranes. *Science* **1972**, *175*, 720–31.

[89] Sackmann, E., Supported Membranes: Scientific and Practical Applications. *Science* **1996**, *271*, 43–48.

[90] Zasadzinski, J.; Kisak, E.; Evans, C., Complex vesicle-based structures. *Curr. Opin. Colloid Interface Sci.* **2001**, *6*, 85–90.

[91] Boyer, C.; Zasadzinski, J., Multiple lipid compartments slow vesicle contents release in lipases and serum. *ACS Nano* **2007**, *1*, 176–182.

[92] Schwille, P., Bottom-up synthetic biology: engineering in a tinkerer's world. *Science* **2011**, *333*, 1252–4.

[93] Loughrey, H.; Wong, K.; Choi, L., Protein-liposome conjugates with defined size distributions. *Biochim. Biophys. Acta* **1990**, *1028*, 73–81.

[94] Chiruvolu, S.; Walker, S.; Israelachvili, J.; Schmitt, F. J.; Leckband, D.; Zasadzinski, J. a., Higher order self-assembly of vesicles by site-specific binding. *Science* **1994**,

264, 1753–6.

[95] Kisak, E.; Kennedy, M.; Trommeshauser, D.; Zasadzinski, J. A., Self-limiting aggregation by controlled ligand-receptor stoichiometry. *Langmuir* **2000**, *16*, 2825–2831.

[96] Lynch, N. J.; Kilpatrick, P. K.; Carbonell, R. G., Aggregation of ligand-modified liposomes by specific interactions with proteins. I: Biotinylated liposomes and avidin. *Biotechnol. Bioeng.* **1996**, *50*, 151–68.

[97] Beales, P.; Vanderlick, T., Specific Binding of Different Vesicle Populations by the Hybridization of Membrane-Anchored DNA. *J. Phys. Chem. A* **2007**, *111*, 12372–12380.

[98] Hadorn, M.; Eggenberger Hotz, P., DNA-mediated self-assembly of artificial vesicles. *PLoS ONE* **2010**, *5*, e9886.

[99] Parolini, L.; Mognetti, B.; Kotar, J., Thermal regulation of volume and porosity in lipid mesophases by coupling mobile ligands to soft membranes. *Nat. Comm.* **2015**, *6*, 5948–5957.

[100] Casagrande, C.; Fabre, P.; Raphael, E.; Veyssie, M., "Janus Beads": Realization and Behaviour at Water/Oil Interfaces. *Europhys. Lett.* **1989**, *9*, 251–255.

[101] de Gennes, P. G., Soft matter. *Rev. Mod. Phys.* **1992**, *64*, 645–648.

[102] Bunge, A.; Kurz, A.; Windeck, A.-K.; Korte, T.; Flasche, W.; Liebscher, J.; Herrmann, A.; Huster, D., Lipophilic oligonucleotides spontaneously insert into lipid membranes, bind complementary DNA strands, and sequester into lipid-disordered domains. *Langmuir* **2007**, *23*, 4455–64.

[103] Beales, P. A.; Vanderlick, T. K., Partitioning of Membrane-Anchored DNA between Coexisting Lipid Phases. *J. Phys. Chem. B* **2009**, *113*, 13678–13686.

[104] Beales, P. A.; Nam, J.; Vanderlick, T. K., Specific adhesion between DNA-functionalized "Janus" vesicles: size-limited clusters. *Soft Matter* **2011**, *7*, 1747.

[105] Christian, D. a.; Tian, A.; Ellenbroek, W. G.; Levental, I.; Rajagopal, K.; Janmey, P. a.; Liu, A. J.; Baumgart, T.; Discher, D. E., Spotted vesicles, striped micelles and Janus assemblies induced by ligand binding. *Nat. Mater.* **2009**, *8*, 843–9.

[106] Bibette, J.; Calderon, F.; Poulin, P., Emulsions: basic principles. *Rep. Prog. Phys.* **1999**, *969*, 969 – 1033.

[107] Hadorn, M.; Boenzli, E.; Sørensen, K. T.; Fellermann, H.; Eggenberger Hotz, P.; Hanczyc, M. M., Specific and reversible DNA-directed self-assembly of oil-in-water emulsion droplets. *Proc. Natl. Acad. Sci. U.S.A.* **2012**, *109*, 1–6.

[108] Pontani, L.-L.; Jorjadze, I.; Viasnoff, V.; Brujic, J., Biomimetic emulsions reveal the effect of mechanical forces on cell-cell adhesion. *Proc. Natl. Acad. Sci. U.S.A.* **2012**, *109*, 9839–44.

[109] Feng, L.; Pontani, L. L.; Dreyfus, R.; Chaikin, P.; Brujic, J., Specificity, flexibility and valence of DNA bonds guide emulsion architecture. *Soft Matter* **2013**, *9*, 9816–23.

[110] Ho, K.; Chan, C.; Soukoulis, C., Existence of a photonic gap in periodic dielectric structures. *Phys. Rev. Lett.* **1990**, *65*, 3152–3155.

[111] John, S., Strong localization of photons in certain disordered dielectric superlattices. *Phys. Rev. Lett.* **1987**, *58*, 2486–2489.

[112] Yablonovitch, E., Inhibited spontaneous emission in solid-state physics and electronics. *Phys. Rev. Lett.* **1987**, *58*, 2059–2062.

[113] Wang, S.; Dormidontova, E., Selectivity of Ligand-Receptor Interactions between Nanoparticle and Cell Surfaces. *Phys. Rev. Lett.* **2012**, *109*, 238102.

[114] Angioletti-Uberti, S.; Varilly, P.; Mognetti, B. M.; Tkachenko, A. V.; Frenkel, D., Communication: A simple analytical formula for the free energy of ligand-receptor-mediated interactions. *J. Chem. Phys.* **2013**, *138*, 021102.

[115] Edagawa, K.; Kanoko, S.; Notomi, M., Photonic Amorphous Diamond Structure with a 3D Photonic Band Gap. *Phys. Rev. Lett.* **2008**, *100*, 1–4.

[116] Pfeiffer, I.; Höök, F., Bivalent cholesterol-based coupling of oligonucleotides to lipid membrane assemblies. *J. Am. Chem. Soc.* **2004**, *126*, 10224–25.

[117] van der Meulen, S. A. J.; Dubacheva, G. V.; Dogterom, M.; Richter, R. P.; Leunissen, M. E., Quartz Crystal Microbalance with Dissipation Monitoring and Spectroscopic Ellipsometry Measurements of the Phospholipid Bilayer Anchoring Stability and Kinetics of Hydrophobically Modified DNA Oligonucleotides. *Langmuir* **2014**, *30*, 6525–6533.

[118] Bell, G., Models for the specific adhesion of cells to cells. *Science* **1978**, *200*, 618–627.

[119] Kusumi, A.; Suzuki, K. G. N.; Kasai, R. S.; Ritchie, K.; Fujiwara, T. K., Hierarchical mesoscale domain organization of the plasma membrane. *Trends Biochem. Sci.* **2011**, *36*, 604–15.

[120] Kusumi, A.; Fujiwara, T. K.; Chadda, R.; Xie, M.; Tsunoyama, T. a.; Kalay, Z.; Kasai, R. S.; Suzuki, K. G. N., Dynamic organizing principles of the plasma membrane that regulate signal transduction: commemorating the fortieth anniversary of Singer and Nicolson's fluid-mosaic model. *Annu. Rev. Cell Dev. Biol.* **2012**, *28*, 215–50.

[121] James, J. R.; Vale, R. D., Biophysical mechanism of T-cell receptor triggering in a reconstituted system. *Nature* **2012**, *487*, 64–9.

[122] Chu, Y.-S.; Thomas, W. a.; Eder, O.; Pincet, F.; Perez, E.; Thiery, J. P.; Dufour, S., Force measurements in E-cadherin-mediated cell doublets reveal rapid adhesion strengthened by actin cytoskeleton remodeling through Rac and Cdc42. *J. Cell Biol.* **2004**, *167*, 1183–94.

[123] Kalb, E.; Frey, S.; Tamm, L., Formation of supported planar bilayers by fusion of vesicles to supported phospholipid monolayers. *Biochim. Biophys. Acta* **1992**, *1103*, 307–316.

[124] McConnell, H. M.; Watts, T. H.; Weis, R. M.; Brian, a. a., Supported planar membranes in studies of cell-cell recognition in the immune system. *Biochim. Biophys. Acta* **1986**, *864*, 95–106.

[125] Richter, R. P.; Bérat, R.; Brisson, A., Formation of solid-supported lipid bilayers: an integrated view. *Langmuir* **2006**, *22*, 3497–3505.

[126] Zhu, D.-M.; Dustin, M. L.; Cairo, C. W.; Golan, D. E., Analysis of two-dimensional dissociation constant of laterally mobile cell adhesion molecules. *Biophys. J.* **2007**, *92*, 1022–34.

[127] Groves, J. T.; Dustin, M. L., Supported planar bilayers in studies on immune cell adhesion and communication. *J. Immunol. Methods* **2003**, *278*, 19–32.

[128] Dustin, M. L., Supported bilayers at the vanguard of immune cell activation studies. *J. Struct. Biol.* **2009**, *168*, 152–60.

[129] Smith, A.-S. A.-S.; Seifert, U., Vesicles as a model for controlled (de-)adhesion of

cells: a thermodynamic approach. *Soft Matter* **2007**, *3*, 275–289.

[130] Smith, A.-S. A.-S.; Sengupta, K.; Goennenwein, S.; Seifert, U.; Sackmann, E., Force-induced growth of adhesion domains is controlled by receptor mobility. *Proc. Natl. Acad. Sci. U.S.A.* **2008**, *105*, 6906–11.

[131] Fenz, S. F.; Bihr, T.; Merkel, R.; Seifert, U.; Sengupta, K.; Smith, A.-S., Switching from ultraweak to strong adhesion. *Adv. Mater.* **2011**, *23*, 2622–6.

[132] Fenz, S. F.; Smith, A.-S.; Merkel, R.; Sengupta, K., Inter-membrane adhesion mediated by mobile linkers: Effect of receptor shortage. *Soft Matter* **2011**, *7*, 952.

[133] Noppl-Simson, D. a.; Needham, D., Avidin-biotin interactions at vesicle surfaces: adsorption and binding, cross-bridge formation, and lateral interactions. *Biophys. J.* **1996**, *70*, 1391–401.

[134] Nam, J.; Santore, M. M., Adhesion plaque formation dynamics between polymer vesicles in the limit of highly concentrated binding sites. *Langmuir* **2007**, *23*, 7216–24.

[135] Fattaccioli, J.; Baudry, J.; Henry, N.; Brochard-Wyart, F.; Bibette, J., Specific wetting probed with biomimetic emulsion droplets. *Soft Matter* **2008**, *4*, 2434.

[136] Bourouina, N.; Husson, J.; Waharte, F.; Pansu, R. B.; Henry, N., Formation of specific receptor-ligand bonds between liquid interfaces. *Soft Matter* **2011**, *7*, 9130.

[137] Knowles, T. P. J.; White, D. a.; Abate, A. R.; Agresti, J. J.; Cohen, S. I. a.; Sperling, R. a.; De Genst, E. J.; Dobson, C. M.; Weitz, D. a., Observation of spatial propagation of amyloid assembly from single nuclei. *Proc. Natl. Acad. Sci. U.S.A.* **2011**, *108*, 14746–14751.

[138] Sang, Y. Y. C.; Lorenceau, E.; Wahl, S.; Stoffel, M.; Angelescu, D. E.; Höhler, R., A microfluidic technique for generating monodisperse submicron-sized drops. *R. Soc. Chem. Adv.* **2013**, *3*, 2330.

[139] Bogush, G.; Tracy, M.; Iv, C. Z., Preparation of monodisperse silica particles: control of size and mass fraction. *J. Non-Cryst. Solids* **1988**, *104*, 95–106.

[140] Bayerl, T. M.; Bloom, M., Physical properties of single phospholipid bilayers adsorbed to micro glass beads. A new vesicular model system studied by 2H-nuclear magnetic resonance. *Biophys. J.* **1990**, *58*, 357–62.

[141] Ross, E. E.; Mok, S.-W.; Bugni, S. R., Assembly of lipid bilayers on silica and modified silica colloids by reconstitution of dried lipid films. *Langmuir* **2011**, *27*, 8634–44.

[142] Conway, J. W.; Madwar, C.; Edwardson, T. G.; McLaughlin, C. K.; Fahkoury, J.; Lennox, R. B.; Sleiman, H. F., Dynamic Behavior of DNA Cages Anchored on Spherically Supported Lipid Bilayers. *J. Am. Chem. Soc.* **2014**.

[143] Schade, M.; Berti, D.; Huster, D.; Herrmann, A.; Arbuzova, A., Lipophilic nucleic acids - A flexible construction kit for organization and functionalization of surfaces. *Adv. Colloid Interface Sci.* **2014**, *208*, 235–251.

[144] Boutorin, A. S.; Gus'kova, L. V.; Ivanova, E. M.; Kobetz, N. D.; Zarytova, V. F.; Ryte, A. S.; Yurchenko, L. V.; Vlassov, V. V., Synthesis of alkylating oligonucleotide derivatives containing cholesterol or phenazinium residues at their 3'-terminus and their interaction with DNA within mammalian cells. *FEBS Lett.* **1989**, *254*, 129–32.

[145] Shea, R. G.; Marsters, J. C.; Bischofberger, N., Synthesis, hybridization properties and antiviral activity of lipid-oligodeoxynucleotide conjugates. *Nucleic Acids Res.*

1990, *18*, 3777–83.

[146] Krieg, A.; Tonkinson, J., Modification of antisense phosphodiester oligodeoxynucleotides by a 5'cholesteryl moiety increases cellular association and improves efficacy. *Proc. Natl. Acad. Sci. U.S.A.* **1993**, *90*, 1048–1052.

[147] Benkoski, J. J.; Höök, F., Lateral Mobility of Tethered Vesicle- DNA Assemblies. *J. Phys. Chem. B* **2005**, *109*, 9773–79.

[148] Yoshina-Ishii, C.; Boxer, S. G., Controlling two-dimensional tethered vesicle motion using an electric field: interplay of electrophoresis and electro-osmosis. *Langmuir* **2006**, *22*, 2384–91.

[149] Chan, Y.-H. M.; van Lengerich, B.; Boxer, S. G., Lipid-anchored DNA mediates vesicle fusion as observed by lipid and content mixing. *Biointerphases* **2008**, *3*, 17–21.

[150] Beales, P. A.; Vanderlick, T. K., DNA as membrane-bound ligand-receptor pairs: duplex stability is tuned by intermembrane forces. *Biophys. J.* **2009**, *96*, 1554–65.

[151] Chung, M.; Lowe, R. D.; Chan, Y.-H. M.; Ganesan, P. V.; Boxer, S. G., DNA-tethered membranes formed by giant vesicle rupture. *J. Struct. Biol.* **2009**, *168*, 190–9.

[152] Chung, M.; Boxer, S. G. S., Stability of DNA-Tethered Lipid Membranes with Mobile Tethers. *Langmuir* **2011**, *27*, 5492–7.

[153] Nasiru, T.; Avila, L.; Levine, M., Determination of Critical Micelle Concentrations Using UV-Visible Spectroscopy. *J. High School Res.* **2011**, *2*, 1–6.

[154] Domack, A.; Prucker, O.; Rühe, J.; Johannsmann, D., Swelling of a polymer brush probed with a quartz crystal resonator. *Phys. Rev. E* **1997**, *56*, 680–689.

[155] Johannsmann, D., Viscoelastic analysis of organic thin films on quartz resonators. *Macromol. Chem. Phys.* **1999**, *200*, 501–516.

[156] Johannsmann, D., Viscoelastic, mechanical, and dielectric measurements on complex samples with the quartz crystal microbalance. *Phys. Chem. Chem. Phys.* **2008**, *10*, 4516–34.

[157] Eisele, N. B.; Andersson, F. I.; Frey, S.; Richter, R. P., Viscoelasticity of thin biomolecular films: a case study on nucleoporin phenylalanine-glycine repeats grafted to a histidine-tag capturing QCM-D sensor. *Biomacromolecules* **2012**, *13*, 2322–32.

[158] Carton, I.; Brisson, A. R.; Richter, R. P., Label-free detection of clustering of membrane-bound proteins. *Anal. Chem.* **2010**, *82*, 9275–81.

[159] De Feijter, J. A.; Benjamins, J.; Veer, F. A., Ellipsometry as a tool to study the adsorption behavior of synthetic and biopolymers at the air-water interface. *Biopolymers* **1978**, *17*, 1759–72.

[160] Richter, R. P.; Rodenhausen, K. B.; Eisele, N. B.; Schubert, M., Coupling Spectroscopic Ellipsometry and Quartz Crystal Microbalance to Study Organic Films at the Solid-Liquid Interface. *In* Ellipsometry of Functional Organic Surfaces and Films, Hinrichs, K.; Eichhorn, K. J., editors (Springer Berlin Heidelberg, 2014), 223–248.

[161] Nicolai, T.; Dijk van, T. N.; Dijk van, J. A.; Smit, J. A., Molar mass characterization of DNA fragments by gel permeation chromatography using a low-angle laser light-scattering detector. *J. Chromatogr. A* **1987**, *389*, 286–92.

[162] Keller, C. A.; Kasemo, B., Surface specific kinetics of lipid vesicle adsorption measured with a quartz crystal microbalance. *Biophys. J.* **1998**, *75*, 1397–1402.

[163] Hermens, W. T.; Benes, M.; Richter, R. P.; Speijer, H., Effects of flow on solute exchange between fluids and supported biosurfaces. *Biotechnol. Appl. Biochem.*

2004, *39*, 277–284.

[164] Fuguet, E.; Ràfols, C.; Rosés, M.; Bosch, E., Critical micelle concentration of surfactants in aqueous buffered and unbuffered systems. *Anal. Chim. Acta.* **2005**, *548*, 95–100.

[165] Murphy, M.; Rasnik, I.; Cheng, W.; Lohman, T. M.; Ha, T., Probing Single-Stranded DNA Conformational Flexibility Using Fluorescence Spectroscopy. *Biophys. J.* **2004**, *86*, 2530–2537.

[166] Woller, J. G.; Börjesson, K.; Svedhem, S.; Albinsson, B., Reversible hybridization of DNA anchored to a lipid membrane via porphyrin. *Langmuir* **2012**, *28*, 1944–53.

[167] Lee, S.-K.; Maye, M. M.; Zhang, Y.-B.; Gang, O.; van der Lelie, D., Controllable g5p-protein-directed aggregation of ssDNA-gold nanoparticles. *Langmuir* **2009**, *25*, 657–60.

[168] Hiddessen, A. L.; Rodgers, S. D.; Weitz, D. a.; Hammer, D. a., Assembly of Binary Colloidal Structures via Specific Biological Adhesion. *Langmuir* **2000**, *16*, 9744–9753.

[169] Mann, S.; Shenton, W.; Li, M.; Connolly, S.; Fitzmaurice, D., Biologically Programmed Nanoparticle Assembly. *Adv. Mater.* **2000**, *12*, 147–150.

[170] Schoen, A. P.; Hommersom, B.; Heilshorn, S. C.; Leunissen, M. E.; Heilshorn, M. E., Tuning colloidal association with specific peptide interactions. *Soft Matter* **2013**, *9*, 6781–6785.

[171] Wang, Y.; Breed, D.; Manoharan, V.; Feng, L.; Hollingsworth, A.; Weck, M.; Pine, D., Colloids with valence and specific directional bonding. *Nature* **2012**, *490*, 51–55.

[172] Licata, N. A.; Tkachenko, A. V., Dynamics of particles with "key-lock" interactions. *Europhys. Lett.* **2008**, *81*, 48009.

[173] Xu, Q.; Feng, L.; Sha, R.; Seeman, N. C.; Chaikin, P. M., Subdiffusion of a Sticky Particle on a Surface. *Phys. Rev. Lett.* **2011**, *106*, 5–8.

[174] Bartlett, P.; Campbell, A., Three-Dimensional Binary Superlattices of Oppositely Charged Colloids. *Phys. Rev. Lett.* **2005**, *95*, 128302.

[175] Shevchenko, E. V.; Talapin, D. V.; Kotov, N. a.; O'Brien, S.; Murray, C. B., Structural diversity in binary nanoparticle superlattices. *Nature* **2006**, *439*, 55–9.

[176] Richter, R. P.; Mukhopadhyay, A., Pathways of lipid vesicle deposition on solid surfaces: a combined QCM-D and AFM study. *Biophys. J.* **2003**, *85*, 3035–3047.

[177] Gopalakrishnan, G.; Rouiller, I.; Colman, D. R.; Lennox, R. B., Supported bilayers formed from different phospholipids on spherical silica substrates. *Langmuir* **2009**, *25*, 5455–8.

[178] Chan, Y.-H. M.; Lenz, P.; Boxer, S. G., Kinetics of DNA-mediated docking reactions between vesicles tethered to supported lipid bilayers. *Proc. Natl. Acad. Sci. U.S.A.* **2007**, *104*, 18913–8.

[179] Wu, K.-T.; Feng, L.; Sha, R.; Dreyfus, R.; Grosberg, A. Y.; Seeman, N. C.; Chaikin, P. M., Polygamous particles. *Proc. Natl. Acad. Sci. U.S.A.* **2012**, *109*, 18731–18736.

[180] Manghi, M.; Aubouy, M., Mobile polymer connectors. *Eur. Phys. J. E* **2003**, *11*, 243–54.

[181] Zhang, C.-Z.; Wang, Z.-G., Polymer-tethered ligand-receptor interactions between surfaces II. *Langmuir* **2007**, *23*, 13024–39.

[182] Effenterre, D. V.; Roux, D., Adhesion of colloids on a cell surface in competition for

mobile receptors. *Europhys. Lett.* **2003**, *543*, 543–49.
[183] Martinez-Veracoechea, F. J. F.; Leunissen, M. M. E., The entropic impact of tethering, multivalency and dynamic recruitment in systems with specific binding groups. *Soft Matter* **2013**, *9*, 3213–3219.
[184] Vial, S.; Nykypanchuk, D.; Yager, K.; Tkachenko, A. V.; Gang, O., Linear Mesostructures in DNA-Nanorod Self-Assembly. *ACS Nano* **2013**, *7*, 5437–5445.
[185] Wu, A. M.; Senter, P. D., Arming antibodies: prospects and challenges for immunoconjugates. *Nat. Biotechnol.* **2005**, *23*, 1137–46.
[186] Schroeder, A.; Heller, D. A.; Winslow, M. M.; Dahlman, J. E.; Pratt, G. W.; Langer, R.; Jacks, T.; Anderson, D. G., Treating metastatic cancer with nanotechnology. *Nat. Rev. Canc.* **2012**, *12*, 39–50.
[187] Mammen, M.; Choi, S. S.-K.; Whitesides, G. M. G., Polyvalent interactions in biological systems: implications for design and use of multivalent ligands and inhibitors. *Angew. Chem. Int. Ed.* **1998**, *37*, 2755–94.
[188] Kiessling, L. L.; Gestwicki, J. E.; Strong, L. E., Synthetic multivalent ligands in the exploration of cell-surface interactions. *Curr. Opin. Chem. Biol.* **2000**, *4*, 696–703.
[189] Carlson, C.; Mowery, P.; Owen, R.; Dykhuizen, E.; Kiessling, L., Selective tumor cell targeting using low-affinity, multivalent interactions. *ACS Chem. Biol.* **2007**, *2*, 119–127.
[190] Davis, M. E.; Zuckerman, J. E.; Choi, C. H. J.; Seligson, D.; Tolcher, A.; Alabi, C. a.; Yen, Y.; Heidel, J. D.; Ribas, A., Evidence of RNAi in humans from systemically administered siRNA via targeted nanoparticles. *Nature* **2010**, *464*, 1067–70.
[191] Seifert, U., Rupture of multiple parallel molecular bonds under dynamic loading. *Phys. Rev. Lett.* **2000**, *84*, 2750–2753.
[192] Kitov, P. I.; Bundle, D. R., On the nature of the multivalency effect: a thermodynamic model. *J. Am. Chem. Soc.* **2003**, *125*, 16271–84.
[193] Huskens, J.; Mulder, A.; Auletta, T.; Nijhuis, C. a.; Ludden, M. J. W.; Reinhoudt, D. N., A model for describing the thermodynamics of multivalent host-guest interactions at interfaces. *J. Am. Chem. Soc* **2004**, *126*, 6784–97.
[194] Diestler, D. J.; Knapp, E. W., Statistical Mechanics of the Stability of Multivalent Ligand - Receptor Complexes. *Phys. Rev. Lett.* **2008**, *100*, 178101 (1–4).
[195] Erdmann, T.; Pierrat, S.; Nassoy, P.; Schwarz, U. S., Dynamic force spectroscopy on multiple bonds: experiments and model. *Europhys. Lett.* **2008**, *81*.
[196] Wang, S.; Dormidontova, E. E., Nanoparticle design optimization for enhanced targeting: Monte Carlo simulations. *Biomacromolecules* **2010**, *11*, 1785–95.
[197] Wang, S.; Dormidontova, E. E., Nanoparticle targeting using multivalent ligands: computer modeling. *Soft Matter* **2011**, *7*, 4435.
[198] Getfert, S.; Reimann, P., Hidden multiple bond effects in dynamic force spectroscopy. *Biophys. J.* **2012**, *102*, 1184–1193.
[199] Martinez-Veracoechea, F. J.; Frenkel, D., Designing super selectivity in multivalent nano-particle binding. *Proc. Natl. Acad. Sci. U.S.A.* **2011**, *108*, 10963–8.
[200] Dubacheva, G. V.; Curk, T.; Mognetti, B. M.; Auzély-Velty, R.; Frenkel, D.; Richter, R. P., Superselective targeting using multivalent polymers. *J. Am. Chem. Soc* **2014**, 8–11.
[201] Evans, E.; Ritchie, K., Dynamic strength of molecular adhesion bonds. *Biophys. J.*

1997, *72*, 1541–55.

[202] Merkel, R.; Nassoy, P.; Leung, a.; Ritchie, K.; Evans, E., Energy landscapes of receptor-ligand bonds explored with dynamic force spectroscopy. *Nature* **1999**, *397*, 50–3.

[203] Friddle, R. W.; Noy, A.; De Yoreo, J. J., Interpreting the widespread nonlinear force spectra of intermolecular bonds. *Proc. Natl. Acad. Sci. U.S.A.* **2012**, *109*, 505–509.

[204] Evans, E., Probing the relation between force–lifetime–and chemistry in single molecular bonds. *Annu. Rev. Biophys. Biomol. Struct.* **2001**, *30*, 105–128.

[205] Evans, E.; Williams, P., Physics of bio-molecules and cells. *In* Les Houches–Ecole d'Ete de Physique Theorique, Flyvbjerg, F.; Julicher, F.; Ormos, P.; David, F., editors, volume 75 (Springer Berlin Heidelberg, 2002), 145–204.

[206] Seifert, U., Dynamic strength of adhesion molecules: Role of rebinding and self-consistent rates. *Europhys. Lett.* **2002**, *58*, 792–798.

[207] Hummer, G.; Szabo, A., Kinetics from nonequilibrium single-molecule pulling experiments. *Biophys. J.* **2003**, *85*, 5–15.

[208] Erdmann, T.; Schwarz, U. S., Stochastic dynamics of adhesion clusters under shared constant force and with rebinding. *J. Chem. Phys.* **2004**, *121*, 8997–9017.

[209] Dudko, O. K.; Hummer, G.; Szabo, A., Intrinsic rates and activation free energies from single-molecule pulling experiments. *Phys. Rev. Lett.* **2006**, *96*, 1–4.

[210] Dudko, O. K.; Hummer, G.; Szabo, A., Theory, analysis, and interpretation of single-molecule force spectroscopy experiments. *Proc. Natl. Acad. Sci. U.S.A.* **2008**, *105*, 15755–15760.

[211] Liang, H. H.; Chen, H. Y., Strength of adhesion clusters under shared linear loading. *Phys. Rev. E* **2011**, *83*, 1–7.

[212] Friddle, R. W.; Podsiadlo, P.; Artyukhin, A. B.; Noy, A., Near-equilibrium chemical force microscopy. *J. Phys. Chem. C* **2008**, *112*, 4986–4990.

[213] Heinrich, V.; Ritchie, K.; Mohandas, N.; Evans, E., Elastic thickness compressibilty of the red cell membrane. *Biophys. J.* **2001**, *81*, 1452–63.

[214] Wong, W.; Heinrich, V.; Evans, E., Exploring reaction pathways of single-molecule interactions through the manipulation and tracking of a potential-confined microsphere in three dimensions. *Mat. Res. Soc. Symp. Proc.* **2003**, *790*, 1–12.

[215] Rädler, J.; Sackmann, E., On the measurement of weak repulsive and frictional colloidal forces by reflection interference contrast microscopy. *Langmuir* **1992**, 848–853.

[216] Te Velthuis, A. J. W.; Kerssemakers, J. W. J.; Lipfert, J.; Dekker, N. H., Quantitative guidelines for force calibration through spectral analysis of magnetic tweezers data. *Biophys. J.* **2010**, *99*, 1292–1302.

[217] Wong, W.; Halvorsen, K., Beyond the frame rate: measuring high-frequency fluctuations with light-intensity modulation. *Opt. Lett.* **2009**, *34*, 277–279.

[218] SantaLucia, J., A unified view of polymer, dumbbell, and oligonucleotide DNA nearest-neighbor thermodynamics. *Proc. Natl. Acad. Sci. U.S.A.* **1998**, *95*, 1460–1465.

[219] Malghani, M. S.; Yang, J., Stable Binding of DNA to Zwitterionic Lipid Bilayers in Aqueous Solutions. *J. Phys. Chem. B* **1998**, *102*, 8930–8933.

[220] Maier, B.; Rädler, J., Conformation and Self-Diffusion of Single DNA Molecules

Confined to Two Dimensions. *Phys. Rev. Lett.* **1999**, *82*, 1911–1914.
[221] Ainalem, M.-L. L.; Kristen, N.; Edler, K. J.; Höök, F.; Sparr, E.; Nylander, T., DNA Binding to Zwitterionic Model Membranes. *Langmuir* **2010**, *26*, 4965–76.
[222] Sitters, G.; Kamsma, D.; Thalhammer, G.; Ritsch-marte, M.; Peterman, E. J. G.; Wuite, G. J. L., Acoustic force spectroscopy. *Nat. Methods* **2015**, *12*, 47–50.
[223] Halvorsen, K.; Wong, W. P., Massively parallel single-molecule manipulation using centrifugal force. *Biophys. J.* **2010**, *98*.
[224] Gittes, F.; Mickey, B.; Nettleton, J.; Howard, J., Flexural rigidity of microtubules and actin filaments measured from thermal fluctuations in shape. *J. Cell Biol.* **1993**, *120*, 923–34.
[225] Karayiannis, N.; Foteinopoulou, K.; Laso, M., Entropy-Driven Crystallization in Dense Systems of Athermal Chain Molecules. *Phys. Rev. Lett.* **2009**, *103*, 045703.
[226] Zou, L.-N.; Cheng, X.; Rivers, M. L.; Jaeger, H. M.; Nagel, S. R., The packing of granular polymer chains. *Science* **2009**, *326*, 408–10.
[227] Karayiannis, N. C.; Foteinopoulou, K.; Abrams, C. F.; Laso, M., Modeling of crystal nucleation and growth in athermal polymers: self-assembly of layered nanomorphologies. *Soft Matter* **2010**, *6*, 2160.
[228] Li, D.; Banon, S.; Biswal, S. L., Bending dynamics of DNA-linked colloidal particle chains. *Soft Matter* **2010**, *6*, 4197.
[229] Vutukuri, H. R.; Demirörs, A. F.; Peng, B.; van Oostrum, P. D. J.; Imhof, A.; van Blaaderen, A., Colloidal analogues of charged and uncharged polymer chains with tunable stiffness. *Angew. Chem. Int. Ed.* **2012**, *51*, 11249–53.
[230] Vutukuri, H. R.; Smallenburg, F.; Badaire, S.; Imhof, A.; Dijkstra, M.; van Blaaderen, A., An experimental and simulation study on the self-assembly of colloidal cubes in external electric fields. *Soft Matter* **2014**, 9110–9119.
[231] Byrom, J.; Han, P.; Savory, M.; Biswal, S. L., Directing assembly of DNA-coated colloids with magnetic fields to generate rigid, semiflexible, and flexible chains. *Langmuir* **2014**.
[232] Zerrouki, D.; Baudry, J.; Pine, D.; Chaikin, P.; Bibette, J., Chiral colloidal clusters. *Nature* **2008**, *455*, 380–382.
[233] Shen, X.; Asenjo-Garcia, A.; Liu, Q.; Jiang, Q.; García De Abajo, F. J.; Liu, N.; Ding, B., Three-dimensional plasmonic chiral tetramers assembled by DNA origami. *Nano Lett.* **2013**, *13*, 2128–2133.

CURRICULUM VITÆ

Stef Aris Jurriaan VAN DER MEULEN

14-06-1987 Born in Edam, The Netherlands.

EDUCATION

1999–2005	VWO Da Vince, Purmerend
2005–2008	BSc. Medical Natural Sciences Vrije Universiteit Amsterdam
2008–2010	MSc. Medical Physics Vrije Universiteit Amsterdam
2011-2016	PhD. Biophysics TU Delft & FOM Institute AMOLF *Thesis:* DNA linkers surfing on colloids: How surface-mobile DNA linkers affect colloidal self-assembly *Promotor:* Prof. dr. M. Dogterom *Copromotor:* Dr. M. E. Leunissen

LIST OF PUBLICATIONS

PUBLICATIONS COVERED IN THIS THESIS

1. S. A. J. van der Meulen, G. Helms, M. Dogterom, *J. Phys.: Condens. Matter* **2015**, *27*, 233101-14. (*chapter 2*)

2. S. A. J. van der Meulen, G. V. Dubacheva, M. Dogterom, R. P. Richter, M. E. Leunissen, *Langmuir* **2014**, *30*, 6525-33. (*chapter 3*)

3. S. A. J. van der Meulen, M. E. Leunissen, *J. Am. Chem. Soc.* **2013**, *135*, 15129–34. (*chapter 4*)

OTHER PUBLICATIONS

1. B. S. Gentry, S. A. J. van der Meulen, P. Noguera, B. Alonso-Latorre, J. Plastino, and G. H. Koenderink, *Eur. Biophys. J.* **2012**, *41*, 979-990.

DANKWOORD

Dit proefscrhift zou ik nooit alleen gemaakt kunnen hebben en daarom zou ik graag de mensen willen bedanken die in grote of minder grote mate hebben bijgedragen aan de totstandkoming van dit werk.

Allereerst, Mirjam, ik wil je hartelijk bedanken voor de kans en het vertrouwen die je me hebt geboden. Je energie, efficiëntie, uitgebreide vakkennis, pragmatisme, humor en interesse voor sport hebben me enorm geïnspireerd en uiteindelijk gestimuleerd om dit tot een goed eind te brengen. Bedankt dat je ondanks je vertrek toch als co-promotor wilde fungeren om zo mijn promotie tot het einde bij te staan.

M'n promotie verliep niet helemaal zoals initieel was gepland, Marileen, ik wil je hierbij bedanken dat je me na het vertrek van Mirjam onder je hoede hebt genomen. Ook al ligt de focus van je onderzoek op een heel ander vlak, je was toch bereid om met volle overtuiging mijn project tot een goed einde te brengen. Ik heb me altijd zeer welkom gevoeld en met je rijke ervaring in de experimentele wetenschap en je scherpe kritische blik wist je me altijd de juiste vragen te stellen en heb je me altijd van nuttig advies voorzien. Ik waardeer je flexibiliteit en ben blij dat je me altijd de ruimte en tijd hebt geboden die ik nodig had om uiteindelijk mijn proefschrift af te kunnen ronden.

En de laatste in het rijtje van vrouwelijke AMOLF groepsleiders waar mijn dank aan toebehoort is Gijsje. Gijsje bedankt voor het in 2010 mij met veel enthousiasme te hebben begeleid tijdens het schrijven van mijn master scriptie. Door jou heb ik AMOLF mogen leren kennen wat uiteindelijk tot dit proefschrift heeft geleid.

Een groot deel van m'n promotie heb ik gespendeerd samen met Bob. Bob, het was een waar genoegen om onze tijd op AMOLF samen door te brengen op dezelfde 12 m^2 van ons kantoor. We zijn tegelijkertijd begonnen onder Mirjam, en hebben dus hetzelfde doorgemaakt, en dan is het fijn dat je de daaruit voortkomende strubbelingen met elkaar kunt delen. Maar ook je uitgebreide chemische kennis, je know-how omtrent het reilen en zeilen binnen AMOLF en je vele ervaringen met familie, vrienden en volleybal zorgden altijd voor interessante en gezellige gesprekken tijdens de vele koffiepauzes, lunches en borrels.

Gesa, thanks for everything. Your presence both in AMOLF and in Delft was a pleasure to experience. And it was nice to have someone in the Delft sitting "in hetzelfde schuitje" as I sat, to either brainstorm about experiments or share our issues with.

Also a warm thank you to the members of the Dogterom lab who I shared the last 2-3 years of my PhD with: Florian, Nuria, Magdalena, Sophie, Marian, Maurits, Mathijs, Louis, Eseng ́ul, and especially Jolijn, Roland and Anne, I don't know where I'd been without your administrative, technical or scientific support.

Thanks to Ralf, for your warm welcome to your group in San Sebastian. Your sincere interest and your vast scientific knowledge greatly motivated me to get the most out of our collaboration. But a thank you should also be sent to the friendly and skillful members of your group who I had the pleasure to spend time with: Galina, Nico, Severin,

Totta, Ram, Leire and Marta. Your scientific advise was invaluable and I greatly enjoyed the work-unrelated things we did in the evenings and weekends.

Thanks to Alfons, Rao, Daniela, Casper and Indrani. Your interest in my work and the directions you proposed provided the necessary input to stay confident about my research. The times we shared were great and insightful, let's hope it will once lead to some exciting new findings.

Bij deze gaat mijn hartelijke dank ook naar de ondersteunde groepen van AMOLF met in het bijzonder Ivo, Erik, Marko, Marco, Marjolein, Henk-Jan, Jan, Richard, Arnelli, Tatiana en Wouter. Of ik nu een aanpassing wenste in de aansturingssoftware voor de microscoop, advies nodig had in het lab of vragen had over financiën, jullie stonden altijd vrijwel meteen voor me klaar. Die efficiënte hulp is van ongekende waarde geweest voor het uitvoeren van mijn onderzoek.

Bedankt Henk-Jan voor het maken van de cover, je enthousiasme siert je en was zeer aanstekelijk. Ben echt ontzettend blij met het resultaat.

The effort of finishing a PhD would have been a much greater challenge if it wouldn't have been for the presence of the many fantastic and diverse personalities of the people that I shared my time at AMOLF with. In no particular order, thanks to Yuval, Jeanette, José, Iza, Lutz, Ioana, Tomek, Wiet, Anouk, Noreen, Marina, Sebastiaan, Nicola, Jacopo, Aditya, Mohammed, Michele, Felipe, Feng, Karin, Corianne, Ruben, Martin, Joris, Roeland, Stefan, Wilbert, Remko, Lars, Ruud, Bob, Arthur, Brian, Björn, Mark.

Thanks to my teammates of our indoor football team Nikhef/AMEF: Stephan, Bart, Timmo, Maarten, Bryn, John, Niels, Michael, Gede, Ido and Fred. I always looked forward to our weekly matches. Too bad there was always at least one team with a few miraculously talented players ruining our endeavors to become champions of the competition.

Bedankt Thomas, dat ik de laatste maanden met je heb mogen samenwerken. Je zorgde voor een flinke boost aan enthousiasme in het staartje van mijn project. En wie weet waartoe dit nog kan leiden.

Dank ook aan de vele nog niet genoemde vrienden voor jullie belangstelling en de soms broodnodige momenten van afleiding in de vorm van concerten, kermisavonden, mannenweekenden, bierproeverijen, festivals, etentjes, etc.

Ook een grote dank aan de familie en schoonfamilie die altijd met veel interesse hebben geluisterd naar mijn pogingen om jullie vragen als: "Maar wat kun je er eigenlijk mee?" overtuigend te beantwoorden. In het bijzonder gaat mijn dankbaarheid naar m'n ouders, Mirron, Mark, Nelly, Wim, Bonny, Niels, Martijn en Ruby voor het feit dat ik altijd ontzettend warm door jullie wordt ontvangen om even de werk-stress te kunnen vergeten.

En ten slotte, een waanzinnig grote dank aan Kelly, zonder jouw onbegrensde steun en liefde had ik allang de spreekwoordelijke handdoek in de ring gegooid. Ik kijk ontzettend uit naar wat de toekomst ons gaat brengen, maar ben er stiekem wel van overtuigd dat die iets moois voor ons in petto heeft.